Durham E-Theses

Inorganic geochemistry and palaeoenvironments of the Early Jurassic Cleveland Basin

ATAR, ELIZABETH,FILIZ,LINDSAY

Inorganic geochemistry and palaeoenvironments of the Early Jurassic Cleveland Basin

Elizabeth Filiz Lindsay Atar

Thesis presented for the degree of Master of Science by Research to the University of Durham

Under the Supervision of Dr. João P. Trabucho-Alexandre

and Professor Andrew Aplin

Research conducted at:

Department of Earth Sciences
Durham University
Science Labs
Durham
DH1 3LE

Abstract

The uppermost Staithes Sandstone Formation to lowermost Alum Shale Member were studied in a core drilled recently approximately 10 km south of Whitby and 7 km west of Robin Hood's Bay to investigate the evolution of Pliensbachian-Toarcian (lower Jurassic) depositional environments of the Cleveland Basin, Yorkshire, UK. Samples were analysed for organic carbon isotopes, total organic carbon (TOC), and elemental geochemistry (major and trace elements). The carbon isotope excursion in the Whitby Mudstone Formation correlates to the Toarcian oceanic anoxic event (T-OAE). The elemental geochemistry data were used to assess the palaeoredox state of the depositional environment, the role of dilution of organic matter by siliciclastic material, and the rates of organic productivity in the photic zone above the site of deposition. The data reveal that the supply of detrital material varied, possibly resulting from climate or relative sea-level variations, during the deposition of the Staithes Sandstone and Cleveland Ironstone Formations, but abruptly stopped at the onset of the deposition of the Grey Shale Member of the Whitby Mudstone Formation. It is proposed that siliciclastic starvation, resulting from a transgression, was responsible for the shutoff of detrital material supply and that from the Pliensbachian-Toarcian boundary deposition was predominantly of palimpsest sediment. The redox proxies suggest that the water column was well oxygenated throughout the deposition of the Staithes Sandstone and Cleveland Ironstone Formations, but became anoxic, and eventually euxinic, during the deposition of the upper half of the Grey Shale Member. It is suggested that the transgression responsible for the detrital shutoff also resulted in the stratification of the water column and that the TOC enrichment during and after the negative carbon isotope excursion may be a product of enhanced preservation.

Contents

List of figures

Acknowledgements

To my Mum, Nigel and John, words cannot express my gratitude to you. I thank you for your endless love and support throughout everything. My past, present and future projects would not have been possible without you.

To Janette and Philip, thank you for your love, kindness and hospitality during my time in London. Thank you for turning your living room in to a bedroom for me and for the endless fun and laughter we enjoyed in your home – I truly felt part of your family.

To Chris, Laura and Erin, thank you for your continued friendship, encouragement and support throughout my time in Durham. I can honestly say that between you, you made it fantastic. I thank my housemates, Fienke, Edward, Ben, Adam and Tom for being the very best friends, for making our home a great place to be, for absolving me of all house-related responsibilities and keeping me sane whilst I wrote this thesis. Finally, thanks go to the postgraduate students and staff in the Department of Earth Sciences at the University of Durham, for creating a nice atmosphere to work in, the much-needed breaks from writing and the endless supply of coffee.

Introduction

During the Early Jurassic, northwest Europe was covered by a shallow, epicontinental sea (Powell, 2010). Sedimentation in this setting was controlled by sediment supply, whether that be derived from the continent or palimpsest, subsidence and uplift associated with regional and global tectonic activity, and changes in sea level. Sediments deposited in the Cleveland Basin, Yorkshire, UK, a basin in the north-western European seaway, throughout the late Pliensbachian-early Toarcian, are the focus of this study.

Oceanic anoxic events (OAEs) were time intervals in the Mesozoic characterised by widespread deposition of organic matter-rich sediments, known as black shales (Jenkyns, 1988; Schlanger and Jenkyns, 1976). The early Toarcian (*c.* 183 Ma) OAE (T-OAE) is the first of such events to be recognised in the sedimentary record, and is synchronous with a large perturbation in the global carbon cycle, a global temperature rise, enhanced continental weathering, and a severe biotic crisis (Bailey et al., 2003; Caruthers et al., 2011; Hesselbo et al., 2000; Kafousia et al., 2011).

Many of the organic matter-rich sediments deposited during the late Pliensbachian-early Toarcian are excellently exposed in Europe and have been extensively studied (Bailey et al., 2003; Farrimond et al., 1989; Kafousia et al., 2011; Rohl et al., 2001). A particularly well-studied succession is that of the Posidonia Shale in the Netherlands and Germany (Rohl et al., 2001; Schwark and Frimmel, 2004; Song et al., 2014; Trabucho-Alexandre et al., 2012), which is a lateral equivalent of the Toarcian of the Cleveland Basin, Yorkshire, UK. Several models have been proposed for the deposition and presevation of the Toarcian shales in the Germanic

basins, i.e. upwelling driven productivity (Kauffman, 1979) or enhanced preservation under a stratified water column. (Brumsack, 1991; Röhl et al., 2001).

The controls on the deposition of black shale are a complex interplay between nutrient supply, whether that be from continental run-off, upwelling or recycling within the water column, dilution of organic matter by inorganic material, and the redox state of the sediment pore and bottom waters (Pedersen and Calvert, 1990; Tyson, 2001; Tyson, 2005). Each of these processes affects the chemistry of the water and sediment and thus they leave signals in the sedimentary record, which can be used to reconstruct the depositional environment (Calvert and Pedersen, 1993; Lezin et al., 2013).

I report high resolution inorganic geochemical data from sediment deposited in the Cleveland Basin, Yorkshire, NE England, during the late Pliensbachian and early Toarcian. Major, trace and rare earth element data were used as proxies for organic productivity, redox state of the sediment pore waters, dilution effects of siliciclastic input and sediment provenance. I propose a local scale model where rising relative sea level starved the Cleveland Basin of detrital material entering the basin and promoted stratification of the water column. Palimpsest sedimentation of relict sediment occurred throughout the deposition of the Whitby Mudstone Formation under predominantly anoxic-euxinic waters.

Geological background

Paleogeography, tectonics, climate, and sea level

The Cleveland Basin, a relatively small extensional basin in North Yorkshire, NE England (fig. 1), was located at around 30°N in the late Pliensbachian (Powell, 2010). The Cleveland Basin formed in the Late Triassic as a product of non-uniform extension across eastern England (Rawson and Wright, 1995). It was one of several basins established in the epicontinental seaway with the Tethys Ocean to the south and the Boreal Ocean towards the north (Bradshaw et al., 1992; Simms et al., 2004). The extent of the sea on the northwest European epicontinental shelf is uncertain. Rawson and Wright (1995) suggest that the Cleveland Basin was within c. 30 km of land while Bradshaw et al. (1992) suggest that there was a distance of c. 120 km between the Cleveland Basin and a landmass. Situated north of the East Midlands Shelf, the Cleveland Basin is bound to the north by the Howardian-Flamborough fault, to the northeast by the Mid-North Sea High, to the west by the Pennine High and to the south by the Market Weighton High (Bradshaw et al., 1992; Powell, 2010; Rawson and Wright, 1995). In the Early Jurassic, regional extension affecting the basin caused rapid subsidence; this, coupled with rising sea level, created accommodation space for sedimentation (Rawson and Wright, 1995).
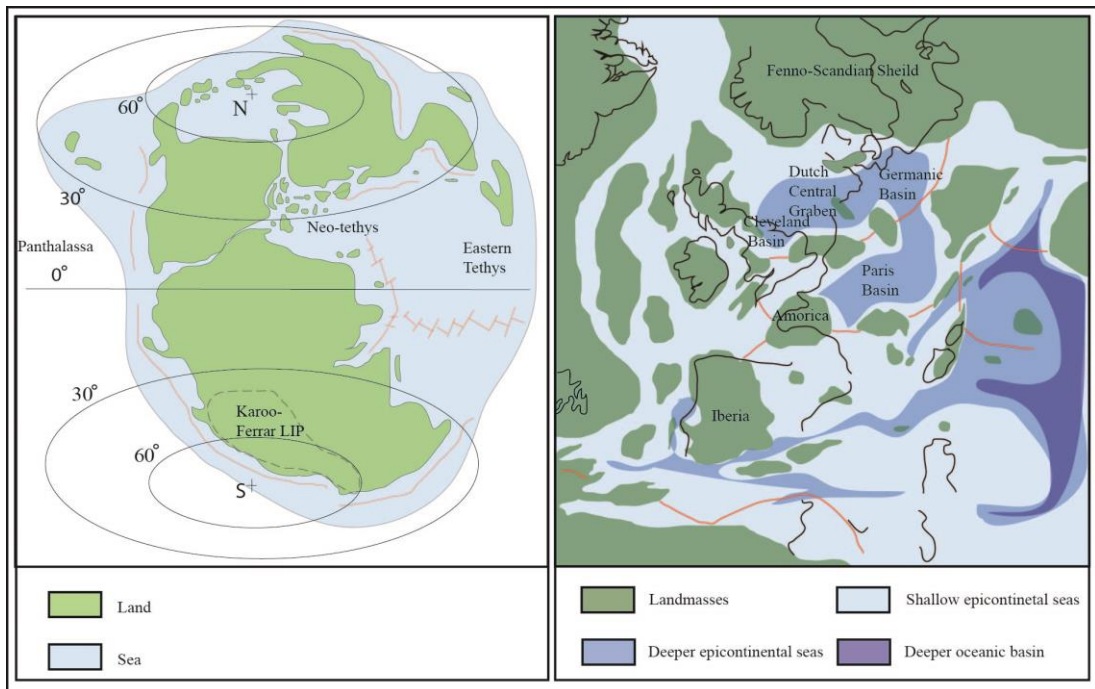
Figure 1. Palaeogeographical map of northwest Europe in the Early Jurassic. Adapted from (Trabucho-Alexandre et al., 2012)

Earth was in a greenhouse period during the Early Jurassic. Global temperatures rose by *c.* 6 ˚C during the Pliensbachian-Toarcian (Svensen et al., 2007); the temperature rise is commonly attributed to elevated pCO$_2$ levels associated with the emplacement of the Karoo-Ferrar Large Igneous Province. The Karoo-Ferrar LIP is estimated to have erupted at 183±1 Ma but more accurate dating needs to be conducted to firmly link the eruptions to the T-OAE (Pálfy and Smith, 2000). The mechanism surrounding the increase in pCO$_2$ is widely debated; Hesselbo et al. (2000) suggest that the emplacement caused mass-dissociation of methane clathrates, while Svensen et al. (2007) suggest contact metamorphism of organic matter-rich rocks, resulting from the emplacement of the LIP, caused a build-up of CO$_2$ in the atmosphere. Suan et al. (2008) suggest that long term degassing from the eruptions can account for the CO$_2$ volume in the atmosphere after an initial input of gas hydrate. The temperature rise may have enhanced the hydrological cycle and weathering of exposed rocks. It

would have also caused the oceans to thermally expand and thus would have served as a mechanism for the transgression recorded throughout the Early Jurassic.

Changes in sea level were a major control on the palaeogeography of northwest Europe in the Early Jurassic. A transgression continued from the Late Triassic well into the Early Jurassic reaching its maximum in the *Hildoceras bifrons* Zone (middle Toarcian); this led to a greater area of submerged continent and a possible increase in marine sedimentation (Bradshaw, 1992). However, it is unlikely that water depth exceeded tens of metres in the Cleveland Basin (Powell, 2010). Within the Cleveland Basin, a regression is commonly reported to have occurred in the late Pliensbachian which increased the area of land exposed and susceptible to weathering processes (Bradshaw et al., 1992). The regression is inferred from lithological changes (Powell, 2010), however this should be considered with caution as grain size is a poor indicator of water depth. Hallam (1981) infers a middle Toarcian regression. A glacio-eustatic model cannot explain the extent of sea-level fluctuation recorded in the sedimentary record because there was little to no ice at the poles at this time; however, tectono-eustatic models can explain the majority of changes in the sea level in the Jurassic (Hallam, 2001).

Lithostratigraphy and biostratigraphy

The Lower Jurassic of the Cleveland Basin is dominated by mudstones which alternate with occasional fine-grained sandstones and oölitic ironstones. The thickness of the succession, often informally referred to as the 'Lias,' does not exceed 454 m.

Figure 2 shows the lithostratigraphical and biostratigraphical thicknesses and divisions of the studied succession. The lowermost formation of the Lower Jurassic sediments in the Cleveland Basin is the Redcar Mudstone Formation, which is a c. 238 m thick shale succession. Overlying the Redcar Formation is the 27.35 m thick Staithes Sandstone Formation. The uppermost beds of the Staithes Sandstone Formation form the base of the studied part of the core. The Staithes Sandstone Formation consists of yellow, fine- to very fine arenites interbedded with brownish siltstones.

Stage/Substage	Ammonite Zone	Lithostratigraphical Division		Thickness (m)
Toarcian	*Haugia variabilis*	Whitby Mudstone Formation *p.p.*	Alum Shale Member *p.p.*	27.85
	Hildoceras bifrons		Mulgrave Shale Member	30
	Harpoceras falciferum		Grey Shale Member	14.64
Upper Pliensbachian	*Dactylioceras tenuicostatum*	Cleveland Ironstone Formation	Kettleness Member	5.84
	Pleuroceras spinatum		Penny Nab Member	18.45
Lower Pliensbachian	*Amaltheus margaritatus*	Staithes Sandstone Formation *p.p.*		27.35

Figure 2. Stratigraphic column showing the biostratigraphical and lithostratigraphical divisions of the studied section.

The Cleveland Ironstone Formation overlies the Staithes Sandstone Formation and comprises the 18.54 m-thick Penny Nab Member and the 5.84 m-thick Kettleness Member. The Penny Nab Member consists of at least four shale parasequences that exhibit small scale (0.1 – 1.0 m thick) upwards coarsening and both large scale (1.0 – 3.0 m thick) upwards fining and coarsening cycles (Macquaker et al., 1996).

Macquaker et al. (1996) interpret the large scale cycles to be retrogradational and progradational, respectively. The sequences are capped by condensed oölitic ironstone horizons, which Powell (2010) interpreted as transgressive deposits but Macquaker et al. (1996) interpret as forced regressions. The younger Kettleness Member consists of grey shale and sandy mudstone beds interbedded with oölitic ironstones.

The Cleveland Ironstone Formation is overlain by the Whitby Mudstone Formation which comprises five members. The lowermost unit is the 14.64 m thick Grey Shale Member; it is predominantly grey mudstone. Above this, sits the 30 m thick Mulgrave Shale Member, informally subdivided into the Jet Rock and the Bituminous Shale; it is dominated by black shale beds with occasional concretionary horizons. The Alum Shale Member is the uppermost lithostratigraphical unit in the studied part of the core. It is 27.85 m thick and made up of black and grey shales with phosphatic nodule horizons.

Materials and methods

Samples were collected from the core drilled by York Potash, a Sirius Minerals project, at the Dove's Nest site, situated 10 km south of Whitby and 7 km west of Robin Hood's Bay in the Cleveland Basin, North Yorkshire, U.K.

The samples were taken from depths between 126.18 m and 219.06 m below the earth's surface at a resolution of 20–50 cm. The sample set comprises 278 samples.

Approximately 1 g of each sample was ground to a fine powder using a Retsch RM100 Agate Mill in the Stable Isotope Biogeochemistry Lab at Durham University and separated in half; half was used for carbon isotope analysis and the other half for elemental analysis.

Inductively coupled plasma – atomic emissions spectrometry (ICP–AES)

A Join Yvon JY70 Plus ICP–AES was used in the geochemistry labs at Kingston University London to determine the major- (Al, Si, Ti, Fe, Mn, Mg, Ca, Na, and P)) and minor- (Ba, Cr, Sr, and Zr) elements within each sample. All of the samples and reference materials (appendices B and C) were prepared in lithium metaborate fusions (see appendix A for method) prior to being run on the ICP–AES. Data are reported as weight percent oxides for the major elements and as µg/g (parts per million) for the trace elements (Appendix G).

Inductively coupled plasma – mass spectrometry (ICP–MS)

ICP–MS was carried out at Kinston University London to determine the trace element (Sc, V, Cr, Mn, Co, Ni, Cu, Zn, Ga, Rb, Sr, Nb, Mo, Cs, Ba, Y, Zr, Hf, Ta,

Th, and U) (Appendix K) and rare earth element concentrations (La, Ce, Pr, Nd, Sm, Eu, Gd, Tb, Dy, Ho, Er, Tm, Yb, and Lu) of 97 samples spread throughout the sample set. The samples and reference materials (appendix C) were prepared in both lithium metaborate fusions and aqua regia leach digestions (see appendix A for methods). The lithium metaborate preparations were analysed for all of the aforementioned elements; however, the solutions had to be run at low concentrations to avoid damaging the machine. The dilution can cause the concentration of elements to fall below detection limits of the machine and thus the data can be unreliable. The loss of some elements, for example Zn, Se, and Cd, during the heating stage is another problem with the fusion preparation. To mitigate these problems, aqua regia leach digestions were analysed for the elements which were unreliable in the lithium metaborate fusions (V, Mn, Co, Ni, Cu, Zn, As, Se, Mo, Cd, and Sb). It is important to note that the aqua regia leach digestions are semi-quantitative because they are partial digestions.

Normalisation against aluminium

Elements are normalised against aluminium because it represents the aluminosilicate fraction of the sedimentary rock, which is unaffected by biological and diagenetic processes (Tribovillard et al., 2006). It is abundant in all aluminosilicate minerals that ultimately enter the system from terrestrial sources but has a relatively low abundance in seawater (Brumsack, 2006) meaning it can be used to assess trace metal concentrations in the samples irrespective of the lithological genesis and of the effect dilution caused by siliciclastic, carbonate, opal and organic material (Dellwig et al., 2000; Tribovillard et al., 2006). The enrichment factors, in reference to 'average shale' values, were not calculated as some discrepancies surround the

composition of average shale e.g. their diagenetic components. The average shale data may not be representative of the average shale of the local area so using the average shale values may further complicate the analysis. To mitigate these problems, I have normalised against Al and will look at relative enrichments and depletions within the succession.

All elements were plotted against Al to see which, if any, are controlled by the detrital flux. Most elements, with the exception of chromium, plotted with a negative or no correlation; this indicates that they are not controlled by detrital flux (Des Combes et al., 1999).

Where samples have very low concentrations of Al, normalisation may produce exaggerated peaks in the element (Van der Weijden, 2002) this needs to be taken in to account when interpreting the results (Hetzel et al., 2009).

Results

Detrital input proxies

The detrital flux to a basin can be inferred using specific element concentrations normalised to aluminium e.g. silicon, titanium and zirconium (Lezin et al., 2013; Murphy et al., 2000; Tribovillard et al., 1994). Si is associated with either the detrital quartz or the biogenic fraction of the sediment while Ti and Zr are related to the clay and heavy mineral fraction of the sediment. The Al-normalised values of these elements can tell us information on the nature and variation in the supply of clastic material to a sedimentary basin during the deposition of a specific formation.

In shallow epicontinental seas, palaeogeography is a dominant control on siliciclastic sedimentation. The sediment accumulation rate of siliciclastic sediment on the shallow epicontinental seafloor depends on the distribution of siliciclastic sediment sources, i.e. river mouths and rocky coastlines, the distance of these sources to the depositional environment, which is partly controlled by relative sea-level, and the amount of sediment that escapes near shore sediment traps to the shelf (Alexandre et al., 2011).

In the Staithes Sandstone and Cleveland Ironstone Formations, the Si/Al, Ti/Al, Zr/Al, Na/Al, and, K/Al profiles (fig. 3) show large amplitude variation relative to the rest of the core. Just above the Pliensbachian-Toarcian boundary, the detrital indicators have a negative shift suggesting the nature of the sediment supply changed here.

In the Whitby Mudstone Formation, the Si/Al profile is stable at a low concentration with the exception of a positive peak at 141.60 m. The Ti/Al profile exhibits less
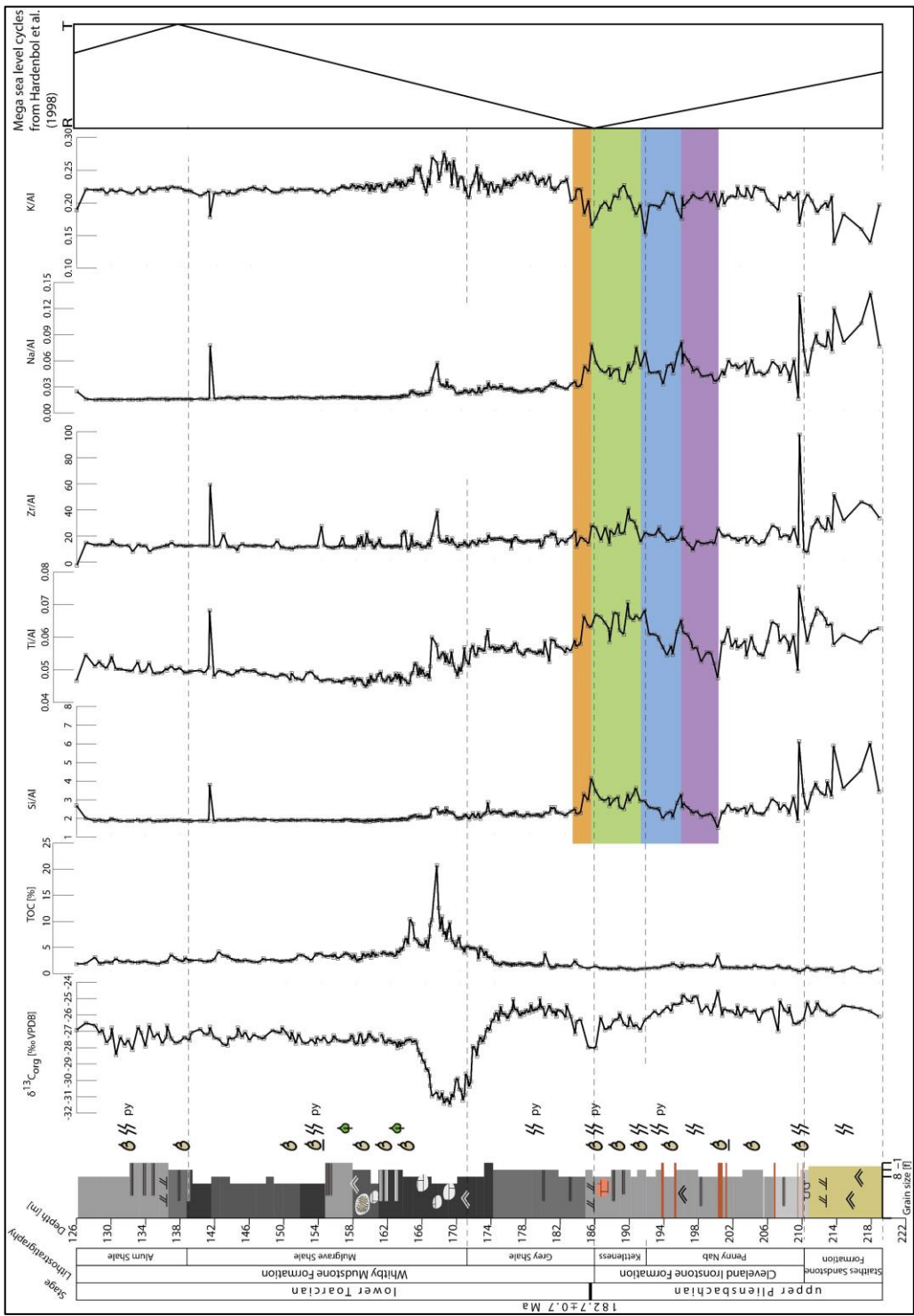
Figure 3. Depth core logs of Al normalised Si, Ti, Zr, Na, and K, which have been used as proxies for detrital input to the basin. The four coloured boxes highlight the observed cyclicity in the Cleveland Ironstone Formation. The mega sea level cycles plot illustrate the long-term regression-transgression cycle.

variation in the Whitby Mudstone Formation than in the Staithes Sandstone and Cleveland Ironstone Formations and it has a slight overall positive increase.

Na/Al and K/Al (fig. 3) show near-opposite trends. The Na/Al profile gets gradually more negative between samples up through the Staithes Sandstone and Cleveland Ironstone Formations, while K/Al becomes progressively more positive. Both profiles flat-line throughout the Whitby Mudstone Formation with the exception of peaks at in Na/Al at 167.89 m and in both elements at 141.06 m. The variation in the Cleveland Ironstone Formation described in Si/Al, Ti/Al, and Zr/Al can be seen in Na/Al but not K/Al.

Palaeoredox proxies

The redox state of sediment-pore and bottom waters depends on oxygen supply and demand in the water column. The supply of oxygen in shallow epicontinental seas is maintained by the mixing of the seas, currents transporting oxygenated water, and primary producers photosynthesising. When the demand for oxygen exceeds the supply, the water is depleted in oxygen and becomes sub-oxic, anoxic or, in the presence of free hydrogen sulphide, euxinic. Anoxia has a dramatic effect on the behaviour of trace metals so the concentrations of these elements can be used to reconstruct the palaeoredox state of the sediment pore and, potentially, bottom waters (Brumsack, 2006; Tribovillard et al., 2006).

Throughout the Staithes Sandstone and Cleveland Ironstone Formations and the lower section of the Grey Shale Member, Al-normalised uranium, molybdenum, iron, cadmium, zinc, and antinomy are relatively flat at low concentrations relative to other formations, which suggests that the waters were well oxygenated during the deposition of these sediments (Brumsack, 2006; Calvert and Pedersen, 1993; Tribovillard et al., 2006). Manganese (fig. 4) shows four pronounced positive peaks, one of which corresponds to the Sulphur Band at the Pliensbachian–Toarcian boundary. The profile is less variable in the Grey Shale Member but peaks again at 167.89 m and 164.91 m. After this, the Mn profile gradually declines with the exception of peaks at 137.61 m and 126.18.V/Al (fig. 4) becomes progressively negative up the core with the exception of three pronounced positive peaks; this is similar to the Si/Al, Ti/Al and Zr/Al (fig. 3) so V concentrations may be affected by the detrital input and thus cannot be used as a redox proxy. Vanadium is linked to the
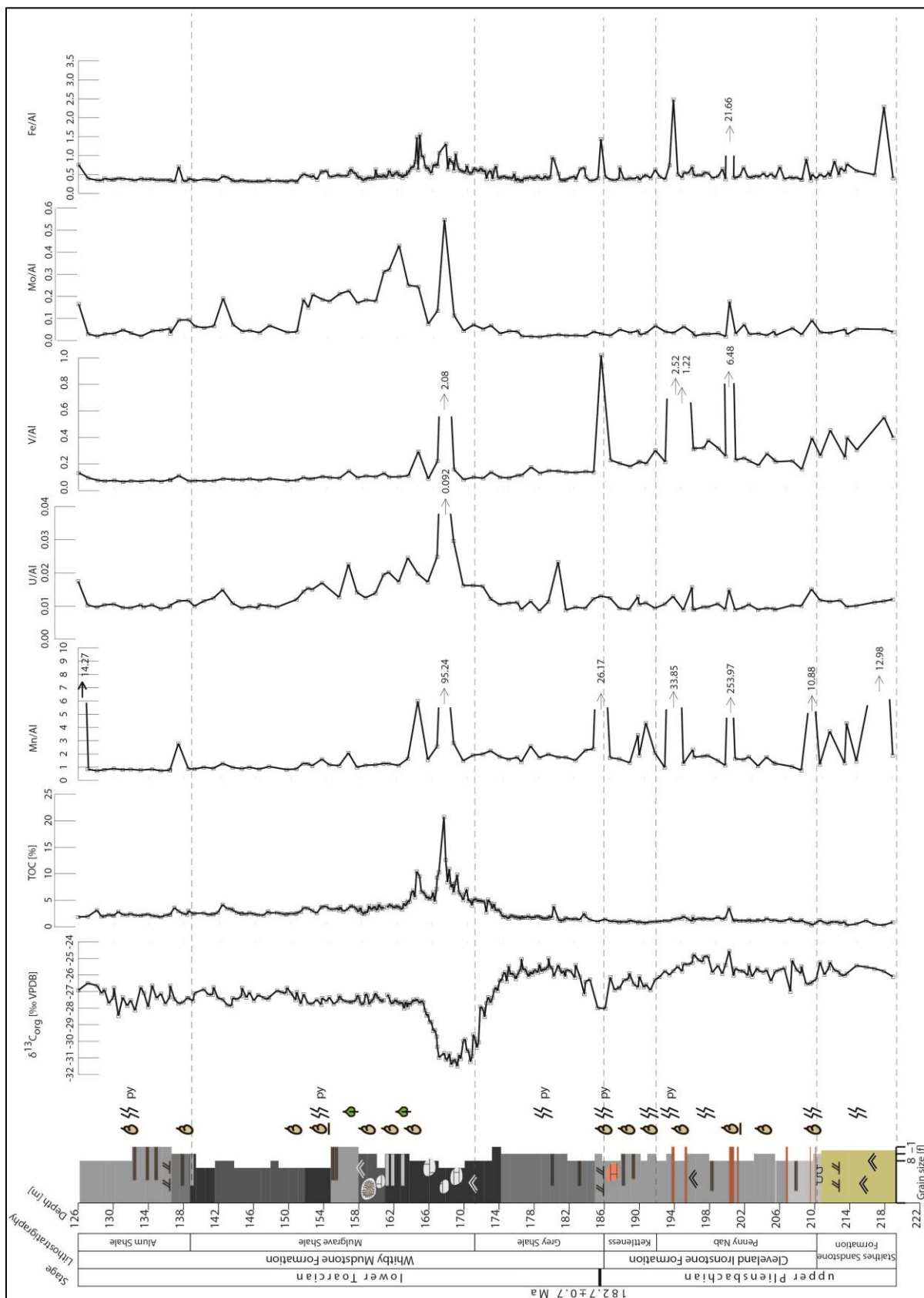
Figure 4. Depth core logs of Al normalised Mn, U, V, Mo, and Fe, which have been used as redox proxies.

manganese cycle (Tribovillard et al., 2006), which may explain why Mn/Al and V/Al peak at the same horizons (fig. 4).

Al-normalised uranium, arsenic, selenium, and iron concentrations start to increase in the upper few metres (from *c.* 175.0 m) of the Grey Shale Member; this suggests sediment-pore waters became anoxic and it coincides with the onset of TOC enrichment.

Chromium (fig. 5) is enriched in the Staithes Sandstone and Cleveland Ironstone Formations and has pronounced positive peaks which correspond to ironstone bands and a negative peak at the Pliensbachian–Toarcian boundary. The values for the rest of the core are slightly depleted, relative to the bottom half of the core, and they remain constant with the exception of the positive peak at 167.89 m.

Cobalt and nickel (fig. 5) are similar to each other in that they exhibit relatively large amplitude variation in the Staithes Sandstone and Cleveland Ironstone formations but are flat at relatively low concentrations in the Grey Shale Member. Concentrations rise again between 175.26 m and 151.07 m, within the Mulgrave Shale Member, and they have pronounced positive peaks at 167.89 m that coincide with a concretionary horizon. At 151.07 m, Co and Ni have a negative shift after which the profiles gradually become more negative up the core. Copper (fig. 5) has lower amplitude variation in the Staithes Sandstone and Cleveland Ironstone Formations and is much flatter in the post-excursion section of the core compared to nickel and cobalt.

Between 170.08 m and 155.93 m, in the Mulgrave Shale Member, Al-normalised uranium, molybdenum, iron, nickel, arsenic, and selenium (fig. 4, 5, and 6) are enriched relative to the rest of the core; this is indicative of strongly anoxic to
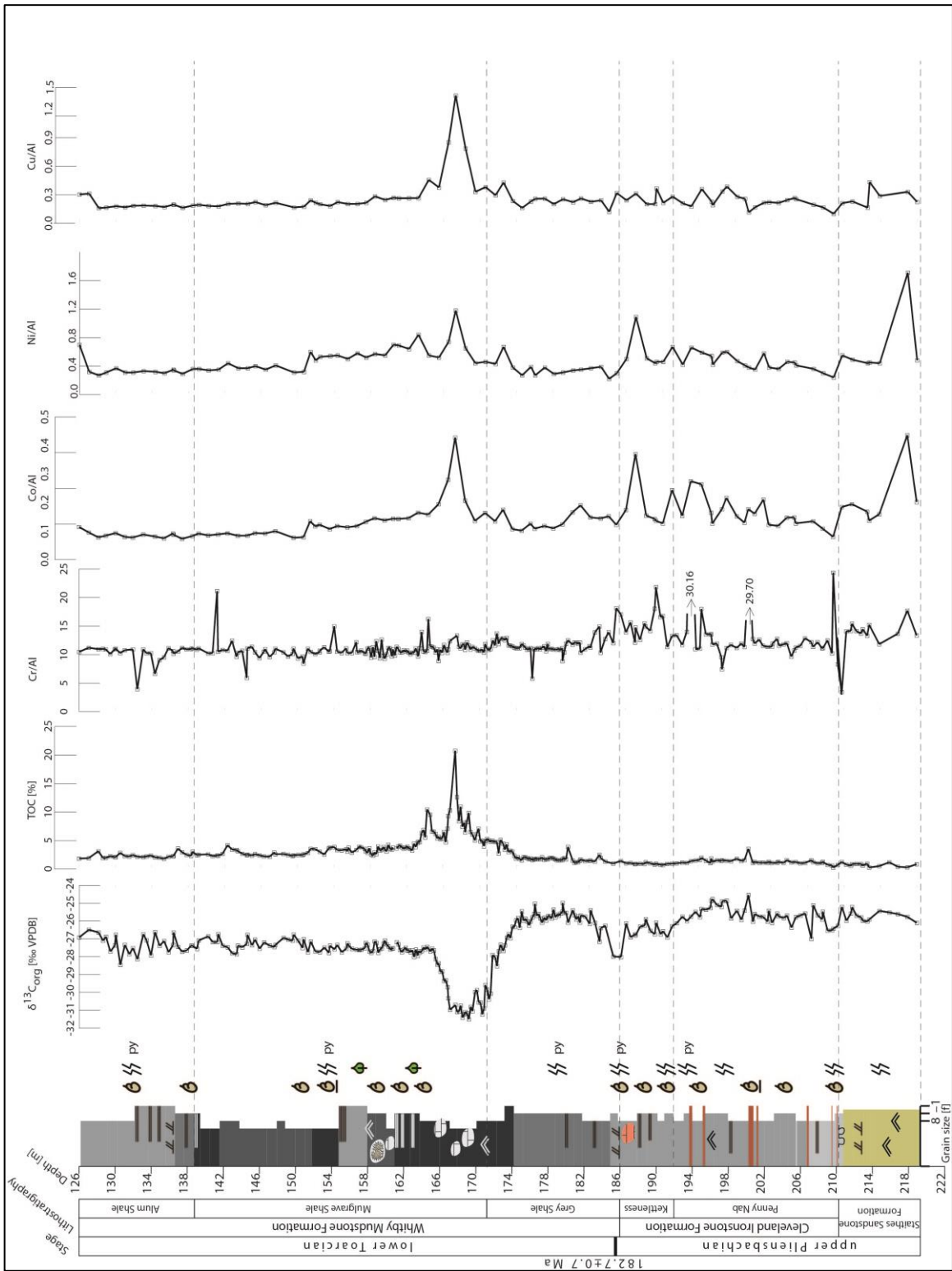
Figure 5. Depth core logs of Al normalised Cr, Co, Ni, and Cu, which have been used as redox proxies, and the d13C and TOC.

11
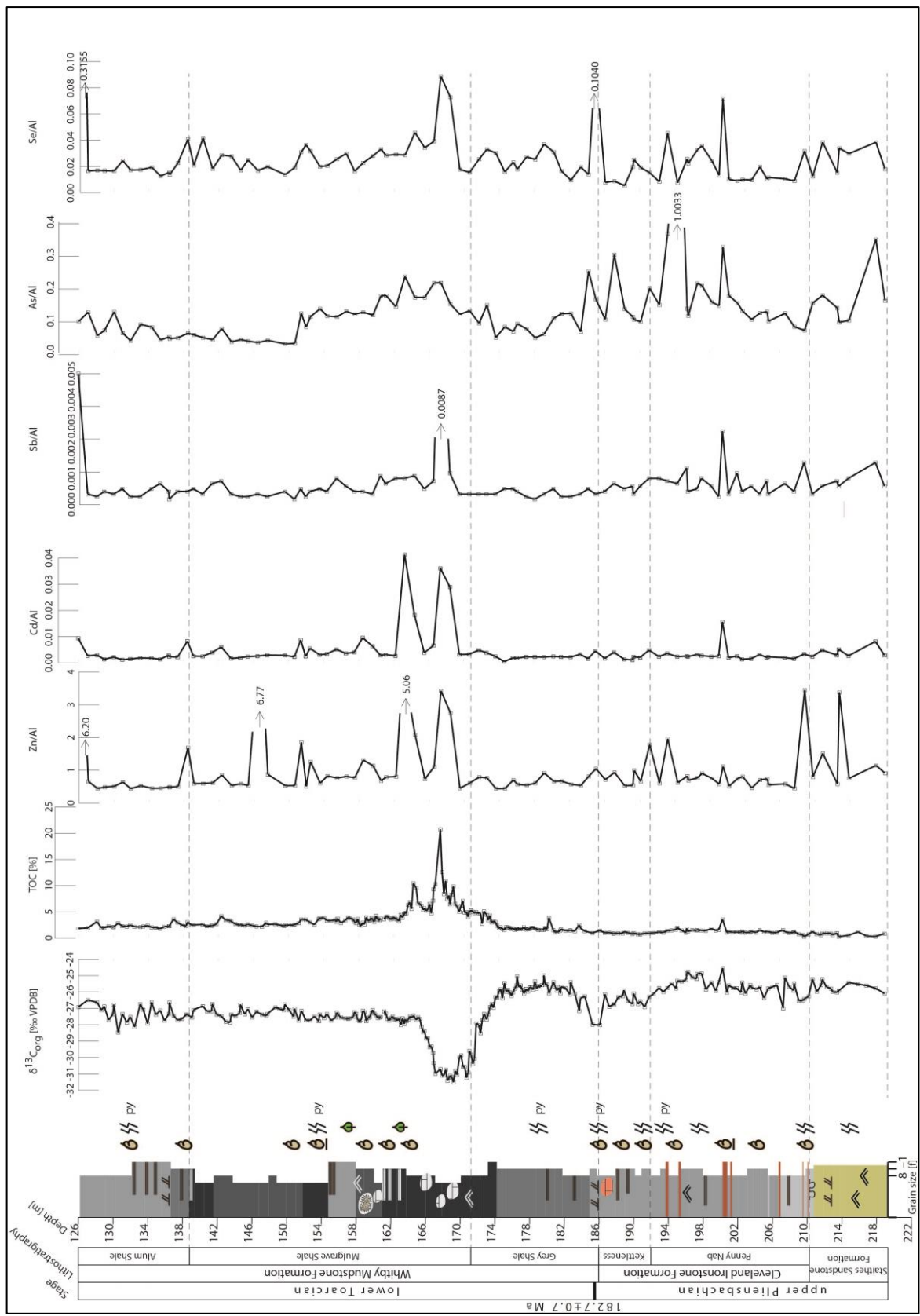
Figure 6. Depth core logs of Al normalised Zn, Cd, Sb, As, and Se, which have been used as redox proxies, carbon isotopes and TOC.

euxinic conditions in the sediment-pore waters during the deposition of these sediments. This is supported by the Ni/Co and U/Th ratios which are reported to be reliable redox proxies (fig. 7) (Jones and Manning, 1994; Lezin et al., 2013). These enrichments occur after the onset of the carbon isotope excursion and continue when after the excursion and the maximum TOC enrichment. The large positive peak at 167.89 m in many of the trace metals (e.g. Mn, U, V, Mo (fig. 4), Cu, Co, Ni (fig. 5), Zn, Cd, Sb, Se (fog. 6)) coincides with the carbonate concretions recorded in the log so the signal is probably diagenetic.

Above 155.93 m, in the upper Mulgrave Shale Member and the Alum Shale Member, most of the redox-sensitive trace metals (e.g. Mn, U, Fe (fig. 4), Co, Ni (fig. 5)) return to low concentrations, which suggest the sediment-pore waters became more frequently oxygenated. The Mo concentration also decreases above 155.93 m but it does not return to pre-enrichment levels; this supports the hypothesis that the waters became more oxygenated throughout the deposition of the Alum Shale Member but suggests that sustained oxygenation of the sediment-pore waters was reached.
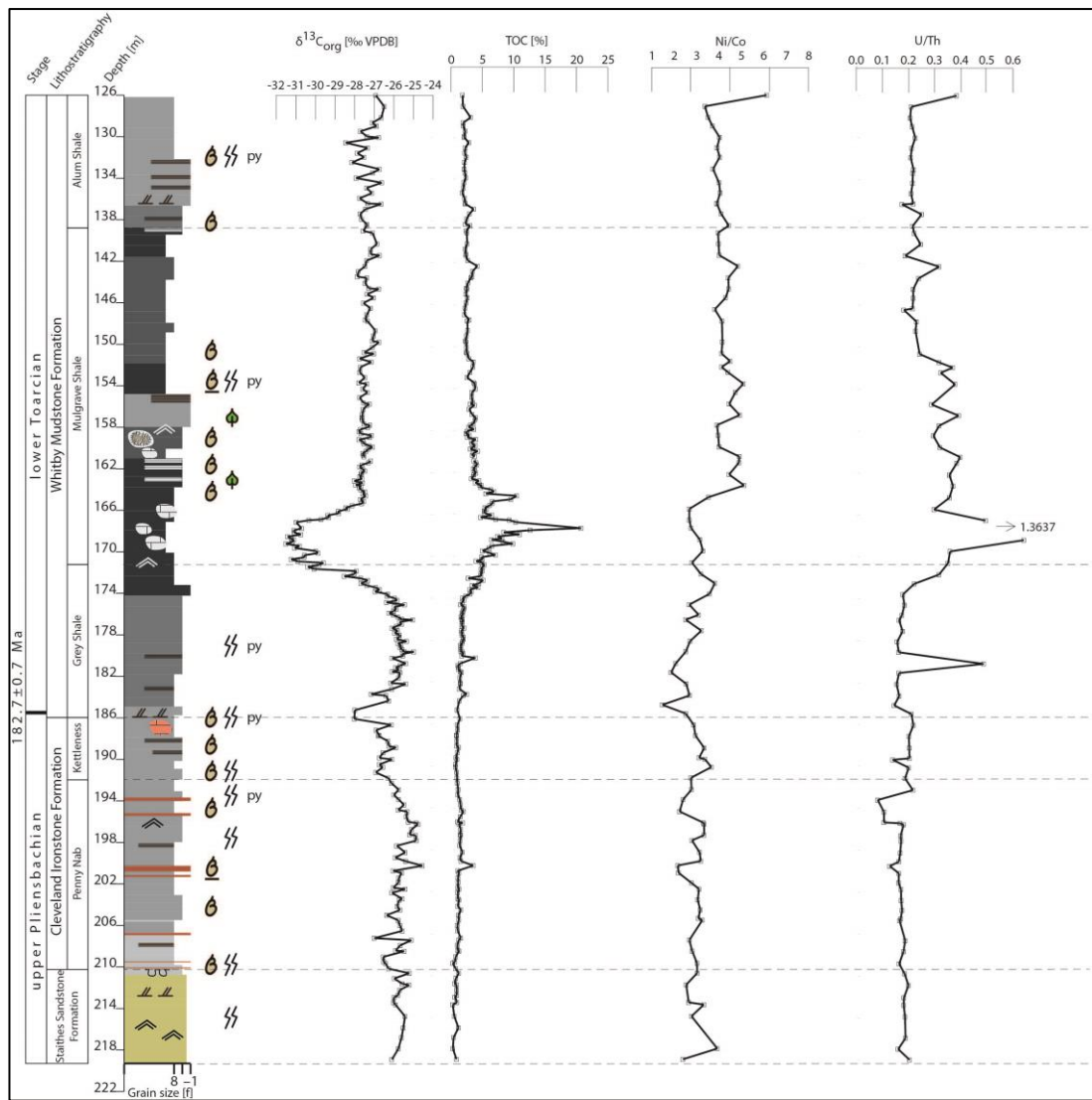
Figure 7. Depth core logs of Ni/Co and U/Th, which have been used as redox proxies, and the d13C and TOC.

Palaeoproductivity proxies

Micro- (e.g. Cd, Ni, and Zn) and macro- nutrients (e.g. P) play an important role in organic productivity and it is widely thought that their concentrations in sediments can be used to determine rates of palaeoproductivity due to their affinity to organic matter (Calvert and Pedersen, 2007). However, many of these elements can be enriched during sedimentation under anoxic conditions through diffusion or remobilisation so these proxies must be applied with caution (Calvert and Pedersen, 2007).

The low concentrations of Al-normalised P, Ba, Cd, Cu, Zn, and Ni (fig. 8) suggest that productivity was low during the deposition of the Staithes Sandstone and Cleveland Ironstone Formations and the lower half of the Grey Shale Member. P/Al starts to increase at c. 183 m, so due to the oxic conditions of the water column at this time, it may indicate that the rate of organic productivity was increasing.

Ba, Cd, Cu, Zn, and Ni are relatively enriched during the deposition of the Mulgrave Shale Member (fig. 8). This may reflect a higher rate of organic productivity. However, because the enrichment coincides with well-developed anoxia in the sediment-pore and, potentially, bottom waters, it may result from diffusion or redox-related remobilisation in the sediment.

TOC (fig. 8) may be used as a palaeoproductivity proxy in settings where the preservation and sedimentation conditions remain constant and stable. However, both the rate of sedimentation and the redox state of the depositional environment varied during the deposition of the succession so it is not possible to determine whether the higher levels of TOC reflect only enhanced preservation, only higher organic productivity, or a combination of both.
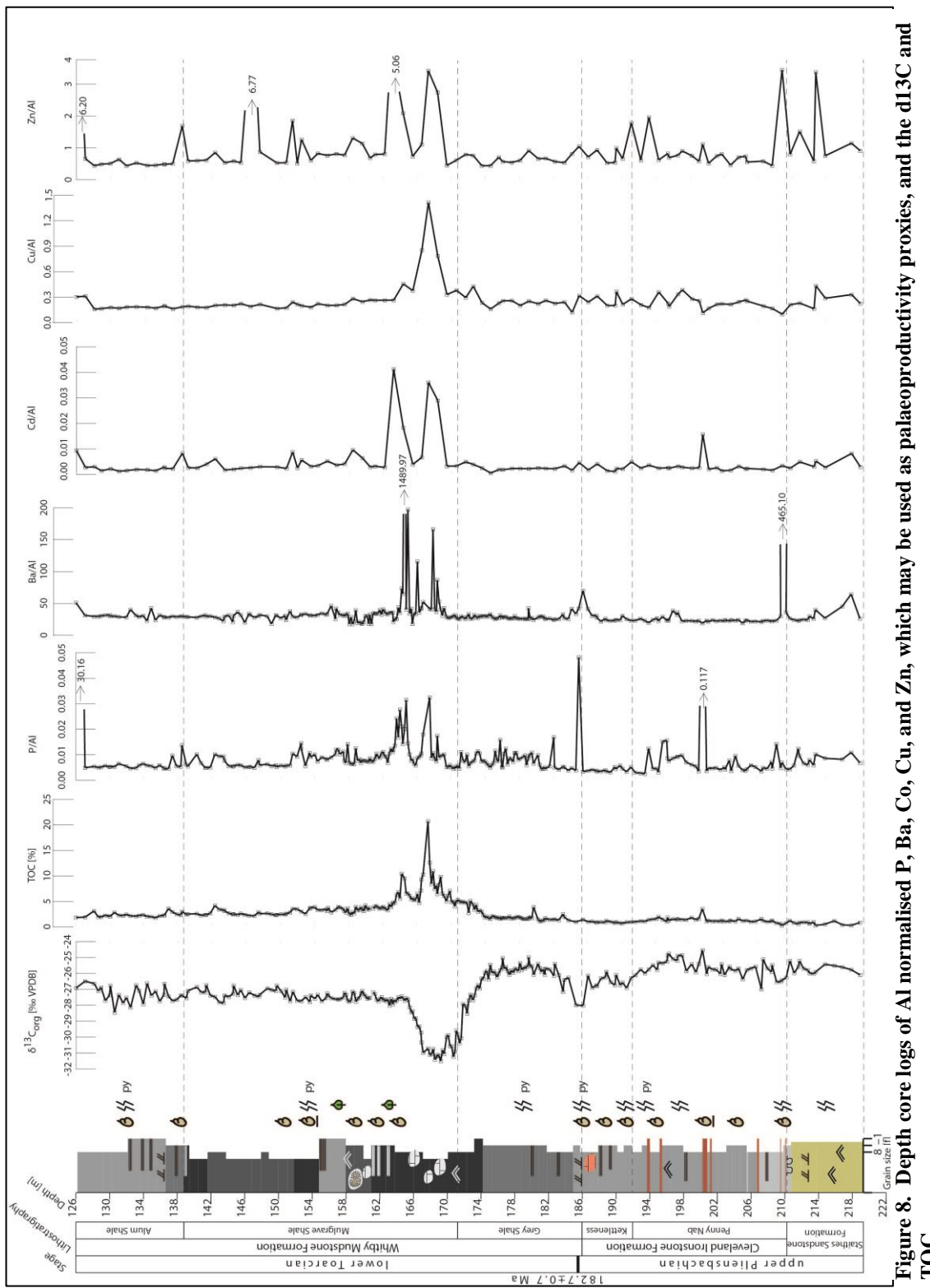
Figure 8. Depth core logs of Al normalised P, Ba, Co, Cu, and Zn, which may be used as palaeoproductivity proxies, and the d13C and TOC.

Discussion

Staithes Sandstone Formation

During the deposition of the Staithes Sandstone Formation, siliciclastic sediment input was highly variable as shown by the Si/Al, Ti/Al, Zr/Al (fig. 3), and Cr/Al (fig. 5) profiles. The poor correlation between silicon and aluminium in the Staithes Sandstone Formation (R^2=0.0023) (fig. 9) suggests that the clay component of the Staithes Sandstone Formation was diluted by other clastic silicates. As there is minimal biogenic material associated with this formation, the abundance of silicon is mostly likely related to the abundance of detrital quartz entering the basin. Based on geochemistry alone, it is not possible to say whether the pulses of clastic material came directly from the continent or if the sediment was reworked from elsewhere on the shelf. However, the sandy nature of this formation suggests that the depositional environment had a relatively high energy and was in a relatively proximal setting.

Typically, the REE concentration is higher in the clay fraction than in the sand/silt fraction of a sedimentary rock (Dypvik and Brunfelt, 1979). This explains why the sandy Staithes Sandstone Formation is characterised by low concentrations of REE relative to other stratigraphic units in the Lower Jurassic of Yorkshire, which are typically more clay-rich (fig. 10). The marginal variation seen within the REE data for the Staithes Sandstone Formation may relate to changes in siliciclastic source and/or abundance, for example, fluctuations in the amount of clastic material weathered from the continent or a change in the course of the river possibly leading to a change in source rock being weathered.

Figure 9. Al$_2$O$_3$ against SiO$_2$, linear trend lines, and R^2 values plotted for each unit to show the correlation.
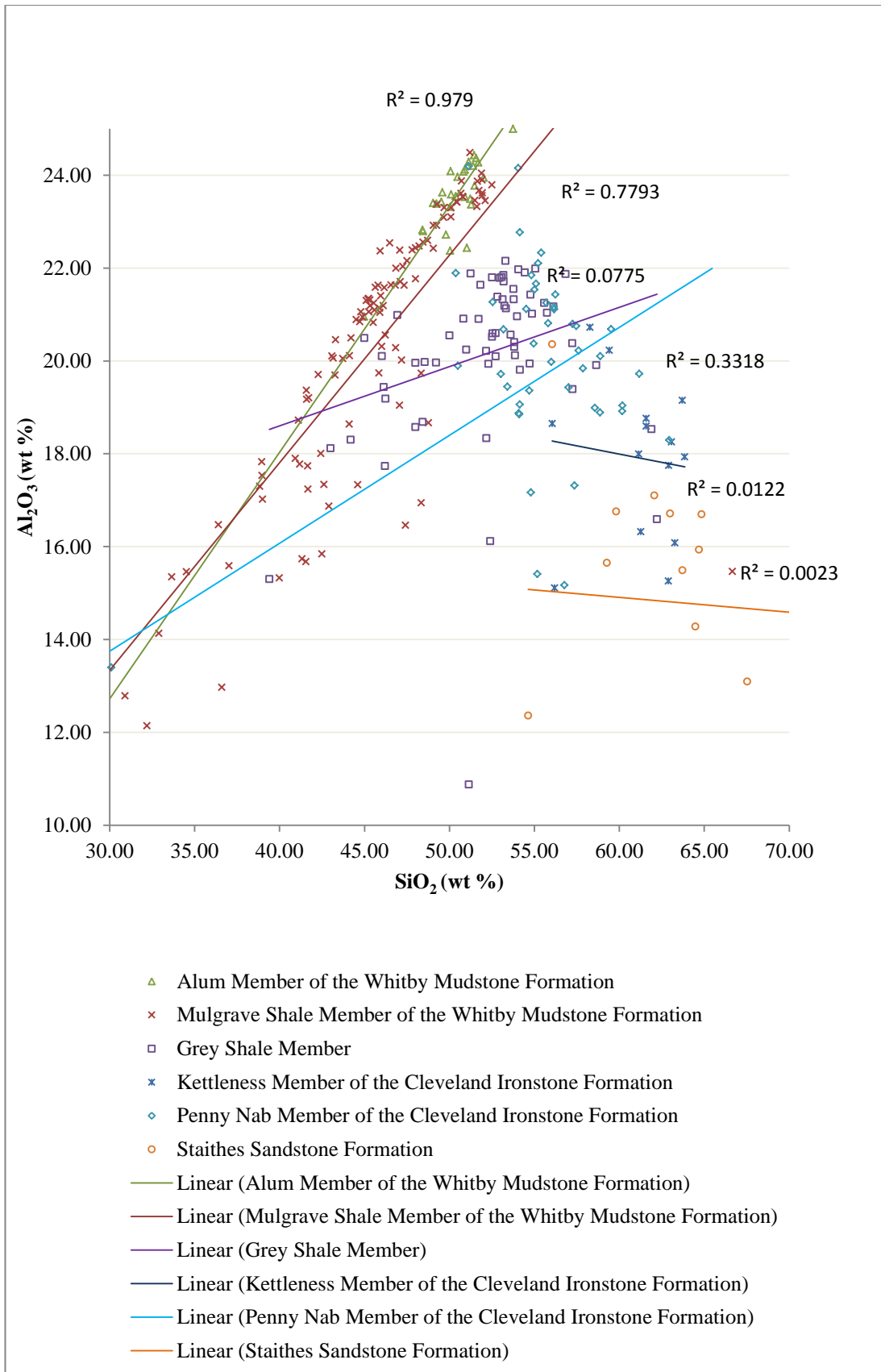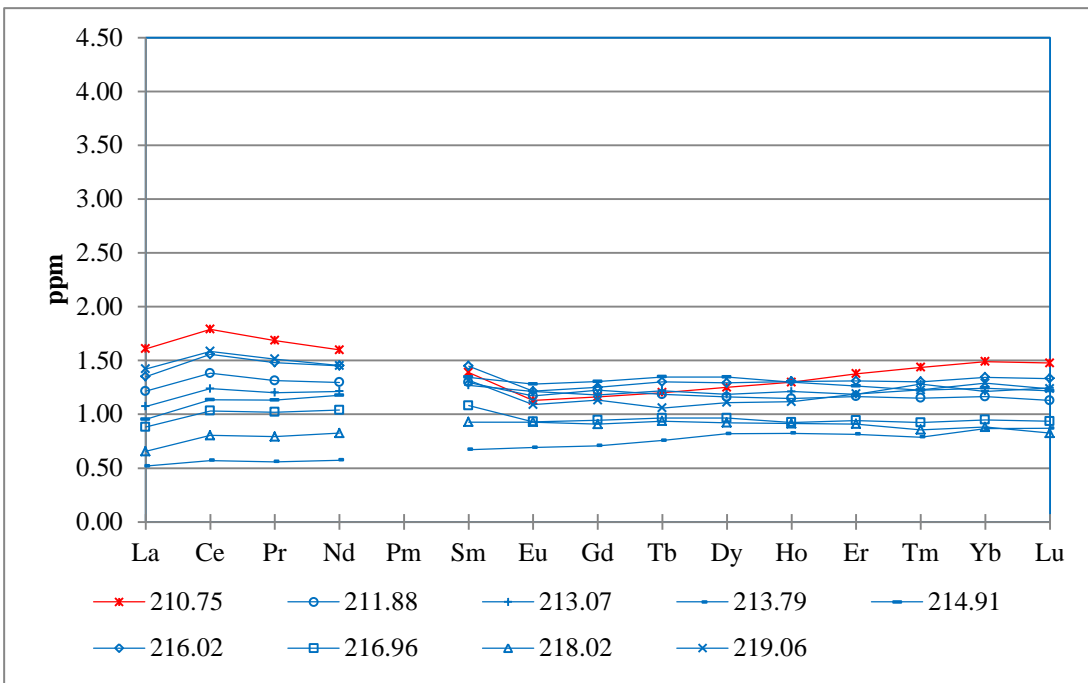
Figure 10. Rare earth element data plotted for the Staithes Sandstone Formation.

The sediment pore and bottom waters were oxygenated throughout the deposition of the Staithes Sandstone Formation as demonstrated by the low concentrations of redox sensitive trace metals (fig. 4, 5, and 6). Well oxygenated waters, dissolved nutrients that entered the basin with the sediment load, and an abundance of light (assumed due to the mid-latitude positioning of the basin) provided all the necessary components required for organic productivity. However, oxygen in the water facilitated the aerobic degradation of organic matter falling through the water column which is why it is not preserved. Fluvial siliciclastic material entering a basin serves as a diluent to the organic matter and thus reduces the concentration of organic matter within the sediment (Murphy et al., 2000); this, and the oxygenated state of the water, explains why, despite optimal conditions for organic productivity, TOC is low is the Staithes Sandstone Formation.

Cleveland Ironstone Formation

The Cleveland Basin received a variable amount of detrital material during the deposition of the Cleveland Ironstone Formation as shown in the Si/Al, Ti/Al, Zr/Al, and Cr/Al profiles (fig. 3). The Si in this formation is most likely related to the abundance of quartz entering the basin; the lack of biogenic material in the sediment rules out an organic source of the silica and the poor correlation between aluminium and silicon in the Penny Nab (R^2=0.3318) and Kettleness (R^2=0.0122) Members (fig. 9) suggests the silicon content is not related to clay mineral abundance.

One of the key controls on the source of the sediment deposited within an epicontinental sea basin is the distance to the shoreline. Rawson and Wright (1995) place the Cleveland Basin close (c. 30 km) to the nearest landmass; if this is correct, variations in continental weathering, resulting from fluctuations in the hydrological cycle, could have caused the input of fluvially-derived siliciclastic material to be cyclical. Bailey et al. (2003) use $\delta^{18}O$ to infer global temperature rise across the late Pliensbachian; this supports hypothesis that weathering was enhanced during the deposition of this formation. At this distance from the coast, the basin is in a proximal setting so sediment is more likely to have entered the basin straight from the continent, and thus be fluvially derived, than if the basin were further from the coast. The upper Pliensbachian of Yorkshire exhibits a general regressive trend thought to be a product of tectonic uplift (Powell, 2010); this supports Rawson and Wright's (1995) reconstruction.

The presence of ironstone bands supports the hypothesis that the basin was situated relatively close to the coast; high iron availability is associated with high detrital input (Brumsack, 2006). Powell (2010) suggests that lateritic soils provided the

source of the iron which was dissolved during periods of sea-level rise, and Rawson and Wright (1995) agree that the iron was probably 'leached from a low-lying, well-vegetated landmass experiencing a tropical climate'. Based on minimal evidence for a Pennine Landmass, Hallam (1966) concludes that the source of the iron is likely to be a Scandinavian river. However, Chowns (1966) counters Hallam's claim, using evidence of littoral facies, and argues in favour of an iron source entering the Cleveland basin through a river lying to the northwest that possibly passed over a Pennine High. Alternatively, the iron may be reworked and originate from elsewhere in the ocean as suggested by Borchert (1960) cited in Hallam (1966) but this model was regarded with much scepticism as it was based on hypothetical depth zones and chemical reactions in the ocean (Hallam, 1966).

Bradshaw et al. (1992) place the basin *c.* 220 km from the coast. Using this reconstruction, it seems unlikely that fluvial input would strongly affect the basin (as there is no evidence for a river large enough to exert this effect). However, if fluctuations in sea-level, which occurred throughout the Early Jurassic (Powell, 2010), are responsible for the cyclicity, through the reworking of shelf deposits, they can provide an alternative mechanism by which clastic material entered the basin.

The Cleveland Ironstone Formation comprises coarsening upwards parasequences of marine mud that are capped by bands of oölitic ironstones (Maquaker and Taylor, 1996). Traditionally, shales are interpreted as deep water facies, and coarser-grained sediments are interpreted as shallower water facies. By this logic, alternating beds of shale and ironstone bands are indicative of transgressive-regressive cycles and forms the basis of the palaeo-sea-level reconstructions. However, more recent work has shown that shales can be deposited in relatively shallow, energetically dynamic

environments; hence they do not have to be deposited in deep water environments (Trabucho-Alexandre et al., 2012). This questions the reliability of the use of lithological indicators to determine palaeo-sea-level and raises the question of which lithology is shallower; shale or ironstone.

I interpret the ironstone horizons to represent stratigraphic condensation during sea level high stands. The horizons are characterised by large positive peaks some elements (e.g. V, Cr, P, Na); these peaks probably formed when the redox interface was fixed. The redox interface, controlled by bacterial degradation-driven anoxia in the sediment pore and bottom waters, moves as sedimentation occurs. So when sedimentation is very low or ceases, for example due to changes in relative sea-level causing a temporary reduction of sediment supply to the basin, the redox interface is fixed allowing elements, remobilised from the anoxic sediment, to precipitate on contact with oxygen thus they concentrate on condensation surfaces.

The MREE depletion that is observed across the core (figs. 10, 11, 12, 13, 15, and 16) may be explained by their post-depositional remobilisation. Subsequent precipitation of the REEs at the redox interface, perhaps when the redox-cline is fixed at possible condensation surfaces during low rates of sedimentation associated with the ironstone bands, could account for the source of the MREE enrichment observed in the convex shaped plots (fig. 14 and 15).

The sediment pore waters in the Cleveland Basin were well oxygenated during the deposition of the Cleveland Ironstone Formation. This is shown by low concentrations in the redox sensitive trace metals (fig. 4, 5, and 6) and the reoccurrence of ironstone bands, which are interpreted to have been deposited under oxygenated waters. As in the Staithes Sandstone Formation, the conditions for

organic productivity were optimal but the majority of organic matter produced in the basin is likely to have been aerobically degraded or scavenged as it passed through the water column; therefore the low concentration of TOC is further indication that the water was oxygenated throughout the deposition of the Cleveland Ironstone Formation.
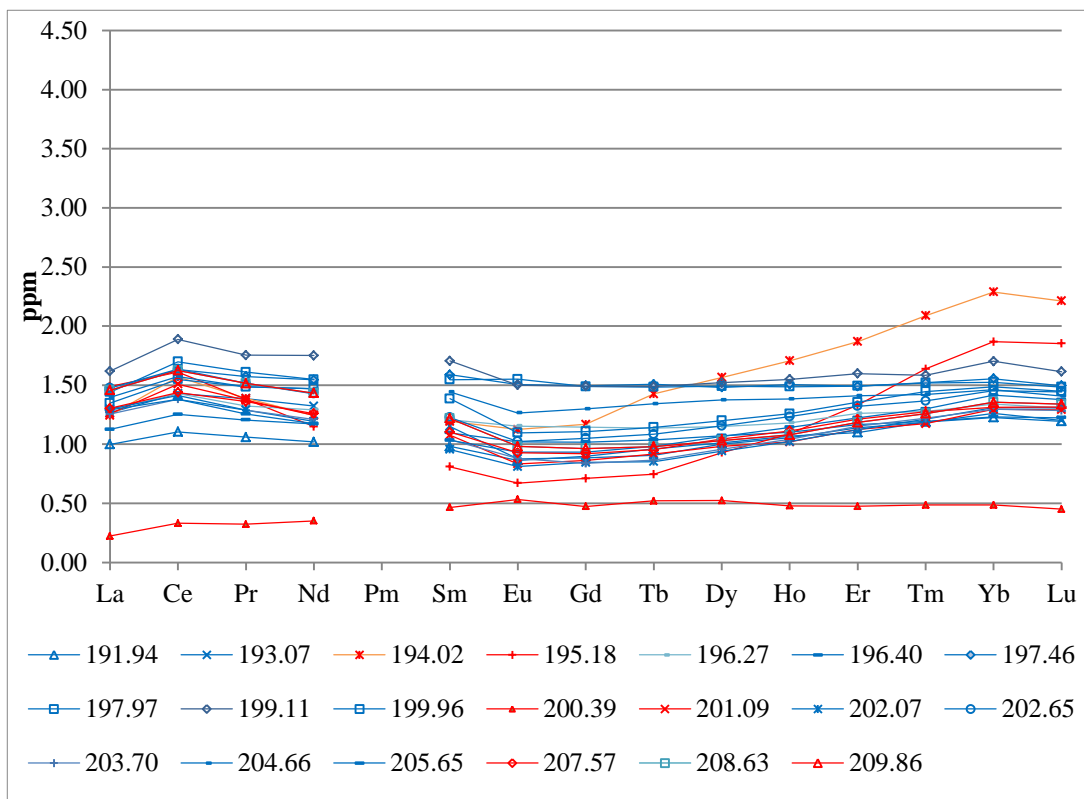
Figure 11. Rare earth element data plotted for the Penny Nab Member of the Cleveland Ironstone Formation.
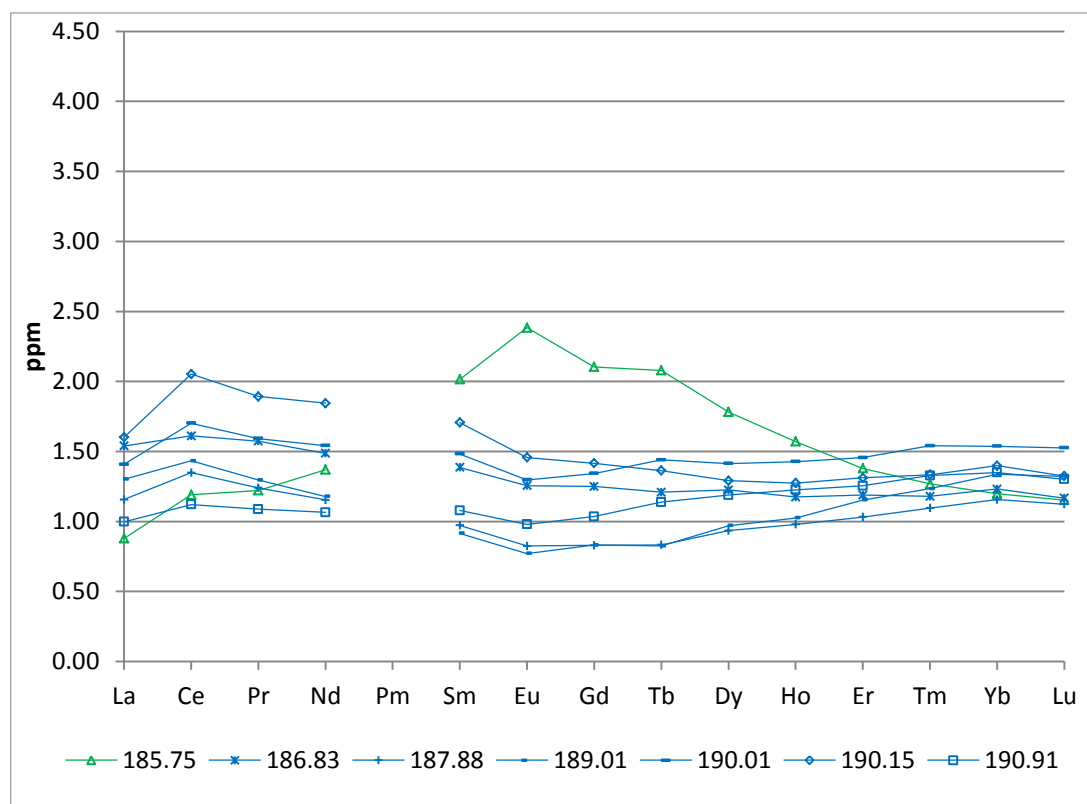
Figure 12. Rare earth element data plotted for the Kettleness Member of the Cleveland Ironstone Formation.

Whitby Mudstone Formation

Grey Shale Member

The Grey Shale Member was deposited during a transitional period from a depositional environment that received a fluctuating amount of continentally-derived clastic material to one that received little or no material directly from the continent. The Pliensbachian-Toarcian boundary marks the onset of a decline in siliciclastic material entering the basin through fluvial channels that continued to diminish throughout the deposition of the member, as shown by the detrital proxies (fig. 3).

The widely reported marine transgression that occurred throughout the Early Jurassic (Bradshaw et al., 1992; Hallam, 2001; Hardenbol, 1998; Powell, 2010) increased the distance between the nearest emerged landmass and the Cleveland Basin so the basin was in a more distal setting. Sediment entering the basin from the landmass had to travel farther so the volume of material that reached the basin decreased as relative sea-level rose. The mechanism by which sediment entering the sea gets trapped at the coast before it can reach basins further from the shore is known as clastic starvation (Murphy et al., 2000). Relative to the other units studied, the Grey Shale Member has less quartz than the stratigraphically lower formations and more quartz than the stratigraphically higher Mulgrave Shale and Alum Shale Members; this is shown by the correlations between silicon and aluminium for each unit (fig. 9). Because the profiles are less varied in this section relative to the three lowermost Formations, the REE data (fig. 10, 11, and 12) supports the hypothesis that the basin became progressively starved of clastic material derived straight from the continent.

The reworking of older sediments is a dominant process in environments that are sediment-starved (Trabucho-Alexandre, 2014). Relict sediment (derived from an earlier, different environment), that has been reworked, is referred to as palimpsest (Swift et al., 1971). I suggest that from the onset of clastic material shutoff, currents acted to transport to and rework relict sediment in the Cleveland Basin and that this is what the Grey Shale Member comprises. Dypvik and Brunfelt (1979) suggest that the processes of weathering and repeated reworking of sediment homogenises the REE across the sediment so all samples from a member deposited in the same environment will have similar plots regardless of the source of the sediment; this explains why sediment derived from different sources show similar REE plots. The homogeneity of the REE plots in figure 13 suggests the Grey Shale Member comprises of repeatedly reworked sediments and therefore supports the hypothesis that the nature of sediments deposited was palimpsest.
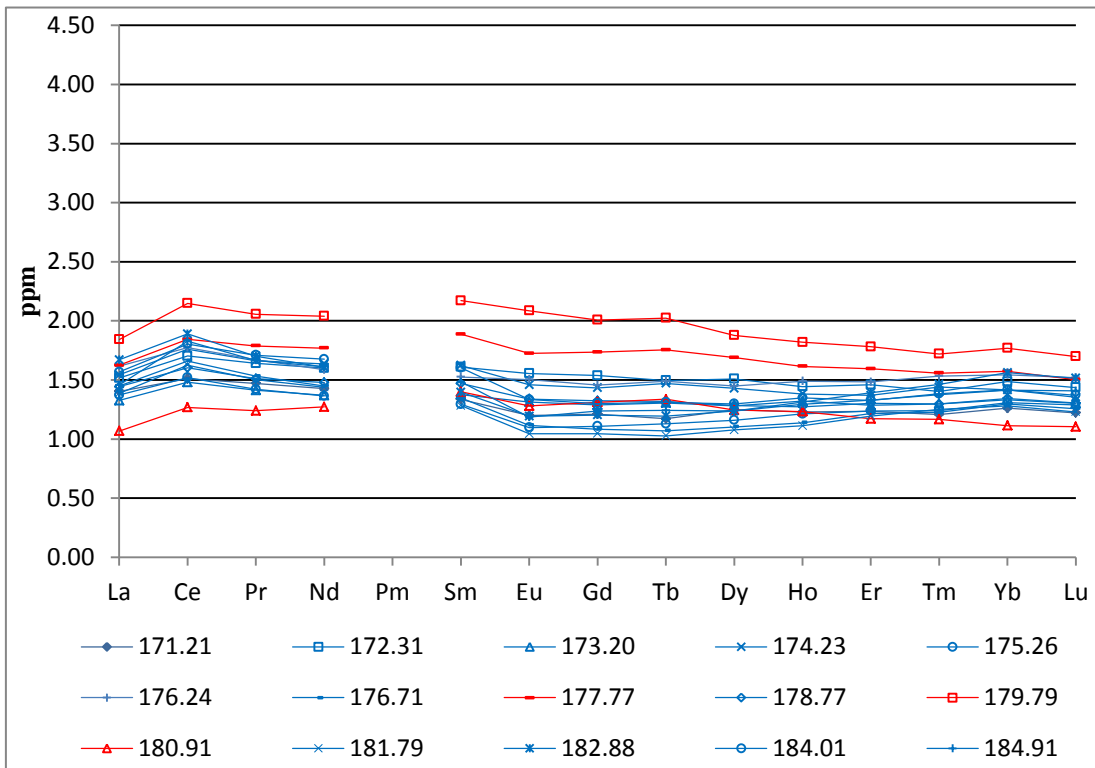
Figure 13. Rare earth element data plotted for the Grey Shale Member of the Whitby Mudstone Formation.

During the deposition of the lower half of the Grey Shale Member, the water was well oxygenated; this is shown by the low levels of transition metals and TOC (fig. 4, 5, and 6). At around 176 m, concentrations of redox sensitive metals, such as uranium, molybdenum, and iron, start to increase suggesting that sediment pore waters became anoxic; this enrichment coincides with the onset of TOC enrichment. The increase in preservation of TOC supports the hypothesis that oxygen was not freely available to degrade the organic material and thus indicates waters were anoxic.

The reduction in clastic material entering the basin reduced the dilution of organic matter so the relative proportion of organic matter preserved in the sediment expected to increase because other clastic material is no longer acting as a diluent. If the shutoff of fluvially-derived clastic material was entirely responsible for the TOC enrichment, the concentration of TOC would increase proportionally to the decline of fluvial material entering the basin. Figure 3, however, shows a lag between the clastic shutoff (Si/Al, Ti/Al, and Zr/Al) and TOC enrichment seen in the uppermost metres of the Grey Shale Member and there is no correlation between the detrital indicators and TOC, as shown in figure 14. I, therefore, suggest that while the starvation model reduced dilution of the organic material in the sediment, it cannot have been the only process responsible for the TOC enrichment.
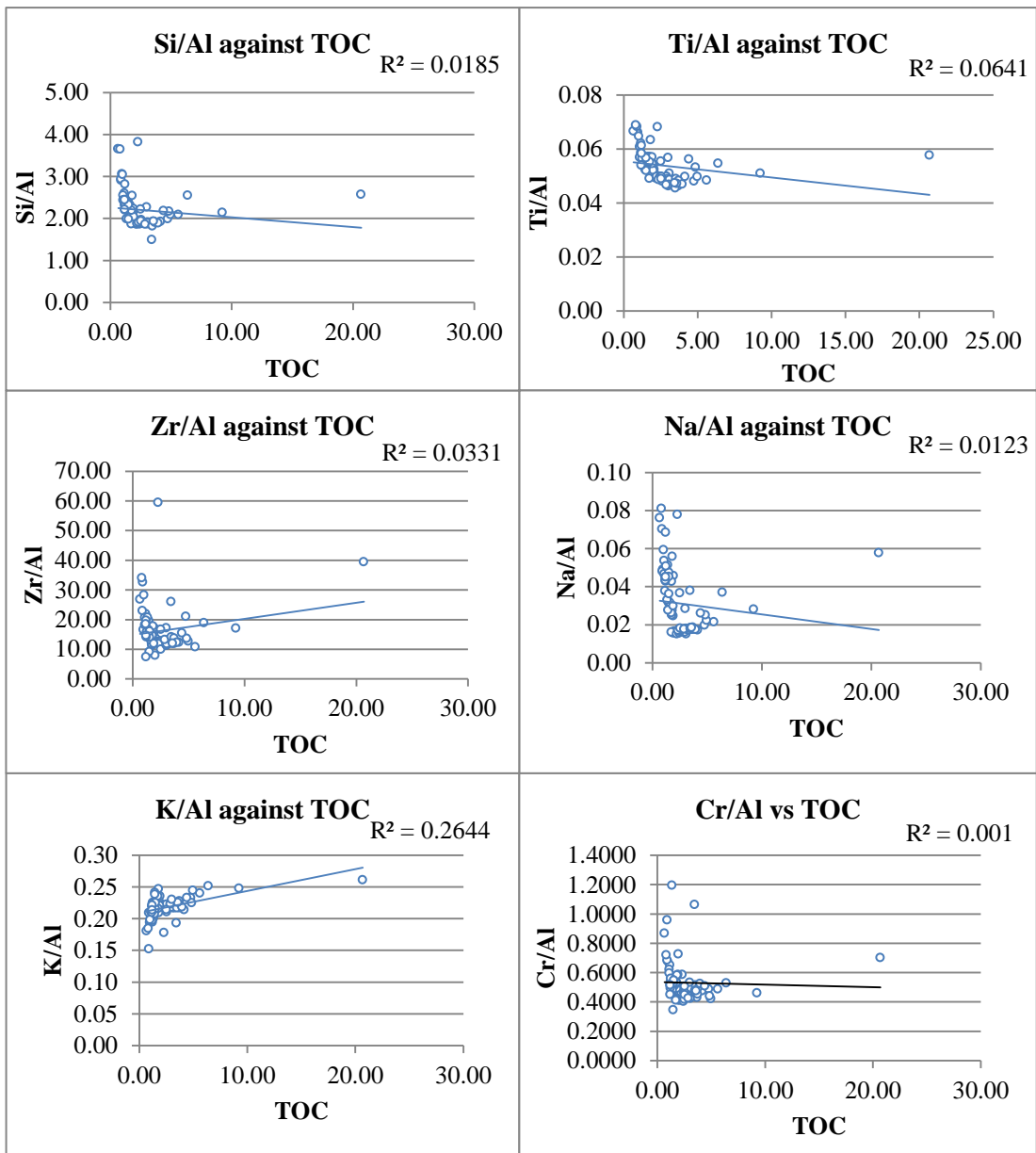
Figure 14. The detrital indicators (Al normalised Si, Ti, Zr, Na, K, and Cr) plotted against TOC (%).

I propose that, during the deposition of the Grey Shale Member, the transgression caused the supply of clastic material derived directly from the continent to be shutoff and led to a deeper, oxygen-stratified water column within the basin. Productivity remained high and worked to deplete oxygen in the newly stable water column; this established anoxia in the sediment pores and enhanced preservation.

An alternative hypothesis explaining the TOC enrichment is that organic productivity was raised and that the preserved TOC proportionally represents how much productivity there was. If nutrients entering the sea did not reach the now distal basin, because they were used up close to the shore (Murphy et al., 2000), upwelling may provide a source of nutrients required to sustain the elevated levels of productivity. On a basin scale, Arthur et al. (1987) proposes the formation saline waters that then sink and displace colder, nutrient-rich water could be a possible upwelling mechanism. On a global scale, general circulation models have reconstructed the convergence of the Hadley and Ferrel Cells over the Cleveland Basin in the Jurassic (Sellwood and Valdes, 2008). The cell convergence would have caused the surface waters to diverge and thus created space for upwelling water. However, applying palaeogeographical and palaeoenvironmental reconstructions to the Cleveland Basin during the Early Jurassic, the mechanism of upwelling cannot be used to explain the deposition of lower Toarcian sediments. The estimated water depths from the time of deposition do not exceed tens of meters (Powell, 2010); bottom waters at this depth are still in the photic zone suggesting they would be depleted in nutrients so would have negligible effect on organic productivity rates even if the waters were to rise. The Cleveland Basin was situated in the middle of an

epicontinental seaway (fig. 1); it is unclear how the connection between the warm Tethys and colder Boreal oceans affected the Cleveland Basin, and there are many aspects of the Toarcian atmosphere that have yet to be reconstructed. Until this is done, we have to make the big assumption that atmospheric circulation in the Jurassic was similar to that of today.

Mulgrave Shale Member

The hypothesis that the basin was progressively starved of continentally-derived clastic material is supported by evidence suggesting that the Cleveland Basin received little quartz during the deposition of the Mulgrave Shale Member. The detrital proxy profiles (fig. 3) show that the volume of coarse clastic material entering the basin continued to decline throughout the deposition of this unit (fig. 3) and the positive correlation (R^2=0.7793) (fig. 9) between silicon and aluminium (R^2=0.979) (fig. 9) shows there was significantly less quartz in the Mulgrave Shale Member than in the Grey Shale Member. The homogeneity of the REE, shown in figure 15, suggests the Mulgrave Shale Member consists of repeatedly reworked sediments (Dypvik and Brunfelt, 1979). Therefore, I propose the Mulgrave Shale Member comprises palimpsest sediment.
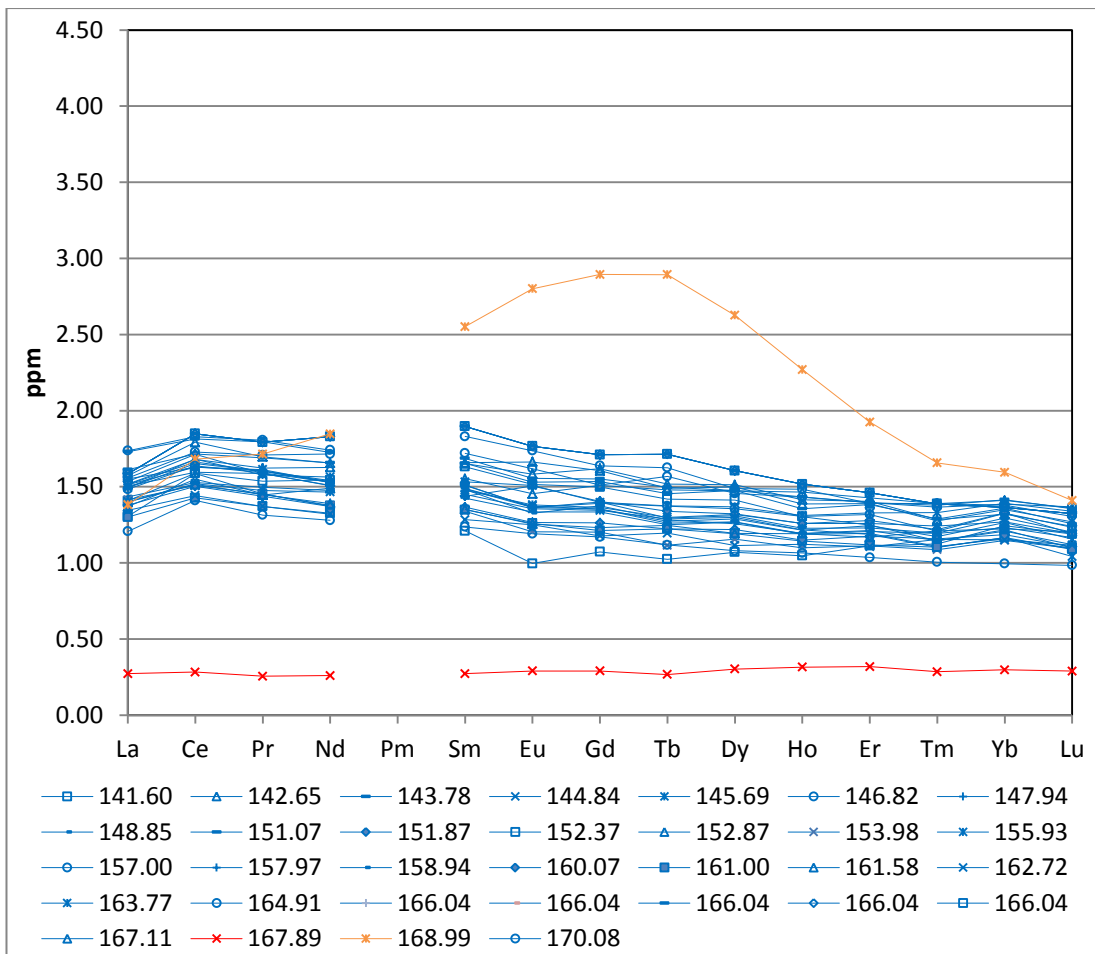
Figure 15. Rare earth element data plotted for the Mulgrave Shale Member of the Whitby Mudstone Formation.

At the beginning of the deposition of the Mulgrave Shale Member, the sediment pore waters were anoxic but, at c. 170.0 m, the waters became strongly sulphidic (euxinic); this is shown by the strong enrichments in molybdenum and uranium (fig. 4). However, it is difficult to determine the depth in the water column to which anoxia and euxinia reached based on the inorganic geochemistry alone. The transition from anoxic waters to euxinic waters suggests oxygen was absent from the water column for prolonged periods of time; this would have enhanced preservation of TOC so may explain the TOC enrichment recorded through the deposition of this member.

The preservation of molybdenum in marine sediment indicates anoxic waters with free H_2S in the water column but debate surrounds the interpretation of Mo enrichments. Erickson and Helz (2000) suggest the mechanism by which Mo is incorporated into the sediment is dependent upon the H_2S activity in the water column and has a slow rate of reaction; further to this Tribovillard et al. (2006) imply prolonged euxinic conditions are required for enrichment to occur. Using this mechanism for the incorporation of Mo in to sediments, I suggest long-term euxinia developed during the deposition of the Mulgrave Shale Member. However, Piper and Perkins (2004) demonstrated that the occurrence of euxinic waters was enough to concentrate Mo in the sediment and that euxinia didn't have to be sustained to generate Mo enrichments as had been earlier suggested. This means that extended periods of euxinic bottom waters, punctuated by oxic intervals, would lead to significant molybdenum enrichment. If this is the case, the Mulgrave Shale Member may have been deposited under predominantly euxinic, but periodically oxic waters.

An ichnological study of the core reveals that there is a dramatic drop in bioturbation at c. 174 m in the core (L. Herringshaw, 2014, pers. comm.) which coincides with onset of the molybdenum (fig. 4) and other trace metal (As, Sb, Se) (fig. 6) enrichment. Seasonal fluctuations in the depth of the redox boundary would have prevented colonisation of the sediments thus it supports the hypothesis that the bottom waters were, at least, periodically anoxic-euxinic.

It is important to consider how sedimentation rates affect the geochemical processes during deposition of a section to mitigate unrealistic interpretation. A rapid sedimentation rate would generate anoxic conditions in the sediment pore waters and thus enhance the preservation of organic material; this is possible during the

deposition of Mulgrave Shale Member assuming sedimentation rates were high. However, a hiatus in deposition would lead to precipitation and concentration of elements upon the condensed surface during the interval of little or no deposition. An example of this are the calcareous nodules in the Jet rock (the lower subdivision of the Mulgrave Shale Member) e.g. at 167.89 m; these nodules are a product of calcium diffusion across the sediment/water interface during a break in deposition (Trabucho-Alexandre, 2014) so it is likely that sedimentation rates were variable throughout the deposition of the Mulgrave Shale Member. It is difficult to constrain the accumulation rate of the studied units because sedimentation rates are likely to have varied and the stratigraphic record is incomplete as shown by the numerous erosional surface recorded in the Yorkshire section (Trabucho-Alexandre, 2014).

If the TOC enrichment is interpreted to indicate increased levels of organic productivity, a nutrient recycling mechanism may be invoked to explain the enhanced supply of nutrients required to raise productivity. Continental shelf waters less than 100 m deep are strongly influenced by storm and wind mixing (Tyson and Pearson, 1991) so can be used as an analogue to ancient epicontinental seas. Tyson and Pearson (1991) model, based on a continental shelf, suggests that in spring, solar insolation increased productivity in the surface waters by providing longer daylight hours, warmer waters, and increased nutrient input due to enhanced continental weathering. A reduction in wind and storm intensity, along with increased thermal buoyancy of the surface waters, associated with increased solar insolation, promoted thermal stratification by decreasing vertical mixing of the water column (assuming tidal stresses were low). The water column separated in to three distinct layers; the mixed layer, the thermo-halocline and the bottom waters. Higher levels of productivity in the surface waters promoted oxygen depletion in the bottoms waters.

Nutrient transfer across the thermo-halocline was reduced, if not stopped completely, preventing the replenishment of nutrients to the mixed surface layer and thus led to a decline in productivity. During autumn and winter, solar insolation and thermal stratification decreased while wind and storm mixing was re-established. Together, these factors led to the re-oxygenation of the bottom waters which led to the recycling of nutrients to the surface waters which then boosted productivity.

Murphy et al. (2000) adapted Ingall and Jahnke's (1997) positive anoxic feedback (PAF) model to present a hypothesis where short-term anoxia developed under a thermally stratified water column. Seasonal and storm-driven mixing of the water column cycled nitrogen and phosphorous back to surface waters, which boosted organic productivity. They propose organic productivity was nitrogen-limited due to inefficient recycling of nitrogen resulting from denitrification which occurred whilst bottom waters were anoxic. Phosphorous remained unutilised until nitrogen was reoxidised in the period between the anoxic intervals.

These two models can be combined to form a hypothesis to explain the TOC enrichment in the Mulgrave Shale Member if it resulted from raised levels of productivity. During periods of deposition when the water column was relatively undisturbed, organic matter, produced in the mixed surface layer of the water column, would have been preserved in the anoxic bottom waters. However, during seasonal or storm-driven wind mixing events, sediment deposited under anoxic waters came in to contact with oxygen; this could have remobilised nutrients from the sediment and cycled them back to the surface layers thus sustaining productivity. Nutrient recycling may also have occurred if the redoxcline sank due to low

productivity, which may have been caused by a lack of nutrients. However, I do not have the required data to constrain nutrient recycling within this setting.

At *c.* 166 m, the TOC (fig. 5) values decrease but remain enriched relative to the levels preserved in the lower section of the Grey Shale Member suggesting the production and/or preservation of organic material decreased but did not cease and the sediment-pore waters become more oxygenated. Above *c.* 166 m, the TOC remains slightly enriched relative to pre-excursion levels; this may be because the return to oxygenated waters was gradual so preservation of TOC was more favourable during the deposition of this sediment compared to during the deposition of the Staithes Sandstone and Cleveland Ironstone Formation.

The return to oxygenated conditions correlates with the regression reported to have occurred in the late early Toarcian (Hallam, 1981; Hardenbol, 1998) (fig 3). The regression increased the area of land exposed and thus moved the shoreline closer to the basin; this would have reduced the stability of the stratification of the water column and enabled the mixing of the water column. Organic matter would have been scavenged and degraded in the water column which explains why the concentration of TOC declines here.

The second suggestion is in a scenario where the mid-Toarcian regression (Hallam, 1981) reduced the distance between the coast and the basin thus shut off the clastic starvation mechanism. Sediments were still predominantly palimpsest.

Alum Shale Member

Redox conditions during the deposition of the studied section of the Alum Shale Member were similar to those during the deposition of the upper Mulgrave Shale

Member; waters were predominantly oxygenated but periods of anoxia may have occurred, inferred from the redox proxies (fig. 4, 5, and 6) and low TOC values.

The majority of the sedimentation is likely to have been of palimpsest sediments; the homogeneity of the REE supports this. However, the detrital indicators show a possible return of quartz entering directly from the continent (fig. 3). The regression would have placed the basin to be in a more proximal setting than it had been during the deposition of the Grey Shale and Mulgrave Shale Members. The reduced the distance between the basin and the coast may have worked to cancel the clastic starvation mechanism; this would have cause fluvial input directly from the continent to return to the basin.
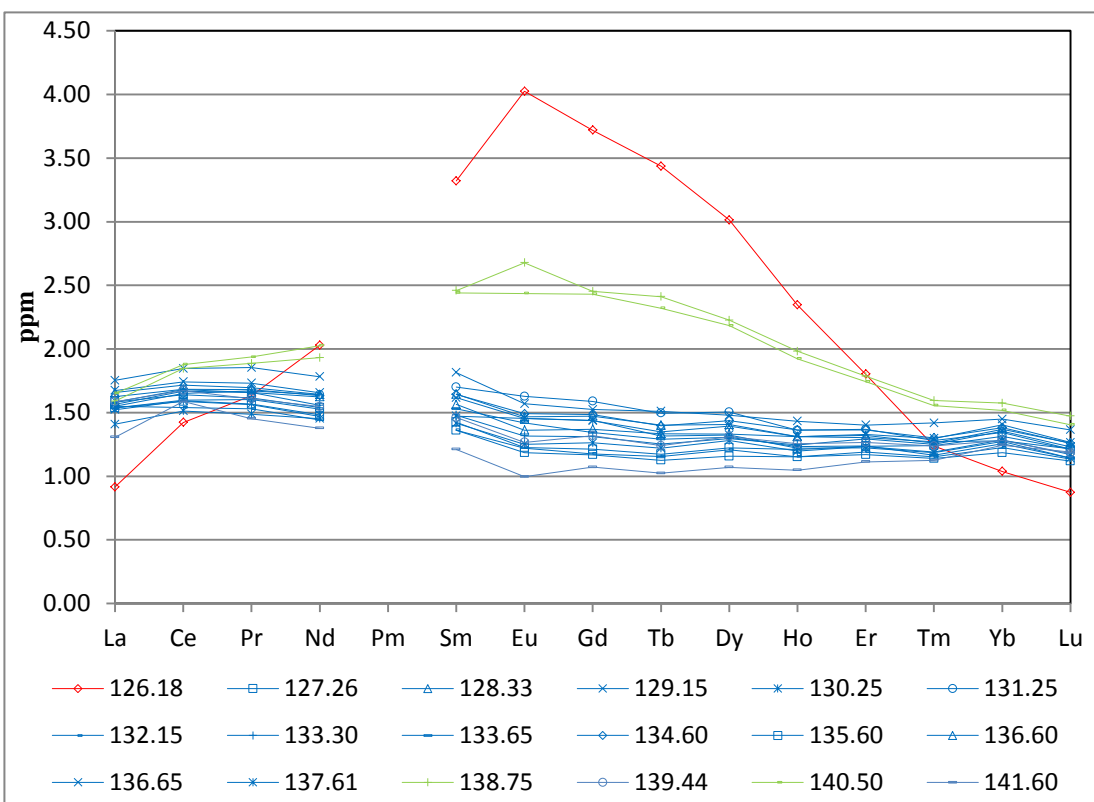
Figure 16. Rare earth element data plotted for the Alum Shale Member of the Whitby Mudstone Formation.

Conclusion

Figure 17 is a schematic diagram showing how the depositional environment of the Cleveland Basin changed through the late Pliensbachian through to the early Toarcian.

Detrital proxies show that the Cleveland Basin received a variable amount of siliciclastic material from a fluvial source during the deposition of the Staithes Sandstone Formation and suggest that the basin was in a proximal setting with a moderately high depositional energy.

During the deposition of the Cleveland Ironstone Formations, the supply of detrital material was variable. The variation observed in the influx of fluvially-derived siliciclastic material may be due to fluctuations in the hydrological cycle or, more likely, relative sea-level change. The fluvial source also transported nutrients to the basin which provided a substrate for the organisms in the photic zone. The conditions in the Cleveland Basin during the deposition of the Staithes Sandstone and Cleveland Ironstone Formations were probably the most favourable towards organic productivity compared to conditions during the deposition of the Whitby Mudstone Formation. However, the dilution of organic matter by clastic material and the aerobic degradation of organic matter in the water column led to little/no organic matter being preserved.

Around the Pliensbachian-Toarcian boundary, the Early Jurassic transgression led to the shutoff of the supply of siliciclastic material derived straight from the continent through fluvial sources by increasing the distance between the coast and the basin. This worked to reduce the effects of dilution of organic matter by other clastic

components and thus organic matter was concentrated in the sediment and is demonstrated by the TOC enrichment. From here, deposition was of palimpsest sediment.

The transgression promoted stratification of the water within the Cleveland Basin; this enabled sediment-pore and, potentially, bottom water anoxia, and eventually euxinia, to be established. It is not possible to determine whether the TOC enrichment, which coincides with the carbon isotope excursion, was caused by enhanced preservation due to the development of anoxia, or because of an increased level of palaeoproductivity. However, it is likely that both these processes played a role. Nutrient recycling involving the periodic mixing of the water column to sustain higher productivity is one possible hypothesis to explain the TOC enrichment but it is not possible to confirm this with this data alone.

The regression which took place in the late early Toarcian may have reduced the stratification of the water column and thus promoted mixing and re-oxygenation of sediment-pore and bottom waters. It may also have reintroduced fluvially derived sediment to the basin which would have been deposited in addition to palimpsest sediments.
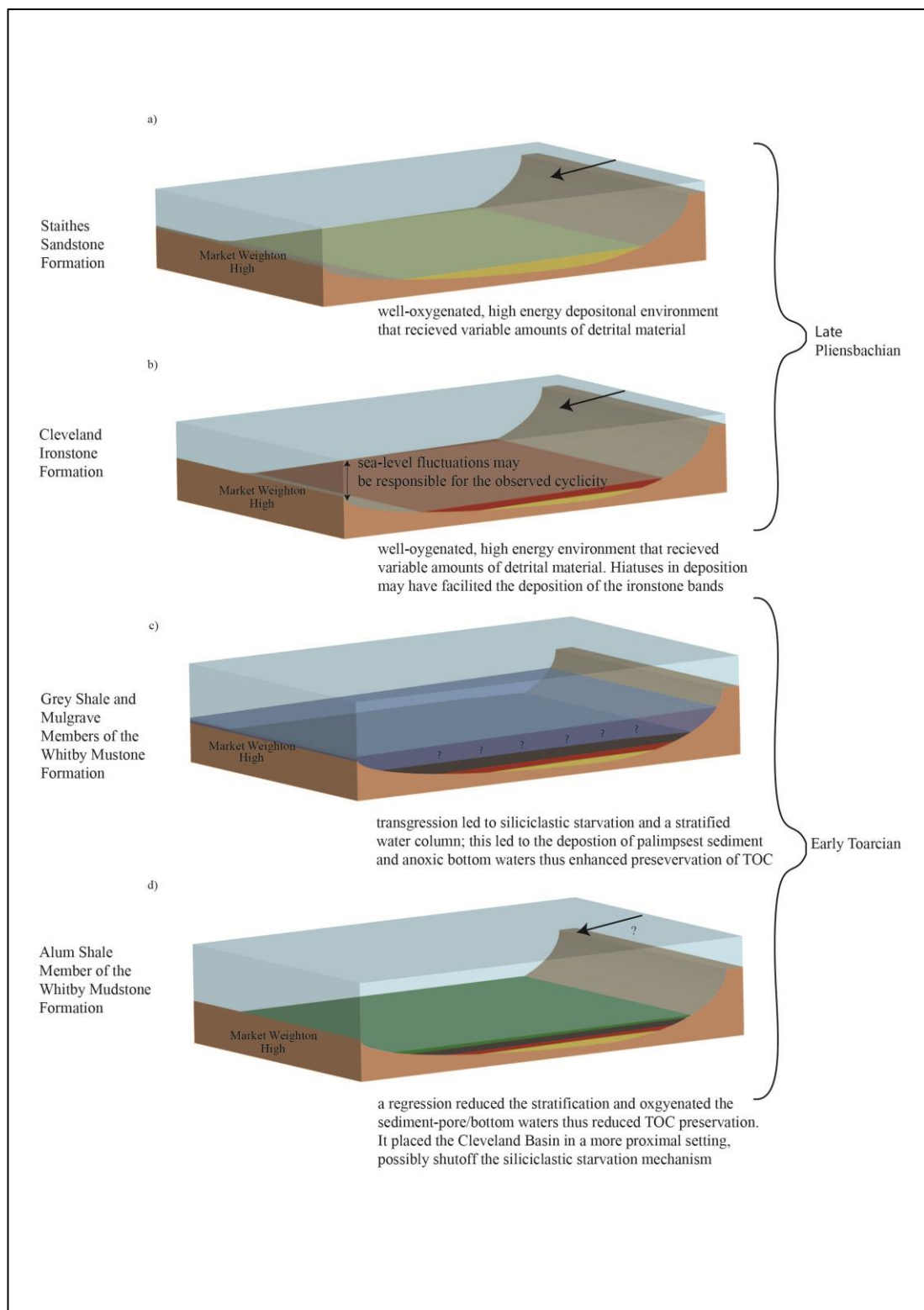
Figure 17. A schematic diagram showing how the depositional environment of the Cleveland Basin changed in the late Pliensbachian through to the early Toarcian. The black arrows indicate detrital input through fluvial channels.

References

Alexandre, J.T., Van Gilst, R.I., RodrÍGuez-LÓPez, J.P., De Boer, P.L., 2011. The sedimentary expression of oceanic anoxic event 1b in the North Atlantic. Sedimentology, 58(5): 1217-1246.

Arthur, M., Schlanger, S.t., Jenkyns, H., 1987. The Cenomanian-Turonian Oceanic Anoxic Event, II. Palaeoceanographic controls on organic-matter production and preservation. Geological Society, London, Special Publications, 26(1): 401-420.

Bailey, T.R., Rosenthal, Y., McArthur, J.M., van de Schootbrugge, B., Thirlwall, M.F., 2003. Paleoceanographic changes of the Late Pliensbachian–Early Toarcian interval: a possible link to the genesis of an Oceanic Anoxic Event. Earth and Planetary Science Letters, 212(3–4): 307-320.

Borchert, H., 1960. Genesis of marine sedimentary iron ores. na.

Bradshaw, M.J. et al., 1992. Jurassic. Geological Society, London, Memoirs, 13(1): 107-129.

Brumsack, H.-J., 1991. Inorganic geochemistry of the German 'Posidonia Shale': palaeoenvironmental consequences. Geological Society, London, Special Publications, 58(1): 353-362.

Brumsack, H.-J., 2006. The trace metal content of recent organic carbon-rich sediments: Implications for Cretaceous black shale formation. Palaeogeography, Palaeoclimatology, Palaeoecology, 232(2–4): 344-361.

Calvert, S., Pedersen, T., 2007. Chapter fourteen elemental proxies for palaeoclimatic and palaeoceanographic variability in marine sediments: interpretation and application. Developments in Marine Geology, 1: 567-644.

Calvert, S.E., Pedersen, T.F., 1993. Geochemistry of Recent oxic and anoxic marine sediments: Implications for the geological record. Marine Geology, 113(1–2): 67-88.

Caruthers, A.H., Gröcke, D.R., Smith, P.L., 2011. The significance of an Early Jurassic (Toarcian) carbon-isotope excursion in Haida Gwaii (Queen Charlotte Islands), British Columbia, Canada. Earth and Planetary Science Letters, 307(1–2): 19-26.

Chowns, T., 1966. Depositional environment of the Cleveland Ironstone series. Nature, 211: 1286-1287.

Dellwig, O., Hinrichs, J., Hild, A., Brumsack, H.J., 2000. Changing sedimentation in tidal flat sediments of the southern North Sea from the Holocene to the present: a geochemical approach. Journal of Sea Research, 44(3–4): 195-208.

Des Combes, H.J., Caulet, J.-P., Tribovillard, N.P., 1999. Pelagic productivity changes in the equatorial area of the northwest Indian Ocean during the last 400,000 years. Marine Geology, 158(1–4): 27-55.

Dypvik, H., Brunfelt, A.O., 1979. Distribution of rare earth elements in some North Atlantic Kimmeridgian black shales.

Erickson, B.E., Helz, G.R., 2000. Molybdenum(VI) speciation in sulfidic waters:: Stability and lability of thiomolybdates. Geochimica et Cosmochimica Acta, 64(7): 1149-1158.

Farrimond, P., Eglinton, G., Brassell, S.C., Jenkyns, H.C., 1989. Toarcian anoxic event in Europe: An organic geochemical study. Marine and Petroleum Geology, 6(2): 136-147.

Hallam, A., 1966. Depositional environment of British Liassic ironstones considered in the context of their facies relationships. Nature, 209: 1306-1309.

Hallam, A., 1981. A revised sea-level curve for the early Jurassic. Journal of the Geological Society, 138(6): 735-743.

Hallam, A., 2001. A review of the broad pattern of Jurassic sea-level changes and their possible causes in the light of current knowledge. Palaeogeography, Palaeoclimatology, Palaeoecology, 167(1–2): 23-37.

Hardenbol, J., 1998. Mesozoic and Cenozoic sequence chronostratigraphic framework of European basins.

Hesselbo, S.P. et al., 2000. Massive dissociation of gas hydrate during a Jurassic oceanic anoxic event. Nature, 406: 392-395.

Hetzel, A., Böttcher, M.E., Wortmann, U.G., Brumsack, H.-J., 2009. Paleo-redox conditions during OAE 2 reflected in Demerara Rise sediment geochemistry (ODP Leg 207). Palaeogeography, Palaeoclimatology, Palaeoecology, 273(3–4): 302-328.

Ingall, E., Jahnke, R., 1997. Influence of water-column anoxia on the elemental fractionation of carbon and phosphorus during sediment diagenesis. Marine Geology, 139(1–4): 219-229.

Jenkyns, H.C., 1988. The early Toarcian (Jurassic) anoxic event; stratigraphic, sedimentary and geochemical evidence. American Journal of Science, 288(2): 101-151.

Jones, B., Manning, D.A.C., 1994. Comparison of geochemical indices used for the interpretation of palaeoredox conditions in ancient mudstones. Chemical Geology, 111(1–4): 111-129.

Kafousia, N., Karakitsios, V., Jenkyns, H.C., Mattioli, E., 2011. A global event with a regional character: the Early Toarcian Oceanic Anoxic Event in the Pindos

Ocean (northern Peloponnese, Greece). Geological Magazine, 148(04): 619-631.

Kauffman, E.G., 1979. Benthic environments and paleoecology of the Posidonienschiefer (Toarcian). Neues Jahrbuch fuer Geologie und Palaeontologie Abhandlungen, 157(1-2): 18-36.

Lezin, C. et al., 2013. Geochemical disturbance and paleoenvironmental changes during the Early Toarcian in NW Europe. Chemical Geology, 341: 1-15.

Macquaker, J.H.S., Taylor, K.G., Young, T.P., Curtis, C.D., 1996. Sedimentological and geochemical controls on ooidal ironstone and 'bone-bed' formation and some comments on their sequence-stratigraphical significance. Geological Society, London, Special Publications, 103(1): 97-107.

Murphy, A.E., Sageman, B.B., Hollander, D.J., Lyons, T.W., Brett, C.E., 2000. Black shale deposition and faunal overturn in the Devonian Appalachian Basin: Clastic starvation, seasonal water-column mixing, and efficient biolimiting nutrient recycling. Paleoceanography, 15(3): 280-291.

Pálfy, J., Smith, P.L., 2000. Synchrony between Early Jurassic extinction, oceanic anoxic event, and the Karoo-Ferrar flood basalt volcanism. Geology, 28(8): 747-750.

Pedersen, T., Calvert, S., 1990. Anoxia vs. Productivity: What Controls the Formation of Organic-Carbon-Rich Sediments and Sedimentary Rocks?(1). AAPG Bulletin, 74(4): 454-466.

Piper, D.Z., Perkins, R.B., 2004. A modern vs. Permian black shale—the hydrography, primary productivity, and water-column chemistry of deposition. Chemical Geology, 206(3–4): 177-197.

Powell, J., 2010. Jurassic sedimentation in the Cleveland Basin: a review. Proceedings of the Yorkshire Geological Society, 58(1): 21-72.

Rawson, P.F., Wright, J.K., 1995. Jurassic of the Cleveland Basin, North Yorkshire. Geological Society, London(173-208).

Röhl, H.-J., Schmid-Röhl, A., Oschmann, W., Frimmel, A., Schwark, L., 2001. The Posidonia Shale (Lower Toarcian) of SW-Germany: an oxygen-depleted ecosystem controlled by sea level and palaeoclimate. Palaeogeography, Palaeoclimatology, Palaeoecology, 165(1–2): 27-52.

Rohl, H.J., Schmid-Rohl, A., Oschmann, W., Frimmel, A., Schwark, L., 2001. The Posidonia Shale (Lower Toarcian) of SW-Germany: an oxygen-depleted ecosystem controlled by sea level and palaeoclimate (vol 165, pg 27, 2001). Palaeogeography Palaeoclimatology Palaeoecology, 169(3-4): 271-+.

Schlanger, S., Jenkyns, H., 1976. Cretaceous oceanic anoxic events: causes and consequences. Geologie en mijnbouw, 55(3-4): 179-184.

Schwark, L., Frimmel, A., 2004. Chemostratigraphy of the Posidonia Black Shale, SW-Germany: II. Assessment of extent and persistence of photic-zone anoxia using aryl isoprenoid distributions. Chemical Geology, 206(3–4): 231-248.

Sellwood, B.W., Valdes, P.J., 2008. Jurassic climates. Proceedings of the Geologists' Association, 119(1): 5-17.

Simms, M.J., Chidlaw, N., Morton, N., Page, K.N., 2004. British Lower Jurassic Stratigraphy C1P1. Geological Conservation Review Series, Peterborough.

Song, J., Littke, R., Maquil, R., Weniger, P., 2014. Organic facies variability in the Posidonia Black Shale from Luxembourg: Implications for thermal maturation and depositional environment. Palaeogeography, Palaeoclimatology, Palaeoecology, 410(0): 316-336.

Suan, G. et al., 2008. Duration of the Early Toarcian carbon isotope excursion deduced from spectral analysis: Consequence for its possible causes. Earth and Planetary Science Letters, 267(3–4): 666-679.

Svensen, H. et al., 2007. Hydrothermal venting of greenhouse gases triggering Early Jurassic global warming. Earth and Planetary Science Letters, 256(3–4): 554-566.

Swift, D.J.P., Stanley, D.J., Curray, J.R., 1971. Relict Sediments on Continental Shelves: A Reconsideration. The Journal of Geology, 79(3): 322-346.

Trabucho-Alexandre, J., 2014. More gaps than shale: erosion of mud and its effect on preserved geochemical and palaeobiological signals. Geological Society, London, Special Publications, 404.

Trabucho-Alexandre, J., Dirkx, R., Veld, H., Klaver, G., de Boer, P.L., 2012. Toarcian Black Shales In the Dutch Central Graben: Record of Energetic, Variable Depositional Conditions During An Oceanic Anoxic Event. Journal of Sedimentary Research, 82(2): 104-120.

Tribovillard, N.-P. et al., 1994. Geochemical study of organic-matter rich cycles from the Kimmeridge Clay Formation of Yorkshire (UK): productivity versus anoxia. Palaeogeography, Palaeoclimatology, Palaeoecology, 108(1–2): 165-181.

Tribovillard, N., Algeo, T.J., Lyons, T., Riboulleau, A., 2006. Trace metals as paleoredox and paleoproductivity proxies: An update. Chemical Geology, 232(1-2): 12-32.

Tyson, R.V., 2001. Sedimentation rate, dilution, preservation and total organic carbon: some results of a modelling study. Organic Geochemistry, 32(2): 333-339.

Tyson, R.V., 2005. The "Productivity versus Preservation" controversy: Cause, Flaws and Resolution. Sedimentary Geology.

Tyson, R.V., Pearson, T.H., 1991. Modern and ancient continental shelf anoxia: an overview. Geological Society, London, Special Publications, 58(1): 1-24.

Van der Weijden, C.H., 2002. Pitfalls of normalization of marine geochemical data using a common divisor. Marine Geology, 184(3–4): 167-187.

Appendix A – Methodology

Sample crushing and powdering

Samples were crushed using a mallet and then ground to a fine powder using a Retsch RM100 Agate Mill in the geochemistry lab at Durham University. The powder is stored in glass vials. Acetone and tissues were used to clean the machine and utensils between each sample to prevent contamination.

Inductively coupled plasma – atomic emissions spectrometry (ICP – AES)

Analysis was carried out by a Join Yvon JY70 Plus ICP –AES at Kingston University London to determine the major- (Si, Ti, Al, Fe, Mn, Mg, Ca, Na, P) and minor- (Ba, Cr, Sr, Zr) elements within each sample. The samples and reference materials were prepared in lithium metaborate fusions prior to being run on the ICP – AES. Data are reported as weight percent oxides for the major elements and as $\mu g/g$ (parts per million) for the trace elements. The bulk of the Ca present is found in the carbonate fraction so the calcium data are given as $CaCO_3$.

Lithium Metaborate Fusion Preparation

All samples in the high resolution sample set were dried overnight at 105°c in glass vials. 0.25 g ($\pm$ 0.005 g) of sample and 1.250 g ($\pm$ 0.005 g) of lithium metaborate powder was weighed out using METTLER AE200 weighing scales and mixed in a plastic weighing boat. The mixtures were transferred in to graphite crucibles and fused in the furnace at 1050°c for one hour. The fused melts were placed in to beakers containing 150 mL of 0.5 M nitric acid (HNO_3) (made from *Nitric Acid PrimarPlus – Trace Analysis Grade*) and stirred continuously for 30 minutes until all the sample had dissolved. The solutions were filtered through *Watman Number 41*

filter papers into clean 250 mL grade A volumetric flasks to ensure all the carbon from the graphite crucibles was removed.

> 18.2 MΩ $^{cm-3}$ deionised water was used to rinse the filter paper and make the solutions up to 250 mL of 0.3 M HNO_3. The solutions were labelled and stored in centrifuge tubes until analysis. The final dilution factor was 1:1000 and the solutions were analysed by ICP – AES without further dilution.

ICP – AES operating conditions, analytical protocol and processing

The samples were run on the 'Chalks 3' method and the ICP – AES was calibrated before each run using the in-house Chalk reference materials: the BHD series. The reference material W-2 (diorite) was run every 5 samples to monitor the drift of the machine. The results were corrected according to the variations in drift using in-house software.

A suite of six standard rock reference materials was chosen based on the expected compositions of the samples. They were prepared in lithium metaborate fusions and run at the beginning and end of each run. The reference materials used were AGV-2 (andesite), SCo-1 (shale), JLS-1 (Limestone), CCH-1 (calcareous shale), SGR-1 (shale) and MAG-1 (marine mud) (Jochum et al. 2005). The drift corrected results were compared to these reference materials and corrections were made for each element in each sample if required, using in-house software.

The samples were run two or three times, in a randomised order, depending on the stability of the machine. The mean of the corrected values for each sample was calculated and is used as the final value for each sample.

Due to the large number of samples, they had to be run over five days. Five 'cross-over' samples, which have a wide range of compositions, were chosen and run on each day. This was done to identify any offset between the runs on different days.

Inductively Coupled Plasma – Mass Spectrometry (ICP – MS)

ICP – MS was carried out at Kinston University London to determine the trace element (Sc, V, Cr, Mn, Co, Ni, Cu, Zn, Ga, Rb, Sr, Nb, Mo, Cs, Ba, Y, Zr, Hf, Ta, Th, U) and rare earth element concentrations (La, Ce, Pr, Nd, Sm, Eu, Gd, Tb, Dy, Ho, Er, Tm, Yb, Lu) of the pilot sample set. The samples and reference materials were prepared in both lithium metaborate fusions (see section 1.3.4) and aqua regia leach digestions. The lithium metaborate preparations were analysed for all of the aforementioned elements. The aqua regia leach preparations were analysed for the elements which were unreliable in the lithium metaborate preparations (V, Mn, Co, Ni, Cu, Zn, As, Se, Mo, Cd, Sb).

Aqua Regia Leach Preparation

0.25 g (± 0.005 g) of sample and 6 mL of aqua regia solution (3:1 HCl:HNO3) (HCl Trace Metal Grade) was heated on a hotplate at 100°c in glass beakers for 45 minutes. The solutions were then evaporated to dryness at 200°c. 1.25 mL of ultrapure hydrogen peroxide (H_2O_2) and 1.25 mL of concentrated HNO_3 was added to the residue. After a few minutes, the solution was filtered through Watman 41 filter paper and made up to 50 mL with > 18.2 MΩ $^{cm-3}$ deionised water. The final solutions had a dilution factor of 1:200 and were stored in 50 mL centrifuge tubes. Method adapted from Moor et al. (2001).

ICP – MS operating conditions, analytical protocol and processing

The ICP – MS was calibrated before the start of each run using standard calibration standards in concentrations of 0, 2, 5, 10, 20 and 50 ppb. The reference materials used were SCo-1 (shale), JLS-1 (Limestone), SGR-1 (shale), MAG-1 (marine mud) and W-2 (diorite) (Jochum et al. 2005).

The 10 ppb standard was run every 5 samples as a drift monitor. Corrections for drift were made accordingly using in-house software.

The lithium metaborate samples were run on the 'LiMB II' method and were diluted to 1:25000. The solutions were diluted with 0.5% HCL and 1% HNO_3 diluent immediately prior to being run and the machine was washed out with the diluent between every sample.

The aqua regia solutions were run the 'LiMB I' method. The solutions were diluted to a factor of 1:10000 with 0.5% HCL and 1% HNO_3 diluent immediately prior to being run and the machine was washed out with the diluent between every sample.

The samples were run across multiple days due to the large number of samples. Five 'cross-over' samples, which had a wide range of compositions, were chosen and run on each day. This was done to identify any offset between the runs on different days.

Appendix B – Major oxide reference material data

Major Oxides (wt %)	AGV-2	CCH-1	JLS-1	MAG-1	SCO-1	SGR-1
SiO2	59.30	0.97	0.12	50.36	62.80	28.20
TiO2	1.05	0.02	0.00	0.75	0.63	0.25
Al2O3	16.91	0.30	0.02	16.37	13.70	6.52
Fe2O3	6.69	0.17	0.02	6.80	5.13	3.03
MnO	0.10	0.01	0.00	0.10	0.05	0.03
MgO	1.79	2.91	0.61	3.00	2.72	4.44
CaO	5.20	52.12	55.09	1.37	2.62	8.38
Na2O	4.19	0.05	0.00	3.83	0.90	2.99
K2O	2.88	0.08	0.00	3.55	2.77	1.66
P2O5	0.48	0.05	0.03	0.16	0.21	0.33
CaCO3	9.28	93.02	98.32	2.45	4.68	14.96
Total	102.67	97.58	99.12	87.37	93.59	62.41

Appendix C – Trace element reference material data

Element (ppm)	AGV-2	CCH-1	JLS-1	MAG-1	SCO-1	SGR-1	W-2
Sc			0.03	17.00	11.00	4.60	36.00
V			3.59	140.00	130.00	130.00	260.00
Cr	17.00	7.40	3.37	97.00	68.00	30.00	92.00
Mn			16.20	760.00	410.00	267.00	1290.00
Co			0.08	20.00	11.00	12.00	43.00
Ni			0.36	53.00	27.00	29.00	70.00
Cu			0.27	30.00	29.00	66.00	110.00
Zn			3.19	130.00	100.00	74.00	80.00
Ga				20.00	15.00	12.00	3.30
As			0.15	9.20	12.00	67.00	
Se				1.16	0.89	3.50	
Rb			0.18	150.00	100.00	83.00	21.00
Sr	658.00	284.00	295.00	146.00	170.00	420.00	190.00
Y			0.22	28.00	26.00	13.00	23.00
Zr	230.00	8.00	4.19	126.00	160.00	53.00	
Nb			1.00	12.00	11.00	5.20	7.90
Mo				1.60	1.40	35.00	0.70
Cd			0.16	0.20	0.20	0.93	
Sb			0.02	0.96	0.96	3.40	
Cs			0.02	8.60	7.80	5.20	0.99
Ba	1140.00	6.60	476.00	480.00	570.00	290.00	170.00
Hf			0.13	3.70	4.44	1.40	2.60
Ta			0.01	1.10	0.91	0.42	0.50
La			0.15	43.00	30.00	20.00	10.00
Ce			0.52	88.00	62.00	36.00	23.00
Pr			0.03	9.30	6.60	3.90	1.30
Nd			0.14	38.00	26.00	16.00	13.00
Sm			0.14	7.50	4.84	2.70	3.30
Eu			0.01	1.60	1.18	0.20	1.00
Gd			0.03	5.80	4.58	2.00	3.60
Tb			0.00	0.96	0.67	0.36	0.63
Dy			0.03	5.20	3.82	1.90	3.60
Ho				1.00	0.78	0.40	0.76
Er				3.00	2.50	1.10	2.50
Tm				0.43	0.32	0.17	0.38
Yb			0.02	2.60	2.03	0.94	2.10
Lu			0.02	0.40	0.34	0.14	0.33
Th			0.03	12.00	9.70	4.80	2.40
U			1.75	2.70	2.94	5.40	0.53

Appendix D – Exemplar ICP-AES detection limits

Element	Detection Limit (ppm)	Determination limit (ppm)
45 Sc	0.0297	2.4726
51 V	0.0542	4.5178
52 Cr	0.0237	1.9742
55 Mn	0.0257	2.1419
59 Co	0.0054	0.4504
60 Ni	0.0878	7.3170
63 Cu	0.2959	24.6615
65 Cu	0.2889	24.0788
66 Zn	1.0512	87.5962
69 Ga	0.0038	0.3176
71 Ga	0.0055	0.4605
85 Rb	0.0086	0.7191
88 Sr	0.0083	0.6884
93 Nb	0.5163	43.0229
95 Mo	1.1477	95.6406
133 Cs	0.0253	2.1070
137 Ba	0.0109	0.9094

Appendix E – Exemplar ICP-AES data accuracy

	SiO$_2$	TiO$_2$	Al$_2$O$_3$	Fe$_2$O$_3$	MnO	MgO	CaO
Reference							
AGV-2	59.30	1.05	16.91	6.69	0.10	1.79	5.20
CCH-1	0.97	0.02	0.30	0.17	0.01	2.91	52.12
JLS-1	0.12	0.00	0.02	0.02	0.00	0.61	55.09
MAG-1	50.36	0.75	16.37	6.80	0.10	3.00	1.37
SCO-1	62.80	0.63	13.70	5.13	0.05	2.72	2.62
SGR-1	28.20	0.25	6.52	3.03	0.03	4.44	8.38
Values measured							
AGV-2	57.4	1.0	16.4	6.5	0.1	1.7	5.0
CCH-1	1.3	0.0	0.4	0.2	0.0	2.8	50.2
JLS-1	0.3	0.0	0.1	0.0	0.0	0.7	52.4
MAG-1	51.2	0.7	16.3	7.0	0.1	3.0	1.7
SCO-1	63.1	0.6	13.7	5.2	0.1	2.7	3.0
SGR-1	27.5	0.2	6.4	2.9	0.0	4.3	8.1
% offset							
AGV-2	3.1	6.4	3.3	3.5	0.9	4.0	3.8
CCH-1	-37.6	-34.3	-27.5	-18.8	-1.3	4.0	3.7
JLS-1	-180.8	-200.5	-274.6	-189.1	-96.9	-12.9	4.9
MAG-1	-1.6	5.4	0.2	-3.1	-5.8	-0.8	-20.8
SCO-1	-0.5	6.5	0.0	-1.1	-2.9	-0.3	-14.8
SGR-1	2.3	6.2	2.4	3.2	0.7	4.0	2.9
	Na$_2$O	**K$_2$O**	**P$_2$O$_5$**	**Ba**	**Cr**	**Sr**	**Zr**
Reference							
AGV-2	4.19	2.88	0.48	1140.00	17.00	658.00	230.00
CCH-1	0.05	0.08	0.05	6.60	7.40	284.00	8.00
JLS-1	0.00	0.00	0.03	476.00	3.37	295.00	4.19
MAG-1	3.83	3.55	0.16	479.00	97.00	146.00	126.00
SCO-1	0.90	2.77	0.21	570.00	68.00	170.00	160.00
SGR-1	2.99	1.66	0.33	290.00	30.00	420.00	53.00
Values measured							
AGV-2	4.0	2.8	0.5	1162.4	22.7	612.4	199.1
CCH-1	0.0	0.1	0.0	-10.9	15.7	280.9	12.5
JLS-1	0.0	0.0	0.0	500.6	9.0	278.2	3.9
MAG-1	3.8	3.6	0.2	519.6	99.9	142.2	126.2
SCO-1	0.9	2.8	0.2	611.4	71.8	168.5	176.2
SGR-1	2.9	1.6	0.3	296.1	35.2	366.3	54.3
% offset							
AGV-2	4.1	1.6	1.4	-2.0	-33.4	6.9	13.4
CCH-1	7.0	-21.6	4.3	265.2	-112.7	1.1	-55.9
JLS-1	-591.3	-390.9	-6.9	-5.2	-166.7	5.7	5.7
MAG-1	0.3	-2.7	-13.1	-8.5	-2.9	2.6	-0.1
SCO-1	-1.3	-0.3	-6.0	-7.3	-5.6	0.9	-10.1
SGR-1	3.1	6.4	16.6	-2.1	-17.3	12.8	-2.5

Appendix F – Exemplar ICP-AES precision

	SiO_2	TiO_2	Al_2O_3	Fe_2O_3	MnO	MgO	CaO
AGV-2	58.6	1.1	16.8	6.5	0.1	1.7	5.1
AGV-2	58.2	1.0	16.7	6.5	0.1	1.7	5.0
AGV-2	59.7	1.1	17.1	6.7	0.1	1.8	5.2
AGV-2	57.8	1.0	16.6	6.5	0.1	1.7	5.0
AGV-2	58.5	1.1	16.8	6.6	0.1	1.7	5.1
AGV-2	57.8	1.0	16.6	6.5	0.1	1.7	5.0
AGV-2	58.4	1.1	16.8	6.5	0.1	1.7	5.0
2SD	1.4	0.0	0.4	0.2	0.0	0.1	0.1
%	2.4	2.5	2.1	2.5	2.4	3.1	2.9
CCH-1	1.2	0.0	0.3	0.2	0.0	2.8	52.3
CCH-1	1.2	0.0	0.3	0.2	0.0	2.8	51.5
CCH-1	1.0	0.0	0.3	0.2	0.0	2.8	51.8
CCH-1	1.2	0.0	0.4	0.2	0.0	2.9	53.5
CCH-1	1.1	0.0	0.3	0.2	0.0	2.8	52.3
CCH-1	1.1	0.0	0.3	0.2	0.0	2.8	52.3
2SD	0.1	0.0	0.1	0.0	0.0	0.1	1.5
%	12.4	19.9	18.4	8.8	5.3	2.1	2.9
JLS-1	0.3	0.0	0.1	0.1	0.0	0.6	54.8
JLS-1	0.4	0.0	0.1	0.1	0.0	0.6	55.4
JLS-1	0.4	0.0	0.1	0.1	0.0	0.6	56.1
JLS-1	0.6	0.0	0.1	0.1	0.0	0.6	53.6
JLS-1	0.4	0.0	0.1	0.1	0.0	0.6	55.0
2SD	0.2	0.0	0.0	0.0	0.0	0.0	2.1
%	48.8	46.5	45.9	8.2	10.4	7.8	3.9
MAG-1	51.4	0.7	16.5	7.0	0.1	3.1	1.4
MAG-1	51.4	0.8	16.5	7.0	0.1	3.1	1.4
MAG-1	50.5	0.7	16.2	6.9	0.1	3.1	1.3
MAG-1	51.5	0.8	16.6	7.0	0.1	3.1	1.5
MAG-1	51.1	0.7	16.5	7.0	0.1	3.1	1.4
2SD	1.1	0.0	0.4	0.2	0.0	0.1	0.2
%	2.1	2.3	2.2	2.5	2.9	2.6	16.5
SCO-1	63.5	0.6	13.9	5.2	0.1	2.8	3.0
SCO-1	64.5	0.6	14.1	5.3	0.1	2.9	3.0
SCO-1	63.1	0.6	13.9	5.2	0.1	2.8	2.8
SCO-1	62.1	0.6	13.6	5.1	0.1	2.8	2.8
SCO-1	63.3	0.6	13.9	5.2	0.1	2.8	2.9
2SD	2.0	0.0	0.4	0.1	0.0	0.1	0.2
%	3.1	3.1	2.9	2.8	2.8	3.2	7.1

	SiO$_2$	TiO$_2$	Al$_2$O$_3$	Fe$_2$O$_3$	MnO	MgO	CaO
SGR-1	27.5	0.2	6.4	2.9	0.0	4.4	8.2
SGR-1	27.5	0.2	6.4	2.9	0.0	4.4	8.2
SGR-1	26.6	0.2	6.2	2.8	0.0	4.3	8.0
SGR-1	27.0	0.2	6.3	2.8	0.0	4.4	8.2
SGR-1	27.2	0.2	6.3	2.9	0.0	4.4	8.1
2SD	0.9	0.0	0.2	0.1	0.0	0.1	0.2
%	3.4	3.4	3.3	3.6	3.2	3.2	2.6

	Na$_2$O	K$_2$O	P$_2$O$_5$	Ba	Cr	Sr	Zr
AGV-2	4.1	2.9	0.5	1133.2	10.8	659.5	221.2
AGV-2	4.2	2.8	0.5	1113.5	20.5	653.3	207.5
AGV-2	4.3	3.0	0.5	1151.2	20.8	671.4	214.8
AGV-2	4.2	3.0	0.5	1134.6	18.4	646.9	205.1
AGV-2	4.2	2.9	0.5	1133.1	17.6	657.8	212.2
AGV-2	4.2	3.0	0.5	1134.6	18.4	646.9	205.1
AGV-2	4.2	2.9	0.5	1133.4	17.8	656.0	211.0
2SD	0.1	0.1	0.0	23.9	7.3	18.4	12.7
%	2.2	2.9	4.6	2.1	40.9	2.8	6.0
CCH-1	0.1	0.1	0.1	-2.2	-2.2	291.5	-2.9
CCH-1	0.0	0.1	0.1	-1.3	9.1	287.7	8.1
CCH-1	0.0	0.1	0.1	-2.2	9.4	286.9	6.4
CCH-1	0.0	0.1	0.1	-1.8	13.1	292.3	11.8
CCH-1	0.0	0.1	0.1	-1.9	7.4	289.6	5.8
CCH-1	0.0	0.1	0.1	-1.9	7.4	289.6	5.8
2SD	0.0	0.0	0.0	0.7	11.5	4.7	10.8
%	51.0	13.9	7.4	-39.2	155.7	1.6	185.4
JLS-1	0.0	0.0	0.0	473.6	-4.9	289.4	-8.1
JLS-1	0.0	0.0	0.0	481.2	6.9	293.3	2.0
JLS-1	0.0	0.0	0.0	477.1	7.2	295.1	2.0
JLS-1	0.0	0.0	0.0	464.7	5.3	283.8	1.4
JLS-1	0.0	0.0	0.0	474.2	3.6	290.4	-0.7
2SD	0.0	0.0	0.0	14.1	11.5	10.0	10.0
%	224.6	37.9	11.7	3.0	316.8	3.4	-1456.6
MAG-1	3.9	3.7	0.2	490.7	100.3	143.3	136.5
MAG-1	3.9	3.6	0.2	488.5	97.7	144.2	128.7
MAG-1	3.9	3.7	0.2	485.1	94.5	141.9	129.2
MAG-1	3.9	3.8	0.2	496.4	97.3	144.2	132.2
MAG-1	3.9	3.7	0.2	490.0	96.5	143.4	130.1
2SD	0.1	0.2	0.0	11.6	3.5	2.6	3.8
%	2.3	5.0	2.1	2.4	3.6	1.8	2.9

	Na$_2$O	K$_2$O	P$_2$O$_5$	Ba	Cr	Sr	Zr
SCO-1	0.9	2.8	0.2	581.9	66.2	172.4	188.1
SCO-1	1.0	2.9	0.2	589.7	69.1	176.0	183.7
SCO-1	0.9	2.8	0.2	568.5	66.5	172.1	179.8
SCO-1	0.9	2.7	0.2	564.4	68.5	167.1	178.3
SCO-1	0.9	2.8	0.2	576.1	67.6	171.9	182.5
2SD	0.1	0.1	0.0	23.5	2.8	7.3	8.8
%	6.6	4.0	4.6	4.1	4.2	4.2	4.8
SGR-1	2.9	1.6	0.3	269.9	24.8	382.8	48.6
SGR-1	2.9	1.5	0.3	267.8	32.8	382.0	51.7
SGR-1	2.9	1.6	0.3	256.6	26.6	372.1	46.9
SGR-1	2.8	1.5	0.3	248.6	32.3	372.9	51.6
SGR-1	2.9	1.5	0.3	260.7	29.1	377.4	49.7
2SD	0.1	0.1	0.0	19.9	8.1	11.4	4.7
%	4.7	4.7	6.2	7.6	27.7	3.0	9.5

Appendix G – ICP-AES data

Sample	SiO_2 (wt %)	TiO_2 (wt %)	Al_2O_3 (wt %)	Fe_2O_3 (wt %)	MnO (wt %)	MgO (wt %)	CaO (wt %)	Na_2O (wt %)
126.18	16.86	0.23	5.54	3.19	0.07	1.70	36.75	0.18
127.26	51.02	1.08	22.43	6.77	0.02	1.68	0.38	0.47
128.33	51.45	1.10	24.43	6.46	0.02	1.75	0.31	0.48
128.83	51.48	1.10	23.77	6.25	0.02	1.76	0.25	0.48
129.15	51.69	1.10	24.27	7.32	0.02	1.75	0.27	0.49
129.65	49.03	1.04	23.40	6.54	0.02	1.68	0.19	0.47
130.15	49.79	1.06	22.72	6.20	0.02	1.62	0.23	0.46
130.25	50.04	1.07	22.37	6.39	0.02	1.60	0.90	0.46
130.75	50.92	1.04	23.53	7.14	0.02	1.64	0.11	0.47
131.25	49.23	1.04	23.38	6.92	0.02	1.72	0.35	0.47
132.15	50.83	1.06	24.07	6.70	0.02	1.75	0.19	0.48
132.65	50.90	1.06	24.12	6.31	0.02	1.68	0.10	0.48
133.30	51.22	1.09	23.49	7.00	0.02	1.61	0.30	0.47
133.65	49.58	1.03	23.63	6.71	0.02	1.69	0.47	0.47
134.15	50.38	1.03	23.54	6.69	0.02	1.72	0.38	0.49
134.60	51.28	1.07	23.37	6.74	0.03	1.76	0.37	0.50
135.10	50.08	1.04	24.08	6.44	0.02	1.78	0.35	0.50
135.60	51.06	1.05	24.20	6.54	0.02	1.80	0.22	0.50
136.10	51.13	1.05	24.28	6.55	0.02	1.78	0.32	0.51
136.60	50.05	1.04	23.31	6.23	0.02	1.70	0.23	0.49
136.65	51.39	1.06	24.20	6.24	0.02	1.76	0.18	0.47
137.15	53.74	1.13	24.99	6.02	0.02	1.79	0.30	0.52
137.61	44.97	0.92	20.96	11.30	0.07	2.30	2.38	0.44
138.11	52.02	1.07	23.95	6.00	0.02	1.74	0.34	0.50
138.61	51.58	1.06	24.37	6.06	0.02	1.75	0.49	0.50
138.75	48.44	0.99	22.79	6.95	0.03	1.66	2.31	0.47
139.25	50.11	1.03	23.58	6.29	0.02	1.69	0.86	0.49
139.44	50.49	1.05	23.96	6.18	0.02	1.70	0.58	0.48
140.50	48.41	1.00	22.82	6.45	0.03	1.65	2.52	0.48
141.00	49.53	1.01	23.42	6.57	0.03	1.68	1.63	0.48
141.50	50.71	1.07	23.87	6.37	0.03	1.72	0.49	0.49
141.60	66.66	0.93	15.46	7.29	0.04	1.39	1.71	1.56
142.10	51.21	1.04	24.48	6.46	0.02	1.76	0.67	0.50
142.65	45.89	0.93	21.13	7.34	0.03	1.71	2.65	0.47
143.15	48.44	0.98	22.56	7.30	0.03	1.81	1.32	0.49
143.65	49.05	0.97	22.42	6.13	0.03	1.82	2.46	0.52
143.78	50.45	1.01	23.42	5.88	0.02	1.85	0.91	0.54
144.28	49.66	0.98	23.09	5.63	0.02	1.78	0.28	0.51
144.78	51.65	1.04	23.87	6.25	0.02	1.83	0.31	0.49
144.84	51.92	1.04	23.90	6.27	0.02	1.83	0.44	0.53
145.34	52.51	1.06	23.79	5.72	0.02	1.84	0.50	0.56

Sample	SiO$_2$ (wt %)	TiO$_2$ (wt %)	Al$_2$O$_3$ (wt %)	Fe$_2$O$_3$ (wt %)	MnO (wt %)	MgO wt %)	CaO (wt %)	Na$_2$O (wt %)
145.69	52.11	1.03	23.45	5.68	0.02	1.85	0.43	0.53
146.19	51.94	1.03	23.62	5.63	0.02	1.88	0.35	0.54
146.69	51.92	1.04	23.55	5.77	0.02	1.86	0.48	0.54
146.82	51.62	1.02	23.32	5.72	0.02	1.81	0.30	0.54
147.32	50.80	1.01	23.53	5.65	0.02	1.80	0.29	0.52
147.82	50.08	0.99	23.10	6.45	0.03	1.88	1.16	0.51
147.94	51.50	1.01	23.45	5.81	0.02	1.85	0.66	0.54
148.85	48.72	0.96	22.59	5.71	0.02	1.74	0.59	0.50
149.35	49.69	0.98	23.30	5.76	0.02	1.78	0.72	0.51
149.85	50.40	1.00	23.43	5.66	0.02	1.80	0.57	0.51
149.96	51.89	1.03	24.04	5.72	0.02	1.83	0.61	0.53
150.46	50.79	1.00	23.53	6.13	0.02	1.88	0.82	0.54
150.96	50.68	0.97	23.61	5.78	0.02	1.87	1.16	0.54
151.07	51.75	1.02	23.67	5.49	0.02	1.90	0.81	0.55
151.55	44.88	0.87	20.94	7.24	0.02	1.67	0.77	0.47
151.87	45.26	0.88	21.05	8.22	0.03	1.67	2.19	0.50
152.37	45.59	0.87	21.10	7.41	0.03	1.70	4.37	0.48
152.87	46.10	0.92	21.19	6.88	0.03	1.60	2.89	0.48
153.37	49.24	1.00	22.92	6.39	0.02	1.70	1.45	0.50
153.87	43.09	0.85	20.10	8.90	0.03	1.63	4.51	0.45
153.98	44.21	0.86	20.49	8.81	0.04	1.74	4.77	0.46
154.48	41.57	0.80	19.36	8.83	0.05	1.79	5.20	0.45
154.80	47.81	0.92	22.39	7.41	0.03	1.70	3.01	0.50
155.30	47.51	0.92	22.16	7.58	0.03	1.68	2.99	0.51
155.80	45.34	0.88	21.19	8.00	0.03	1.67	4.58	0.49
155.93	45.10	0.87	21.30	7.52	0.03	1.65	3.93	0.49
157.00	42.27	0.80	19.70	8.26	0.05	2.01	6.79	0.47
156.43	45.24	0.88	21.34	7.48	0.03	1.65	3.95	0.48
156.93	45.31	0.87	21.31	7.55	0.03	1.77	4.61	0.50
157.25	41.10	0.78	18.72	9.24	0.05	2.00	6.50	0.45
157.45	43.26	0.82	19.69	8.43	0.04	1.72	6.23	0.47
157.85	43.71	0.83	20.05	7.93	0.03	1.62	5.78	0.47
157.97	47.26	0.91	22.03	7.30	0.03	1.64	3.13	0.51
158.17	48.00	0.94	22.43	7.20	0.03	1.69	2.76	0.51
158.37	45.64	0.87	21.58	6.92	0.03	1.63	4.32	0.50
158.57	49.05	0.95	22.92	6.05	0.02	1.71	1.65	0.53
158.77	50.09	0.97	23.30	6.21	0.03	1.80	1.94	0.54
158.94	47.08	0.92	22.38	6.91	0.02	1.68	1.74	0.51
159.14	49.26	0.97	23.37	6.77	0.02	1.70	1.58	0.52
159.34	43.29	0.83	20.45	6.75	0.03	1.55	6.20	0.46
159.54	46.48	0.90	22.54	6.74	0.03	1.64	3.02	0.52
159.74	46.85	0.87	21.99	6.80	0.03	1.70	3.50	0.51
159.94	46.82	0.90	21.63	6.69	0.03	1.72	4.19	0.51
160.07	45.93	0.90	22.36	10.84	0.03	1.64	4.17	0.52
160.27	48.22	0.96	22.47	7.10	0.03	1.66	2.39	0.51

Sample	SiO₂ (wt %)	TiO₂ (wt %)	Al₂O₃ (wt %)	Fe₂O₃ (wt %)	MnO (wt %)	MgO (wt %)	CaO (wt %)	Na₂O (wt %)
160.47	45.21	0.88	21.33	7.82	0.03	1.57	4.12	0.47
160.47	44.78	0.87	21.05	7.74	0.03	1.56	4.09	0.47
160.67	45.80	0.89	21.63	6.84	0.03	1.54	3.82	0.47
160.87	46.16	0.89	21.58	7.56	0.03	1.60	2.71	0.50
161.00	43.16	0.86	20.06	7.52	0.02	1.55	2.53	0.46
161.20	47.11	0.93	21.70	6.91	0.03	1.62	2.85	0.50
161.40	47.34	0.94	21.63	7.40	0.02	1.57	2.77	0.49
161.58	44.51	0.87	20.89	9.73	0.03	1.53	4.30	0.47
161.78	44.72	0.86	20.85	8.41	0.03	1.53	4.28	0.47
161.98	45.95	0.88	21.40	7.11	0.03	1.60	3.59	0.49
162.18	46.56	0.91	21.64	8.38	0.03	1.69	3.26	0.50
162.38	45.55	0.90	21.24	8.80	0.03	1.64	2.88	0.48
162.58	41.71	0.78	19.20	8.25	0.03	1.55	6.85	0.45
162.72	45.91	0.88	21.04	7.19	0.03	1.52	5.13	0.50
162.92	44.12	0.84	20.11	7.68	0.03	1.49	4.09	0.48
163.12	48.01	0.94	21.77	6.81	0.03	1.59	3.21	0.51
163.32	41.59	0.80	19.17	7.30	0.03	1.48	7.81	0.47
163.52	45.52	0.90	20.83	7.28	0.03	1.45	3.41	0.47
163.72	38.96	0.72	17.83	7.63	0.03	1.35	9.14	0.44
163.77	38.83	0.74	17.30	7.20	0.03	1.34	9.71	0.44
163.97	38.97	0.73	17.53	8.31	0.03	1.38	9.77	0.44
164.17	34.51	0.64	15.46	8.35	0.04	1.54	13.62	0.40
164.37	36.41	0.67	16.47	8.54	0.03	1.46	9.11	0.41
164.57	33.65	0.62	15.35	9.73	0.04	1.55	12.54	0.38
164.77	19.29	0.33	8.20	9.26	0.06	1.55	23.79	0.26
164.91	32.89	0.61	14.13	6.71	0.07	2.69	15.76	0.45
165.11	9.37	0.17	3.90	4.60	0.11	2.44	40.00	0.13
165.31	30.90	0.58	12.79	9.33	0.09	3.43	13.29	0.36
165.51	28.97	0.54	11.86	8.95	0.10	3.79	17.03	0.36
165.71	39.00	0.72	17.02	9.15	0.03	1.45	7.22	0.44
165.91	42.62	0.78	17.34	8.41	0.04	1.72	6.95	0.52
166.04	42.43	0.77	18.00	9.52	0.03	1.48	5.26	0.50
166.24	41.19	0.79	17.78	7.84	0.03	1.36	6.26	0.48
166.44	45.84	0.84	19.74	8.03	0.03	1.32	3.15	0.55
166.64	41.66	0.75	17.74	10.24	0.04	1.32	7.09	0.56
166.84	44.10	0.81	18.64	10.35	0.03	1.44	3.49	0.54
167.04	37.03	0.65	15.59	9.33	0.04	1.25	9.27	0.50
167.11	41.67	0.78	17.24	9.41	0.04	1.53	3.65	0.63
167.31	36.59	0.69	12.97	10.50	0.08	2.69	7.05	0.66
167.89	5.68	0.10	1.96	2.43	0.16	1.09	45.53	0.15
168.09	20.21	0.37	7.86	7.83	0.14	3.10	26.64	0.38
168.29	39.99	0.73	15.33	7.37	0.08	2.71	7.45	0.63
168.49	32.19	0.59	12.14	8.62	0.07	2.92	8.84	0.51
168.69	42.49	0.77	15.84	9.84	0.05	1.91	4.30	0.64
168.89	42.90	0.78	16.87	10.55	0.04	1.46	3.30	0.65

Sample	SiO$_2$ (wt %)	TiO$_2$ (wt %)	Al$_2$O$_3$ (wt %)	Fe$_2$O$_3$ (wt %)	MnO (wt %)	MgO (wt %)	CaO (wt %)	Na$_2$O (wt %)
168.99	47.41	0.79	16.46	7.52	0.04	1.60	4.02	0.79
168.99	48.34	0.81	16.94	8.27	0.04	1.65	4.15	0.80
169.19	41.56	0.73	15.68	12.54	0.04	1.42	2.82	0.59
169.39	41.33	0.72	15.74	8.92	0.06	2.00	5.29	0.63
169.59	48.76	0.92	18.67	8.75	0.03	1.70	1.65	0.73
169.79	44.61	0.79	17.34	7.96	0.05	2.04	4.36	0.64
170.08	47.19	0.88	20.02	8.73	0.03	1.54	1.09	0.58
170.28	46.23	0.87	20.56	8.74	0.03	1.52	1.19	0.59
170.48	40.93	0.81	17.90	9.98	0.05	1.98	2.20	0.56
170.68	46.01	0.88	20.31	8.38	0.04	1.84	1.56	0.60
170.88	46.84	0.93	20.29	8.19	0.05	2.08	2.21	0.63
171.08	47.06	0.96	19.05	7.84	0.08	2.08	3.99	0.67
171.21	48.34	0.93	19.74	9.87	0.04	1.50	0.95	0.64
171.41	46.25	0.89	19.18	9.44	0.04	1.60	1.74	0.61
171.61	45.00	0.93	20.49	9.59	0.05	1.86	2.43	0.59
171.81	43.01	0.90	18.12	7.95	0.07	2.30	5.20	0.62
172.07	48.43	0.95	18.69	9.60	0.03	1.50	1.77	0.63
172.31	46.04	0.97	20.10	8.63	0.04	1.84	2.76	0.58
172.51	46.14	0.93	19.43	9.15	0.05	1.86	2.67	0.57
172.71	53.61	1.03	20.56	6.01	0.04	1.71	1.57	0.81
172.91	46.94	1.04	20.98	8.92	0.03	1.68	1.02	0.61
173.20	49.22	0.99	19.96	9.13	0.04	1.65	1.53	0.67
173.40	52.72	1.01	20.59	5.93	0.04	1.84	2.09	0.79
173.60	48.01	0.98	18.58	8.85	0.04	1.63	1.51	0.65
173.80	52.41	0.89	16.12	8.91	0.04	1.42	2.59	0.74
174.00	52.30	1.00	19.93	6.26	0.04	1.76	2.57	0.75
174.23	52.52	1.03	20.52	6.36	0.04	1.77	1.81	0.75
174.43	54.16	1.00	19.80	6.57	0.03	1.71	1.66	0.79
174.63	53.82	1.00	20.40	6.83	0.03	1.70	1.19	0.77
174.83	55.76	1.06	21.03	7.15	0.03	1.75	0.99	0.78
175.03	54.88	1.04	21.01	6.44	0.03	1.80	1.46	0.78
175.26	54.73	1.00	19.94	6.27	0.04	1.74	1.57	0.83
175.46	52.55	1.04	20.59	6.41	0.03	1.75	1.04	0.76
175.66	53.19	1.09	21.84	6.43	0.03	1.81	1.18	0.75
175.86	48.55	0.98	19.97	8.01	0.03	1.65	1.79	0.71
176.06	53.31	1.09	22.15	5.42	0.03	1.86	1.18	0.77
176.24	53.33	1.05	21.13	6.54	0.04	1.90	2.05	0.75
176.42	53.25	1.05	21.19	6.53	0.04	1.88	2.04	0.74
176.44	51.00	1.00	20.24	5.27	0.05	1.89	4.21	0.75
176.64	54.79	1.08	21.42	5.49	0.03	1.88	1.30	0.76
176.71	54.45	1.10	21.90	5.40	0.03	1.89	1.14	0.71
176.91	53.83	1.05	20.30	5.79	0.03	1.76	1.67	0.68
177.11	52.73	1.03	20.10	6.43	0.04	1.82	1.98	0.66
177.31	53.08	1.07	21.80	6.29	0.03	1.92	0.98	0.68
177.51	50.83	1.02	20.90	6.80	0.04	1.92	1.90	0.66

Sample	SiO_2 (wt %)	TiO_2 (wt %)	Al_2O_3 (wt %)	Fe_2O_3 (wt %)	MnO (wt %)	MgO (wt %)	CaO (wt %)	Na_2O (wt %)
177.77	50.00	0.99	20.55	6.74	0.05	2.00	2.30	0.65
177.97	51.25	1.05	21.88	6.58	0.04	2.02	1.81	0.70
178.17	53.20	1.07	21.71	6.44	0.04	2.04	1.82	0.75
178.37	52.17	1.00	20.21	6.83	0.04	1.91	1.64	0.71
178.57	52.84	1.06	21.38	7.42	0.04	1.99	1.38	0.70
178.77	52.95	1.07	21.78	6.51	0.04	2.01	1.44	0.71
179.17	54.06	1.07	21.97	6.31	0.04	2.06	1.69	0.75
179.37	51.73	1.02	20.90	7.46	0.05	2.06	1.86	0.74
179.57	53.77	1.04	21.54	6.54	0.04	1.99	1.70	0.76
179.77	53.14	1.05	21.32	6.65	0.04	1.99	1.69	0.76
179.79	52.51	1.07	21.79	6.75	0.04	2.02	1.59	0.74
179.99	51.83	1.06	21.64	7.24	0.04	2.00	1.63	0.69
180.19	44.19	0.88	18.30	13.20	0.12	2.97	2.62	0.62
180.39	46.21	0.92	17.73	12.07	0.08	1.72	1.38	0.67
180.91	39.40	0.71	15.30	10.02	0.04	1.53	3.13	0.63
181.11	57.26	1.02	19.39	5.09	0.03	1.70	1.34	0.89
181.31	57.24	1.06	20.38	5.54	0.03	1.77	1.29	0.83
181.51	58.65	1.04	19.90	5.23	0.03	1.76	1.22	0.93
181.71	56.13	1.07	21.16	5.60	0.03	1.88	0.81	0.83
181.79	55.59	1.07	21.25	5.95	0.03	1.89	0.67	0.86
182.29	53.99	1.05	20.95	6.67	0.03	1.83	0.61	0.80
182.79	48.01	0.97	19.95	6.85	0.04	1.96	1.64	0.71
182.88	55.07	1.10	21.98	6.01	0.03	1.93	0.65	0.79
183.38	53.87	0.99	20.12	9.88	0.06	1.79	4.01	0.86
183.88	52.18	0.96	18.33	9.48	0.05	1.66	0.53	0.86
184.01	53.79	1.07	21.32	7.13	0.04	1.86	0.39	0.82
184.51	56.85	1.12	21.87	5.57	0.03	1.83	0.34	0.88
184.91	62.22	0.98	16.59	4.38	0.04	1.38	1.99	1.16
185.41	61.90	1.04	18.53	5.64	0.03	1.55	0.53	1.13
185.75	51.15	0.61	10.88	11.86	0.17	2.30	4.97	1.11
186.25	63.26	0.95	16.08	5.42	0.03	1.44	0.61	1.21
186.83	63.07	1.07	18.25	5.04	0.03	1.58	0.21	1.16
187.33	63.72	1.09	19.15	5.08	0.03	1.67	0.29	1.14
187.83	62.91	0.98	17.75	5.25	0.04	1.62	0.88	1.21
187.88	56.05	0.96	18.65	9.76	0.03	1.59	0.44	0.99
188.38	61.14	1.07	17.99	5.13	0.03	1.74	0.50	1.16
188.88	63.85	1.06	17.93	5.15	0.03	1.69	0.38	1.17
189.01	59.41	1.11	20.23	6.30	0.03	1.89	0.24	0.99
189.51	58.27	1.11	20.72	6.01	0.03	1.93	0.17	0.95
190.01	61.27	1.02	16.32	5.54	0.05	1.66	2.20	1.20
190.15	61.59	1.10	18.76	4.99	0.04	1.73	1.77	1.17
190.65	56.20	0.87	15.11	5.32	0.09	1.65	6.68	1.13
190.91	62.90	0.90	15.26	5.61	0.06	1.57	2.85	1.50
191.41	61.58	1.07	18.60	5.70	0.03	1.63	0.34	1.28
191.94	57.37	1.05	17.31	8.26	0.08	3.29	4.31	1.57

Sample	SiO$_2$ (wt %)	TiO$_2$ (wt %)	Al$_2$O$_3$ (wt %)	Fe$_2$O$_3$ (wt %)	MnO (wt %)	MgO (wt %)	CaO (wt %)	Na$_2$O (wt %)
192.44	58.88	1.08	20.10	6.80	0.02	1.69	0.15	1.20
193.07	59.51	1.11	20.68	5.84	0.02	1.73	0.10	1.25
193.57	54.70	1.03	19.36	10.98	0.02	1.61	0.27	1.18
193.57	54.14	1.00	19.06	10.80	0.02	1.56	0.15	1.15
194.02	30.09	0.67	13.40	25.19	0.30	3.44	3.31	0.57
194.52	54.52	1.01	21.12	8.12	0.04	2.13	0.22	1.48
195.02	55.82	1.06	20.81	6.55	0.03	2.09	0.07	1.53
195.18	50.37	1.06	21.89	9.23	0.03	2.34	0.11	1.29
195.68	54.80	0.94	17.17	6.91	0.03	1.83	0.67	1.52
196.18	56.77	0.88	15.17	8.13	0.06	1.72	2.54	1.61
196.27	54.11	1.05	18.85	7.89	0.04	1.99	0.32	1.36
196.40	60.17	1.02	18.92	6.69	0.03	1.93	0.18	1.67
196.90	57.87	1.07	19.84	7.22	0.03	2.00	0.31	1.56
197.40	53.03	1.01	19.72	7.13	0.03	2.00	0.36	1.32
197.46	53.19	1.03	20.68	8.71	0.03	2.05	0.75	1.27
197.97	54.96	1.02	20.37	8.36	0.03	2.03	0.40	1.35
198.47	54.14	1.05	22.77	6.99	0.03	2.12	0.30	1.25
199.11	52.54	1.04	21.27	7.30	0.03	2.03	0.12	1.17
199.61	50.49	0.97	19.89	9.79	0.03	1.83	0.27	1.15
199.96	54.06	1.11	24.15	6.91	0.03	2.11	0.10	1.13
200.39	4.90	0.12	2.90	47.16	0.58	5.88	4.33	0.14
200.89	56.15	1.09	21.11	6.71	0.03	1.95	0.49	1.34
201.09	55.71	1.09	21.25	6.67	0.03	1.86	0.55	1.18
201.59	58.86	1.05	18.89	6.60	0.03	1.83	0.34	1.49
202.01	53.41	0.98	19.44	10.20	0.03	1.82	0.25	1.35
202.51	57.60	1.06	20.22	6.57	0.03	1.93	0.19	1.45
202.65	56.15	1.06	21.16	7.15	0.04	2.04	0.16	1.39
203.01	56.00	1.01	19.98	6.42	0.03	1.91	0.20	1.37
203.58	57.01	1.01	19.43	6.82	0.03	1.90	0.37	1.46
203.70	55.40	1.07	22.33	7.36	0.03	2.13	0.13	1.26
204.30	58.56	1.01	18.99	7.74	0.03	1.89	0.57	1.52
204.66	56.23	1.07	21.43	7.03	0.03	2.10	0.44	1.25
205.16	55.00	1.04	21.54	8.54	0.03	2.12	0.23	1.33
205.48	55.10	1.05	21.66	7.33	0.03	2.09	0.06	1.26
205.65	55.22	1.05	22.10	7.10	0.03	2.08	0.14	1.24
206.15	54.09	0.98	18.87	10.08	0.02	1.64	0.12	1.16
206.67	62.94	1.05	18.29	5.25	0.02	1.53	0.36	1.40
207.37	60.18	1.07	19.04	6.28	0.02	1.58	0.48	1.30
207.57	57.25	1.08	20.79	6.34	0.02	1.81	0.35	1.21
208.07	61.17	1.05	19.72	6.30	0.03	1.75	0.31	1.44
208.57	57.47	1.07	20.75	5.76	0.02	1.79	0.21	1.22
208.63	54.83	1.07	21.85	6.10	0.02	1.79	0.08	1.03
209.17	55.18	0.82	15.41	10.69	0.11	2.05	1.86	1.22
209.67	51.13	1.06	24.19	6.35	0.02	1.74	0.60	0.51
209.80	65.47	0.63	9.45	3.63	0.11	0.95	7.57	1.66

Sample	SiO$_2$ (wt %)	TiO$_2$ (wt %)	Al$_2$O$_3$ (wt %)	Fe$_2$O$_3$ (wt %)	MnO (wt %)	MgO wt %	CaO (wt %)	Na$_2$O (wt %)
210.31	63.86	1.00	17.32	5.21	0.03	1.54	0.55	1.61
210.75	56.06	1.05	20.36	7.85	0.02	1.78	0.18	1.19
211.25	63.00	0.94	16.71	5.42	0.03	1.60	0.61	1.59
211.75	54.64	0.73	12.36	5.22	0.17	1.96	9.64	1.45
211.88	63.72	0.94	15.49	5.22	0.04	1.52	0.89	1.62
212.38	59.27	0.93	15.65	10.18	0.03	1.47	0.25	1.58
212.88	62.07	0.99	17.10	6.19	0.03	1.60	0.21	1.67
213.07	64.49	0.80	14.28	7.32	0.04	1.38	1.13	1.74
213.57	59.82	0.95	16.76	7.35	0.03	1.61	0.18	1.53
213.79	70.30	0.54	10.55	6.23	0.04	0.93	2.25	1.64
214.91	64.70	0.85	15.93	7.19	0.03	1.50	0.67	1.67
216.96	67.54	0.67	13.09	4.87	0.02	1.17	0.69	1.75
218.02	55.00	0.44	8.06	14.01	0.11	1.41	5.70	1.44
219.06	64.85	0.92	16.70	5.06	0.02	1.44	0.17	1.65

Sample	K_2O (wt %)	P_2O_5 (wt %)	$CaCO_3$ (wt %)	Ba (ppm)	Cr (ppm)	Sr (ppm)	Zr (ppm)
126.18	0.67	1.64	65.60	148	26	621	
127.26	3.16	0.13	0.67	369	133	169	179
128.33	3.43	0.16	0.55	380	142	172	168
128.83	3.33	0.14	0.45	370	139	167	170
129.15	3.43	0.15	0.49	387	141	176	168
129.65	3.19	0.16	0.34	387	125	167	160
130.15	3.19	0.14	0.42	380	132	162	167
130.25	3.15	0.15	1.60	351	128	177	199
130.75	3.25	0.15	0.19	373	128	168	167
131.25	3.29	0.18	0.62	356	134	161	156
132.15	3.31	0.16	0.34	356	139	155	164
132.65	3.29	0.14	0.17	512	51	201	103
133.30	3.33	0.14	0.54	386	136	174	171
133.65	3.25	0.17	0.83	360	129	175	155
134.15	3.24	0.19	0.67	381	128	180	157
134.60	3.33	0.16	0.66	276	82	253	99
135.10	3.36	0.16	0.62	542	116	260	134
135.60	3.44	0.14	0.40	302	122	176	143
136.10	3.44	0.17	0.56	403	143	171	154
136.60	3.33	0.14	0.41	355	132	167	162
136.65	3.38	0.13	0.33	363	131	170	160
137.15	3.59	0.12	0.54	368	145	175	202
137.61	2.99	0.24	4.24	329	124	159	139
138.11	3.41	0.16	0.61	364	139	168	164
138.61	3.42	0.15	0.87	383	142	179	162
138.75	3.17	0.38	4.12	357	134	214	149
139.25	3.30	0.18	1.54	360	136	177	157
139.44	3.32	0.15	1.04	363	141	170	160
140.50	3.07	0.28	4.50	335	124	193	152
141.00	3.20	0.19	2.91	370	127	186	155
141.50	3.34	0.14	0.87	396	267	178	159
141.60	1.76	0.11	3.06	201	183	109	487
142.10	3.37	0.15	1.20	388	141	173	152
142.65	2.89	0.26	4.74	315	120	176	137
143.15	3.14	0.26	2.36	316	149	153	256
143.65	3.05	0.26	4.39	260	114	190	147
143.78	3.25	0.22	1.63	364	129	180	143
144.28	3.15	0.15	0.51	382	131	154	146
144.78	3.28	0.16	0.55	261	75	193	110
144.84	3.34	0.16	0.79	387	141	161	150
145.34	3.34	0.16	0.89	454	141	172	178
145.69	3.28	0.17	0.77	397	130	169	156
146.19	3.35	0.15	0.62	247	118	156	157
146.69	3.38	0.15	0.85	421	131	175	155
146.82	3.30	0.15	0.54	393	135	162	159

Sample	K$_2$O (wt %)	P$_2$O$_5$ (wt %)	CaCO$_3$ (wt %)	Ba (ppm)	Cr (ppm)	Sr (ppm)	Zr (ppm)
147.32	3.32	0.14	0.52	347	120	307	160
147.82	3.22	0.22	2.07	364	127	173	147
147.94	3.36	0.17	1.17	397	137	164	151
148.85	3.12	0.17	1.05	356	125	160	142
149.35	3.21	0.16	1.29	217	120	143	202
149.85	3.25	0.17	1.02	387	126	300	137
149.96	3.39	0.15	1.08	393	141	161	150
150.46	3.30	0.16	1.47	332	117	210	132
150.96	3.31	0.15	2.06	382	121	274	137
151.07	3.36	0.17	1.45	297	106	279	125
151.55	2.91	0.15	1.38	418	123	276	129
151.87	2.97	0.27	3.91	322	117	190	134
152.37	2.97	0.23	7.80	312	113	279	129
152.87	2.98	0.37	5.15	365	117	230	136
153.37	3.24	0.16	2.58	406	137	202	143
153.87	2.80	0.26	8.05	329	112	331	128
153.98	2.84	0.22	8.52	339	115	399	129
154.48	2.72	0.23	9.28	314	154	126	285
154.80	3.10	0.20	5.37	378	125	305	153
155.30	3.01	0.24	5.34	402	121	275	135
155.80	2.98	0.22	8.18	363	125	374	124
155.93	2.96	0.21	7.02	374	116	375	127
157.00	2.84	0.29	12.12	438	111	475	137
156.43	3.02	0.23	7.05	522	116	521	131
156.93	3.06	0.26	8.23	284	138	147	217
157.25	2.67	0.27	11.59	354	104	396	117
157.45	2.80	0.24	11.12	328	112	366	126
157.85	2.84	0.27	10.31	341	109	340	124
157.97	3.19	0.20	5.58	350	119	301	138
158.17	3.26	0.18	4.93	380	132	282	144
158.37	3.10	0.37	7.71	388	128	346	126
158.57	3.23	0.19	2.95	209	115	142	156
158.77	3.38	0.18	3.47	353	140	130	235
158.94	3.19	0.17	3.11	204	114	133	156
159.14	3.37	0.18	2.82	268	153	110	249
159.34	2.88	0.31	11.06	426	116	321	124
159.54	3.23	0.21	5.39	227	112	166	160
159.74	3.23	0.22	6.26	246	147	130	266
159.94	3.11	0.18	7.47	220	113	160	183
160.07	3.10	0.21	7.45	207	110	140	168
160.27	3.28	0.21	4.27	243	119	113	195
160.47	3.00	0.19	7.35	342	127	304	131
160.47	3.00	0.19	7.29	339	117	303	134
160.67	3.03	0.19	6.82	347	128	305	126
160.87	3.13	0.19	4.85	202	111	140	166

Sample	K₂O (wt %)	P₂O₅ (wt %)	CaCO₃ (wt %)	Ba (ppm)	Cr (ppm)	Sr (ppm)	Zr (ppm)
161.00	2.92	0.20	4.52	348	116	268	146
161.20	3.11	0.20	5.09	199	113	104	209
161.40	3.17	0.19	4.94	399	131	328	148
161.58	2.91	0.21	7.67	375	122	372	136
161.78	2.90	0.26	7.64	369	115	298	132
161.98	2.99	0.23	6.41	390	118	262	135
162.18	3.12	0.23	5.81	453	124	262	142
162.38	3.12	0.27	5.14	362	119	259	141
162.58	2.78	0.26	12.23	415	109	333	118
162.72	3.03	0.24	9.16	416	116	284	134
162.92	2.94	0.23	7.30	360	107	215	130
163.12	3.28	0.18	5.74	379	120	212	145
163.32	2.77	0.25	13.94	361	105	257	121
163.52	3.09	0.31	6.08	389	123	200	140
163.72	2.53	0.24	16.31	337	98	254	105
163.77	2.58	0.25	17.34	189	89	120	192
163.97	2.59	0.29	17.43	241	104	105	212
164.17	2.22	0.45	24.31	204	115	139	192
164.37	2.40	0.33	16.26	380	92	239	102
164.57	2.32	0.51	22.38	283	85	267	73
164.77	1.21	0.21	42.46	319	46	382	54
164.91	2.15	0.24	28.13	484	122	175	157
165.11	0.58	0.09	71.39	3082	24	496	28
165.31	2.05	0.48	23.71	272	77	322	83
165.51	1.94	0.21	30.39	1241	71	516	96
165.71	2.68	0.21	12.89	304	94	249	116
165.91	2.83	0.16	12.40	383	100	255	131
166.04	2.76	0.18	9.38	167	85	203	102
166.24	2.64	0.14	11.18	322	102	202	113
166.44	2.81	0.14	5.61	345	108	172	124
166.64	2.43	0.19	12.65	1087	110	207	108
166.84	2.84	0.21	6.24	350	110	178	150
167.04	2.25	0.18	16.55	339	85	199	96
167.11	2.73	0.21	6.52	389	103	178	156
167.31	2.24	0.28	12.58	356	87	173	145
167.89	0.33	0.12	81.26	342	7	210	41
168.09	1.17	0.31	47.55	173	56	189	82
168.29	2.39	0.16	13.30	328	93	192	127
168.49	2.03	0.16	15.78	1092	75	171	106
168.69	2.81	0.16	7.67	343	99	168	137
168.89	2.88	0.15	5.89	328	105	154	135
168.99	2.65	0.35	7.17	757	95	180	165
168.99	2.70	0.35	7.40	754	102	185	172
169.19	2.61	0.17	5.03	440	101	143	134
169.39	2.61	0.18	9.44	338	97	163	119

Sample	K$_2$O (wt %)	P$_2$O$_5$ (wt %)	CaCO$_3$ (wt %)	Ba (ppm)	Cr (ppm)	Sr (ppm)	Zr (ppm)
169.59	2.69	0.22	2.94	302	108	142	182
169.79	2.95	0.21	7.77	393	105	195	133
170.08	3.12	0.13	1.95	305	118	139	134
170.28	2.93	0.13	2.11	291	118	142	118
170.48	2.73	0.12	3.92	257	104	138	133
170.68	3.11	0.12	2.79	308	115	154	136
170.88	3.09	0.11	3.94	320	117	173	149
171.08	2.65	0.12	7.12	321	105	207	163
171.21	2.84	0.11	1.69	290	124	135	142
171.41	2.55	0.13	3.11	263	112	140	129
171.61	2.73	0.11	4.34	271	118	159	133
171.81	2.62	0.24	9.28	284	105	184	150
172.07	2.76	0.17	3.16	278	124	136	159
172.31	3.11	0.17	4.92	269	124	158	148
172.51	3.18	0.24	4.76	292	141	150	135
172.71	2.85	0.14	2.81	362	130	150	190
172.91	3.27	0.17	1.83	285	142	157	173
173.20	2.97	0.18	2.73	277	136	136	163
173.40	2.93	0.19	3.72	347	137	156	185
173.60	2.73	0.24	2.70	279	127	153	147
173.80	2.17	0.22	4.61	230	99	126	180
174.00	2.93	0.25	4.59	323	122	159	191
174.23	3.02	0.18	3.22	313	125	160	186
174.43	2.75	0.18	2.96	321	118	146	189
174.63	2.85	0.18	2.12	331	120	142	192
174.83	3.04	0.17	1.77	322	125	144	200
175.03	3.03	0.15	2.61	341	124	148	198
175.26	2.74	0.12	2.81	351	125	139	199
175.46	2.94	0.15	1.86	317	127	156	193
175.66	3.29	0.18	2.11	313	130	168	195
175.86	2.87	0.28	3.20	267	115	160	173
176.06	3.29	0.21	2.10	311	129	155	188
176.24	3.10	0.19	3.66	300	125	151	188
176.42	3.11	0.19	3.63	307	133	148	184
176.44	2.90	0.39	7.51	334	62	251	113
176.64	3.14	0.14	2.33	322	125	163	197
176.71	3.30	0.13	2.03	322	128	166	197
176.91	3.02	0.26	2.98	307	118	155	212
177.11	3.10	0.30	3.53	308	119	159	195
177.31	3.36	0.16	1.76	311	126	155	184
177.51	3.14	0.22	3.39	286	124	156	179
177.77	3.09	0.21	4.10	290	125	151	167
177.97	3.42	0.19	3.24	304	123	165	173
178.17	3.32	0.28	3.25	309	127	170	186
178.37	3.00	0.26	2.93	288	118	149	176

Sample	K$_2$O (wt %)	P$_2$O$_5$ (wt %)	CaCO$_3$ (wt %)	Ba (ppm)	Cr (ppm)	Sr (ppm)	Zr (ppm)
178.57	3.32	0.21	2.46	298	125	159	186
178.77	3.43	0.22	2.57	296	126	162	183
179.17	3.36	0.24	3.02	303	127	168	191
179.37	3.08	0.25	3.31	280	122	161	177
179.57	3.12	0.15	3.04	297	124	166	186
179.77	3.21	0.22	3.02	283	126	170	191
179.79	3.28	0.25	2.83	491	102	144	135
179.99	3.23	0.26	2.90	306	120	195	139
180.19	2.79	0.24	4.68	262	116	167	149
180.39	2.57	0.14	2.46	227	118	138	187
180.91	2.36	0.17	5.58	327	89	148	160
181.11	2.75	0.14	2.39	305	125	140	237
181.31	2.90	0.11	2.30	310	131	151	218
181.51	2.77	0.11	2.17	312	125	144	236
181.71	3.01	0.13	1.45	300	136	156	196
181.79	3.02	0.11	1.20	282	117	181	147
182.29	3.11	0.14	1.08	291	122	141	194
182.79	2.97	0.41	2.94	252	122	157	154
182.88	3.35	0.13	1.16	290	131	156	200
183.38	2.59	0.10	7.15	267	148	175	206
183.88	2.42	0.12	0.95	319	145	148	234
184.01	3.01	0.13	0.69	302	117	173	134
184.51	3.09	0.10	0.61	293	148	148	224
184.91	1.93	0.10	3.55	365	122	196	151
185.41	2.41	0.09	0.94	327	118	177	138
185.75	1.14	0.62	8.87	239	108	117	163
186.25	1.81	0.07	1.09	596	146	97	225
186.83	2.26	0.08	0.38	398	135	168	160
187.33	2.47	0.09	0.51	309	159	113	274
187.83	2.16	0.08	1.57	291	114	197	130
187.88	2.27	0.08	0.79	272	146	110	244
188.38	2.43	0.08	0.89	204	120	163	199
188.88	2.38	0.09	0.68	246	147	105	283
189.01	2.84	0.08	0.43	253	160	113	235
189.51	3.01	0.08	0.31	247	156	117	244
190.01	2.17	0.10	3.93	200	156	129	357
190.15	2.51	0.10	3.16	242	217	140	324
190.65	1.84	0.11	11.93	189	133	133	252
190.91	1.76	0.08	5.09	247	136	117	217
191.41	2.35	0.07	0.61	249	112	175	151
191.94	1.68	0.11	7.69	209	122	139	210
192.44	2.53	0.07	0.27	244	143	116	222
193.07	2.59	0.07	0.18	283	128	148	226
193.57	2.40	0.06	0.48	233	149	104	275
193.57	2.33	0.07	0.27	223	141	102	239

Sample	K$_2$O (wt %)	P$_2$O$_5$ (wt %)	CaCO$_3$ (wt %)	Ba (ppm)	Cr (ppm)	Sr (ppm)	Zr (ppm)
194.02	1.72	0.20	5.91	138	214	149	147
194.52	2.92	0.11	0.40	269	123	145	183
195.02	2.82	0.12	0.13	294	122	123	203
195.18	2.99	0.08	0.20	257	209	107	199
195.68	2.07	0.32	1.20	265	124	222	174
196.18	1.70	0.28	4.53	185	109	116	214
196.27	2.52	0.20	0.58	245	136	107	177
196.40	2.35	0.17	0.33	231	118	105	186
196.90	2.56	0.21	0.56	405	126	198	148
197.40	2.64	0.22	0.64	331	100	267	109
197.46	2.82	0.23	1.33	393	81	315	100
197.97	2.70	0.24	0.72	236	121	113	179
198.47	3.00	0.19	0.54	272	141	118	171
199.11	2.93	0.16	0.21	254	126	113	164
199.61	2.56	0.13	0.48	228	126	101	166
199.96	3.32	0.10	0.18	290	145	118	179
200.39	0.36	0.41	7.72	28	44	75	40
200.89	2.91	0.09	0.88	257	143	111	230
201.09	2.68	0.12	0.97	237	135	116	222
201.59	2.52	0.11	0.60	238	127	111	211
202.01	2.62	0.12	0.44	227	119	112	187
202.51	2.69	0.10	0.34	243	122	115	194
202.65	3.05	0.11	0.29	268	134	116	177
203.01	2.70	0.12	0.35	237	121	109	189
203.58	2.59	0.18	0.66	230	132	115	199
203.70	3.20	0.10	0.24	281	137	116	166
204.30	2.50	0.22	1.02	229	119	114	194
204.66	3.08	0.15	0.78	274	137	119	183
205.16	3.05	0.11	0.41	213	110	143	154
205.48	3.03	0.10	0.11	261	123	113	182
205.65	3.13	0.12	0.25	275	132	113	172
206.15	2.46	0.13	0.22	213	115	106	214
206.67	2.32	0.11	0.63	210	125	99	273
207.37	2.29	0.08	0.86	211	123	116	258
207.57	2.78	0.12	0.63	246	125	121	204
208.07	2.59	0.11	0.55	241	127	110	216
208.57	2.85	0.18	0.37	241	122	117	221
208.63	2.99	0.12	0.15	255	129	122	193
209.17	2.03	0.26	3.32	187	102	100	216
209.67	3.33	0.14	1.07	381	131	177	162
209.80	1.01	0.08	13.51	2313	124	176	491
210.31	2.23	0.09	0.98	329	76	257	81
210.75	2.78	0.11	0.32	282	37	280	80
211.25	2.17	0.12	1.09	213	125	106	236
211.75	1.49	0.18	17.20	147	93	172	204

Sample	K$_2$O (wt %)	P$_2$O$_5$ (wt %)	CaCO$_3$ (wt %)	Ba (ppm)	Cr (ppm)	Sr (ppm)	Zr (ppm)
211.88	1.83	0.18	1.59	193	127	105	279
212.38	1.94	0.12	0.45	204	117	98	224
212.88	2.19	0.12	0.37	216	124	105	220
213.07	1.75	0.14	2.02	221	110	98	261
213.57	2.26	0.12	0.32	229	118	106	217
213.79	0.93	0.13	4.02	223	85	79	291
214.91	1.86	0.16	1.20	226	102	95	268
216.96	1.34	0.13	1.24	311	96	90	321
218.02	0.72	0.11	10.18	273	76	112	185
219.06	2.11	0.14	0.30	229	118	115	299

Appendix H – ICP-MS precision – lithium metaborate preparation

ppm	45 Sc	51 V	52 Cr	55 Mn	59 Co	60 Ni	65 Cu	66 Zn
JLS-1	0.0	1.1	0.2	1.0	0.1	0.4		0.0
JLS-1	0.0	1.0	0.2	1.0	0.1	0.4		0.0
JLS-1	0.0	1.2	0.3	1.2	0.2	0.4		
JLS-1	0.0	0.9	0.2	1.0	0.1	0.3		0.3
mean	0.0	1.1	0.2	1.1	0.1	0.4		0.1
2SD	0.0	0.2	0.1	0.2	0.0	0.1		0.4
%	106.1	19.9	33.3	18.1	28.8	27.4		346.4
MAG-1	0.7	6.3	4.0	30.3	0.9	2.3	0.9	2.8
MAG-1	0.7	6.3	3.9	30.1	0.9	2.2	0.9	3.1
MAG-1	0.8	6.9	4.3	32.9	1.1	2.5	0.8	3.6
MAG-1	0.7	6.0	3.8	28.9	0.9	2.1	0.5	2.7
mean	0.7	6.4	4.0	30.5	0.9	2.2	0.8	3.0
2SD	0.1	0.7	0.4	3.4	0.2	0.3	0.4	0.8
%	12.6	11.2	11.2	11.1	20.5	14.2	56.0	25.5
SCO-1	0.6	6.7	3.0	17.0	0.5	1.5	1.1	1.6
SCO-1	0.5	6.4	2.8	16.3	0.5	1.4	1.2	2.7
SCO-1	0.6	7.0	3.1	17.7	0.6	1.4	0.8	2.0
SCO-1	0.5	6.4	2.8	15.8	0.5	1.2	0.5	1.6
mean	0.5	6.6	2.9	16.7	0.5	1.4	0.9	2.0
2SD	0.1	0.6	0.3	1.7	0.1	0.2	0.6	1.0
%	15.9	9.8	10.6	9.9	16.4	15.7	70.3	52.7
SGR-1	0.2	4.9	1.1	9.0	20.2	9.3	1.9	1.0
SGR-1	0.2	5.6	1.3	10.3	23.0	10.6	2.2	0.9
SGR-1	0.2	5.3	1.2	9.9	24.6	10.3	1.9	1.3
SGR-1	0.2	5.2	1.2	9.5	24.2	9.8	1.5	0.7
mean	0.2	5.3	1.2	9.7	23.0	10.0	1.9	1.0
2SD	0.0	0.6	0.1	1.1	4.0	1.1	0.6	0.5
%	16.0	10.8	10.3	11.6	17.3	11.4	31.4	46.2
W2	1.5	11.5	3.7	52.1	1.6	2.8	3.8	1.0
W2	1.5	11.7	3.7	53.4	1.6	2.9	3.8	1.5
W2	1.5	12.2	3.9	54.8	1.9	3.0	3.8	2.2
W2	1.4	11.4	3.6	51.2	1.8	2.7	2.9	1.7
mean	1.5	11.7	3.7	52.9	1.7	2.8	3.6	1.6
2SD	0.1	0.7	0.2	3.2	0.3	0.2	0.8	1.0
%	4.7	5.8	6.5	6.1	15.3	7.0	23.6	63.7

	71 Ga	71 Ga	85 Rb	88 Sr	92 Nb	95 Mo	133 Cs	137 Ba
JLS-1	0.8	0.0	0.1	12.2	0.3	0.5	0.0	19.3
JLS-1	0.9	0.0	0.1	13.9	0.0	0.1	0.0	20.3
JLS-1	1.1	0.0	0.1	15.1	0.2	0.3		23.1
JLS-1	1.0	0.0	0.1	14.1				19.0
mean	0.9	0.0	0.1	13.8	0.2	0.3	0.0	20.4
2SD	0.2	0.0	0.0	2.4	0.2	0.4	0.0	3.8
%	24.4	275.7	30.7	17.4	146.2	124.8	33.5	18.5
MAG-1	1.5	0.8	4.7	5.3	0.9	0.5	0.2	18.5
MAG-1	1.5	0.8	4.7	5.7	0.8	0.1	0.2	18.6
MAG-1	1.8	1.0	5.4	5.9	1.3	0.4	0.2	19.9
MAG-1	1.6	0.8	4.9	5.7	0.5		0.2	17.6
mean	1.6	0.9	4.9	5.7	0.9	0.3	0.2	18.6
2SD	0.2	0.1	0.7	0.5	0.6	0.4	0.0	1.9
%	14.7	15.7	14.2	9.0	71.5	104.8	15.1	10.0
SCO-1	1.5	0.6	3.8	6.5	1.1	1.1	0.2	22.5
SCO-1	1.5	0.6	3.8	6.7	0.7	0.3	0.2	22.2
SCO-1	1.8	0.7	4.4	7.2	1.0	0.2	0.2	24.3
SCO-1	1.7	0.7	4.0	7.2	0.4		0.2	22.1
mean	1.6	0.7	4.0	6.9	0.8	0.5	0.2	22.8
2SD	0.3	0.1	0.6	0.8	0.6	0.9	0.0	2.1
%	16.2	18.3	14.2	11.3	73.4	174.7	13.6	9.2
SGR-1	0.6	0.3	2.2	13.1	0.6	2.1	0.1	9.2
SGR-1	0.8	0.3	2.6	16.7	0.4	2.1	0.1	10.9
SGR-1	0.8	0.3	2.7	15.7	0.8	2.4	0.1	10.5
SGR-1	0.8	0.3	2.6	17.0		1.7	0.1	10.0
mean	0.7	0.3	2.5	15.6	0.6	2.1	0.1	10.1
2SD	0.1	0.1	0.4	3.5	0.4	0.6	0.0	1.4
%	18.9	18.7	16.8	22.6	76.0	27.2	17.8	13.8
W2	0.9	0.7	0.7	7.2	0.5	0.4	0.0	6.4
W2	0.9	0.7	0.7	8.1	0.4	0.1	0.0	6.6
W2	1.0	0.8	0.8	8.0	0.8	0.4	0.0	6.9
W2	1.0	0.7	0.7	8.2	0.1		0.0	6.4
mean	0.9	0.7	0.7	7.9	0.4	0.3	0.0	6.6
2SD	0.1	0.1	0.1	0.9	0.6	0.4	0.0	0.5
%	14.2	13.1	13.7	12.0	129.5	109.0	27.6	7.2

Appendix I – ICP-MS precision – aqua regia preparation

ppm	51 V	55 Mn	59 Co	60 Ni	63 Cu	65 Cu	68 Zn
JLS-1	0.26	1.20	0.01	0.10	0.29	0.29	4.02
JLS-1	0.23	1.26	0.02	0.00	0.00	0.00	0.87
JLS-1	0.14	1.49	0.01	0.05	0.07	0.08	3.72
JLS-1	0.12	1.31	0.01	0.05	0.07	0.07	3.61
mean	0.19	1.32	0.01	0.05	0.11	0.11	3.05
2SD	0.13	0.25	0.01	0.08	0.25	0.25	2.94
%	70.3	19.2	114.8	162.1	233.2	224.8	96.2
MAG-1	4.90	54.76	1.61	3.59	2.23	2.21	10.83
MAG-1	4.55	51.84	1.51	3.25	1.39	1.40	2.54
MAG-1	4.82	55.14	1.42	3.65	2.12	2.11	10.60
MAG-1	4.11	47.87	1.21	3.10	1.82	1.80	9.32
mean	4.60	52.40	1.44	3.40	1.89	1.88	8.32
2SD	0.71	6.72	0.33	0.53	0.75	0.73	7.83
%	15.5	12.8	23.3	15.6	39.6	38.9	94.0
SCO-1	2.61	31.30	0.84	1.83	2.32	2.31	8.62
SCO-1	2.42	29.49	0.81	1.53	1.45	1.46	1.92
SCO-1	2.87	36.68	0.88	2.09	2.49	2.49	9.15
SCO-1	2.19	28.59	0.68	1.63	1.91	1.91	7.27
mean	2.52	31.52	0.80	1.77	2.04	2.04	6.74
2SD	0.58	7.24	0.17	0.50	0.92	0.91	6.62
%	22.9	23.0	21.1	28.1	45.2	44.6	98.3
SGR-1	6.56	19.06	0.92	2.29	4.92	4.90	8.86
SGR-1	6.20	18.09	0.87	2.02	4.04	4.06	2.02
SGR-1	6.57	19.21	0.81	2.29	4.80	4.80	8.39
SGR-1	5.84	17.51	0.73	2.05	4.27	4.25	7.87
mean	6.29	18.47	0.83	2.16	4.51	4.50	6.78
2SD	0.69	1.61	0.16	0.30	0.84	0.82	6.40
%	11.0	8.7	18.8	13.7	18.5	18.2	94.4

	75 As	77 Se	95 Mo	98 Mo	111 Cd	121 Sb	123 Sb
JLS-1	0.09	0.06	1.96	1.63	0.03	0.04	0.04
JLS-1	0.04	0.07	0.00	0.00	0.04	0.02	0.02
JLS-1	0.03	0.02	0.77	0.72	0.02	0.01	0.01
JLS-1	0.03	0.01	0.32	0.30	0.02	0.01	0.01
mean	0.05	0.04	0.76	0.66	0.03	0.02	0.02
2SD	0.06	0.06	1.72	1.41	0.02	0.03	0.03
%	124.2	148.2	224.9	213.7	68.6	149.6	169.6
MAG-1	0.64	0.36	1.50	1.25	0.03	0.04	0.03
MAG-1	0.55	0.35	0.00	0.00	0.02	0.01	0.01
MAG-1	0.59	0.32	0.94	0.87	0.02	0.02	0.02
MAG-1	0.50	0.35	0.24	0.23	0.01	0.01	0.01
mean	0.57	0.35	0.67	0.59	0.02	0.02	0.02
2SD	0.12	0.04	1.36	1.15	0.02	0.03	0.02
%	20.7	10.7	203.3	194.6	78.2	126.2	134.3
SCO-1	0.96	0.30	1.47	1.21	0.03	0.03	0.03
SCO-1	0.88	0.23	0.00	0.00	0.02	0.01	0.01
SCO-1	1.02	0.27	0.62	0.57	0.02	0.02	0.02
SCO-1	0.81	0.21	0.24	0.22	0.01	0.01	0.01
mean	0.92	0.25	0.58	0.50	0.02	0.02	0.02
2SD	0.18	0.08	1.29	1.05	0.02	0.02	0.02
%	20.0	30.1	220.9	210.1	77.4	122.9	132.7
SGR-1	4.76	0.22	4.21	3.54	0.09	0.10	0.10
SGR-1	4.41	0.23	2.52	2.12	0.09	0.07	0.07
SGR-1	4.48	0.17	3.94	3.69	0.09	0.09	0.08
SGR-1	4.01	0.19	2.88	2.71	0.07	0.07	0.07
mean	4.41	0.20	3.39	3.02	0.08	0.08	0.08
2SD	0.62	0.05	1.63	1.48	0.02	0.03	0.03
%	14.0	25.7	48.0	48.9	20.5	35.7	38.0

Appendix J – ICP-MS precision – rare earth elements run

ppm	89 Y	90 Zr	93 Nb	139 La	140 Ce	141 Pr	143 Nd	145 Nd
JLS-1	0.05	0.16	0.16	0.09	0.10	0.01	0.04	0.04
JLS-1	0.06	0.20	0.11	0.09	0.10	0.01	0.04	0.04
JLS-1	0.05	0.14	0.59	0.08	0.10	0.01	0.04	0.04
JLS-1	0.04	0.14	0.16	0.08	0.09	0.01	0.04	0.04
mean	0.05	0.16	0.26	0.09	0.10	0.01	0.04	0.04
2SD	0.02	0.06	0.45	0.01	0.01	0.00	0.00	0.00
%	35.12	37.41	175.19	16.23	10.07	22.21	4.59	6.62
MAG-1	1.03	4.65	0.81	1.72	3.42	0.39	1.44	1.43
MAG-1	1.24	4.82	0.91	1.76	3.46	0.40	1.49	1.48
MAG-1	0.92	4.85	0.80	1.57	3.11	0.36	1.47	1.45
MAG-1	0.94	4.80	1.07	1.59	3.13	0.36	1.45	1.43
mean	1.03	4.78	0.90	1.66	3.28	0.38	1.46	1.45
2SD	0.30	0.18	0.25	0.19	0.37	0.04	0.04	0.04
%	28.65	3.81	27.84	11.40	11.34	10.47	2.68	2.82
SCO-1	1.03	7.06	0.79	1.36	2.56	0.30	1.11	1.09
SCO-1	1.24	7.12	0.81	1.35	2.55	0.29	1.12	1.10
SCO-1	0.86	6.77	0.60	1.15	2.17	0.25	1.06	1.06
SCO-1	0.92	7.04	0.91	1.22	2.26	0.27	1.08	1.07
mean	1.01	7.00	0.78	1.27	2.39	0.28	1.09	1.08
2SD	0.33	0.31	0.25	0.20	0.39	0.04	0.05	0.04
%	32.48	4.37	32.69	15.95	16.41	14.93	4.77	3.25
SGR-1	0.38	1.97	0.43	0.75	1.65	0.15	0.60	0.58
SGR-1	0.47	2.08	0.44	0.76	1.68	0.15	0.61	0.62
SGR-1	0.34	2.07	0.31	0.68	1.51	0.14	0.60	0.61
SGR-1	0.35	2.05	0.64	0.69	1.52	0.14	0.60	0.59
mean	0.39	2.04	0.46	0.72	1.59	0.15	0.60	0.60
2SD	0.12	0.09	0.27	0.08	0.18	0.02	0.01	0.03
%	30.89	4.65	59.74	10.80	11.25	10.38	2.16	5.26

	146 Nd	147 Sm	149 Sm	151 Eu	153 Eu	157 Gd	159 Tb	161 Dy
JLS-1	0.04	0.00	0.005	0.002	0.005	0.008	0.001	0.007
JLS-1	0.04	0.00	0.004	0.002	0.005	0.008	0.001	0.008
JLS-1	0.04	0.01	0.008	0.006	0.007	0.013	0.004	0.011
JLS-1	0.04	0.00	0.005	0.002	0.005	0.009	0.001	0.008
mean	0.04	0.01	0.006	0.003	0.005	0.009	0.002	0.009
2SD	0.00	0.00	0.004	0.004	0.002	0.005	0.003	0.003
%	11.46	58.03	69.30	119.74	45.43	51.51	205.20	35.73
MAG-1	1.36	0.27	0.265	0.055	0.058	0.241	0.030	0.192
MAG-1	1.39	0.27	0.275	0.057	0.068	0.246	0.030	0.194
MAG-1	1.46	0.28	0.284	0.057	0.058	0.247	0.033	0.200
MAG-1	1.43	0.28	0.278	0.053	0.053	0.259	0.035	0.201
mean	1.41	0.27	0.275	0.055	0.059	0.248	0.032	0.197
2SD	0.09	0.02	0.015	0.003	0.013	0.015	0.005	0.009
%	6.57	6.22	5.59	6.27	21.30	6.08	14.49	4.75
SCO-1	1.04	0.20	0.198	0.047	0.050	0.201	0.026	0.171
SCO-1	1.06	0.20	0.198	0.047	0.057	0.199	0.025	0.166
SCO-1	1.06	0.20	0.205	0.046	0.048	0.196	0.026	0.168
SCO-1	1.07	0.20	0.207	0.047	0.044	0.207	0.030	0.172
mean	1.06	0.20	0.202	0.046	0.050	0.201	0.026	0.169
2SD	0.03	0.00	0.009	0.001	0.010	0.009	0.004	0.005
%	2.44	0.65	4.49	2.32	20.89	4.32	16.27	3.01
SGR-1	0.56	0.09	0.088	0.018	0.020	0.084	0.010	0.065
SGR-1	0.59	0.09	0.092	0.018	0.023	0.084	0.010	0.065
SGR-1	0.61	0.09	0.095	0.019	0.020	0.087	0.011	0.068
SGR-1	0.60	0.10	0.097	0.018	0.019	0.091	0.013	0.071
mean	0.59	0.09	0.093	0.018	0.021	0.087	0.011	0.067
2SD	0.05	0.01	0.008	0.001	0.004	0.007	0.002	0.006
%	7.64	6.34	8.46	5.41	17.92	7.73	19.83	8.26

	163 Dy	165 Ho	166 Er	166 Er	169 Tm	172 Yb	173 Yb	175 Lu
JLS-1	0.007	0.001	0.004	0.004	0.000	0.001	0.001	0.000
JLS-1	0.009	0.001	0.004	0.004	0.000	0.001	0.001	0.000
JLS-1	0.011	0.005	0.007	0.007	0.003	0.004	0.005	0.003
JLS-1	0.007	0.001	0.004	0.004	0.000	0.001	0.002	0.000
mean	0.008	0.002	0.005	0.005	0.001	0.002	0.002	0.001
2SD	0.003	0.003	0.003	0.003	0.003	0.003	0.004	0.003
%	40.66	163.31	71.23	55.30	326.567	167.009	165.284	299.250
MAG-1	0.193	0.034	0.108	0.106	0.013	0.097	0.093	0.012
MAG-1	0.202	0.033	0.111	0.109	0.012	0.100	0.094	0.013
MAG-1	0.195	0.035	0.113	0.108	0.013	0.099	0.101	0.013
MAG-1	0.196	0.037	0.110	0.108	0.015	0.096	0.100	0.015
mean	0.197	0.035	0.110	0.108	0.013	0.098	0.097	0.013
2SD	0.007	0.004	0.004	0.003	0.002	0.004	0.008	0.002
%	3.68	10.02	3.96	3.01	13.400	3.683	7.989	15.750
SCO-1	0.170	0.031	0.106	0.103	0.012	0.095	0.093	0.013
SCO-1	0.171	0.031	0.105	0.104	0.012	0.096	0.091	0.013
SCO-1	0.164	0.031	0.101	0.099	0.013	0.090	0.091	0.013
SCO-1	0.169	0.034	0.103	0.101	0.014	0.096	0.096	0.015
mean	0.169	0.032	0.104	0.102	0.013	0.094	0.093	0.013
2SD	0.007	0.003	0.004	0.004	0.001	0.005	0.005	0.002
%	3.89	10.38	4.05	4.31	10.063	5.433	5.236	15.227
SGR-1	0.064	0.012	0.039	0.038	0.005	0.036	0.032	0.005
SGR-1	0.067	0.012	0.042	0.040	0.005	0.038	0.036	0.005
SGR-1	0.063	0.012	0.040	0.038	0.005	0.037	0.038	0.005
SGR-1	0.067	0.013	0.041	0.040	0.006	0.037	0.038	0.006
mean	0.065	0.012	0.041	0.039	0.005	0.037	0.036	0.005
2SD	0.004	0.001	0.002	0.003	0.001	0.002	0.005	0.001
%	5.81	10.31	5.10	6.49	18.051	4.514	15.300	25.215

	177 Hf	178 Hf	179 Hf	181 Ta	232 Th	238 U
JLS-1	0.014	0.014	0.014	0.013	0.011	0.066
JLS-1	0.012	0.013	0.012	0.042	0.011	0.066
JLS-1	0.035	0.035	0.035	0.047	0.021	0.068
JLS-1	0.052	0.050	0.049	0.006	0.018	0.065
mean	0.028	0.028	0.028	0.027	0.015	0.066
2SD	0.038	0.036	0.035	0.041	0.010	0.003
%	135.114	127.416	126.888	153.277	68.580	3.889
MAG-1	0.132	0.145	0.130	0.115	0.465	0.095
MAG-1	0.141	0.149	0.139	0.149	0.469	0.094
MAG-1	0.155	0.152	0.158	0.236	0.414	0.098
MAG-1	0.150	0.149	0.151	0.222	0.424	0.102
mean	0.144	0.149	0.145	0.180	0.443	0.097
2SD	0.020	0.006	0.024	0.116	0.056	0.007
%	14.107	4.053	16.757	64.157	12.750	7.394
SCO-1	0.193	0.204	0.189	0.102	0.407	0.114
SCO-1	0.195	0.210	0.199	0.126	0.393	0.111
SCO-1	0.182	0.182	0.183	0.176	0.328	0.110
SCO-1	0.190	0.192	0.191	0.202	0.350	0.120
mean	0.190	0.197	0.191	0.152	0.370	0.114
2SD	0.012	0.025	0.014	0.091	0.074	0.009
%	6.231	12.623	7.225	60.343	19.975	8.170
SGR-1	0.070	0.072	0.069	0.037	0.186	0.174
SGR-1	0.075	0.081	0.075	0.055	0.182	0.174
SGR-1	0.078	0.078	0.080	0.071	0.158	0.182
SGR-1	0.074	0.075	0.074	0.119	0.167	0.186
mean	0.074	0.076	0.075	0.070	0.173	0.179
2SD	0.007	0.008	0.009	0.071	0.026	0.011
%	9.620	9.843	11.465	100.662	14.884	6.377

Appendix K – ICP-MS Data – lithium metaborate preparation

Sample	Sc (ppm)	Cr (ppm)	Rb (ppm)	Sr (ppm)	Nb (ppm)	Cs (ppm)	Ba (ppm)
126.18	0.89	1.38	1.13	29.84	0.00	0.05	6.67
127.26	0.83	5.41	5.16	7.32	1.27	0.26	13.68
128.33	0.86	5.77	5.79	7.68	1.38	0.30	14.65
129.15	1.01	6.33	6.22	8.51	1.53	0.31	16.26
130.25	0.72	4.87	4.92	7.05	1.13	0.25	12.40
131.25	0.96	5.94	6.08	7.37	1.43	0.31	14.85
132.15	0.73	5.16	5.34	6.19	1.12	0.28	12.55
133.30	0.88	5.72	5.79	7.91	1.46	0.30	15.31
133.65	0.86	5.66	6.05	7.73	1.39	0.32	14.82
134.60	0.87	5.32	5.53	6.99	1.34	0.30	13.19
135.60	0.84	5.39	5.74	7.11	1.36	0.31	14.24
136.60	0.98	5.97	6.17	7.62	1.42	0.32	14.36
136.65	0.97	5.98	5.52	6.65	1.18	0.31	14.61
137.61	0.90	4.89	5.09	6.76	1.16	0.28	12.39
138.75	0.96	5.30	5.45	8.34	1.66	0.30	13.54
139.44	0.89	5.93	6.04	7.67	1.40	0.33	14.13
140.50	1.06	5.47	5.47	8.27	1.15	0.29	13.08
141.60	0.66	7.42	2.51	4.55	2.99	0.09	8.08
142.65	0.91	5.33	5.17	8.47	1.14	0.26	13.27
143.78	1.02	6.13	6.18	7.66	1.50	0.31	17.22
144.84	0.89	5.30	5.49	6.80	1.17	0.27	14.24
145.69	0.91	5.76	5.75	6.99	1.22	0.28	15.28
146.69	1.10	6.93	6.87	8.26	1.77	0.35	19.57
146.82	1.05	7.07	7.07	7.80	1.65	0.36	18.54
147.94	0.91	5.70	6.07	7.51	1.27	0.32	15.81
148.85	0.99	5.89	6.18	7.62	1.27	0.33	14.96
151.07	0.86	5.64	5.82	7.21	1.14	0.29	15.74
151.87	0.93	5.09	5.40	8.45	0.98	0.26	12.67
152.37	0.91	5.08	5.40	10.29	1.01	0.28	14.02
152.87	1.00	5.78	5.75	17.00	1.16	0.27	15.95
153.98	0.83	5.30	5.48	19.99	1.00	0.27	14.27
156.05	0.81	4.45	4.45	19.06	0.82	0.25	17.66
157.97	0.82	4.96	5.57	13.24	1.12	0.30	13.27
158.94	0.85	5.06	5.56	9.45	1.12	0.28	13.65
160.07	0.88	5.66	5.46	12.85	2.83	0.28	14.37
161.00	0.78	4.78	5.13	11.34	0.87	0.26	13.30
161.58	0.93	5.81	5.54	17.19	2.56	0.26	15.84
162.72	0.85	5.31	5.74	12.90	1.30	0.30	17.36
163.77	0.80	4.48	4.61	16.24	0.91	0.21	35.46
164.91	0.60	3.60	3.55	19.13	0.56	0.15	13.95
166.04	0.83	4.65	4.54	10.12	0.89	0.21	13.22

Sample	Sc (ppm)	Cr (ppm)	Rb (ppm)	Sr (ppm)	Nb (ppm)	Cs (ppm)	Ba (ppm)
167.11	0.81	4.15	4.45	6.95	0.84	0.19	15.11
167.89	0.16	0.73	0.67	12.46	0.00	0.01	17.32
168.99	0.93	4.68	4.83	8.17	1.09	0.19	34.13
170.08	0.81	4.48	5.16	5.83	0.92	0.23	11.30
171.21	0.73	4.62	4.36	5.50	0.90	0.18	10.40
172.31	0.83	4.98	4.80	5.97	1.04	0.23	10.10
173.20	0.87	5.38	4.65	5.36	1.25	0.22	10.39
174.23	0.94	5.79	5.16	6.70	1.44	0.25	12.87
175.26	0.79	5.17	4.52	5.74	1.18	0.20	13.63
176.24	0.90	5.56	4.82	5.86	1.14	0.26	12.00
176.71	0.98	6.31	6.06	7.42	1.67	0.29	14.01
177.77	0.95	5.64	5.54	6.73	1.38	0.25	12.25
178.77	0.94	5.68	5.84	6.74	1.69	0.29	12.23
179.79	0.80	4.76	4.67	5.93	1.19	0.22	9.96
180.91	0.70	3.64	3.98	5.90	0.62	0.16	12.84
181.79	0.91	5.76	5.17	6.27	1.45	0.24	12.22
182.88	0.98	5.92	5.41	6.43	1.42	0.24	11.80
184.07	0.97	6.63	5.30	6.44	1.43	0.24	11.85
184.91	0.84	7.39	3.09	6.04	1.00	0.12	18.63
185.75	0.62	4.36	1.62	4.67	0.67	0.06	9.41
186.83	0.76	6.56	3.34	4.53	1.09	0.13	11.89
187.88	0.81	6.15	3.58	4.78	0.99	0.14	10.41
189.01	0.92	7.00	4.70	5.40	1.29	0.22	10.75
190.01	0.77	7.01	3.32	5.20	1.07	0.14	8.50
190.15	0.94	9.54	4.04	6.16	1.42	0.18	10.30
190.91	0.82	7.02	2.69	5.10	1.46	0.10	8.31
191.94	0.82	6.29	3.42	4.58	1.21	0.16	9.98
193.07	0.95	6.82	4.25	4.85	1.32	0.20	10.67
194.02	1.16	8.49	2.44	5.78	0.90	0.10	5.45
195.18	0.87	8.42	4.53	4.38	1.16	0.26	9.79
196.27	0.91	5.83	4.17	4.74	1.15	0.24	10.25
196.40	0.80	5.34	3.42	4.37	0.96	0.19	10.03
197.46	1.02	6.01	4.81	5.49	1.25	0.28	10.85
197.97	0.89	5.21	3.80	4.49	0.88	0.23	9.66
199.11	1.03	6.00	5.10	5.13	1.00	0.30	11.50
199.96	1.18	6.76	5.80	5.50	1.28	0.33	12.58
200.39	0.28	1.62	0.61	3.25	0.33	0.03	1.72
201.09	0.72	5.56	4.11	4.60	1.28	0.23	9.51
202.07	0.98	6.15	4.82	5.56	1.32	0.25	11.45
202.65	1.08	6.28	4.78	5.17	0.96	0.30	11.51
203.70	0.91	5.36	4.32	4.49	1.00	0.27	10.38
204.66	1.04	6.23	5.16	5.48	1.28	0.28	11.73
205.48	0.89	5.33	4.79	4.77	1.08	0.26	10.82
205.65	0.94	5.28	4.33	4.50	1.02	0.27	10.38

Sample	Sc (ppm)	Cr (ppm)	Rb (ppm)	Sr (ppm)	Nb (ppm)	Cs (ppm)	Ba (ppm)
207.57	0.97	5.68	4.16	5.19	0.97	0.23	10.49
208.63	0.99	5.86	4.49	4.90	1.06	0.27	10.71
209.80	0.64	5.50	1.67	7.42	0.57	0.04	103.18
210.75	0.91	5.55	4.14	5.06	1.05	0.24	10.19
211.88	0.70	5.92	3.01	4.54	1.02	0.12	8.63
213.07	0.91	5.77	3.14	5.09	1.01	0.16	11.22
213.79	0.58	3.73	1.24	3.28	0.49	0.06	9.07
214.91	0.93	5.12	3.10	4.54	1.12	0.15	10.91
216.96	0.75	4.73	2.14	4.17	0.65	0.08	13.54
218.02	0.56	3.89	1.21	5.55	0.45	0.03	13.56
219.06	0.70	5.10	3.11	4.70	1.07	0.14	9.57

Appendix L – ICP-MS data – aqua regia preparation

Sample	V (ppm)	Mn (ppm)	Co (ppm)	Ni (ppm)	Cu (ppm)	Zn (ppm)	As (ppm)	Se (ppm)	Mo (ppm)	Cd (ppm)	Sb (ppm)
126.18	0.39	41.79	0.33	2.04	0.89	18.15	0.30	0.92	0.47	0.03	0.01
127.26	1.14	10.12	1.12	3.78	3.72	7.88	1.54	0.20	0.33	0.03	0.00
128.33	0.99	9.47	1.00	3.52	2.03	5.72	0.75	0.22	0.23	0.04	0.00
129.15	0.91	10.44	1.07	3.97	2.13	6.27	0.96	0.21	0.36	0.02	0.01
130.25	0.89	10.57	1.10	4.42	2.14	6.05	1.56	0.20	0.35	0.03	0.00
131.25	0.81	9.99	0.98	3.81	2.09	7.96	0.81	0.30	0.56	0.02	0.01
132.15	0.91	10.71	0.98	3.94	2.35	5.56	0.54	0.22	0.39	0.02	0.00
133.30	0.85	9.76	1.09	4.05	2.33	6.58	1.15	0.22	0.23	0.02	0.00
134.60	0.95	10.49	0.99	3.96	2.28	5.55	1.04	0.24	0.51	0.02	0.01
135.60	0.86	9.34	0.95	3.84	2.20	5.81	0.57	0.16	0.56	0.02	0.01
136.60	1.01	9.67	1.12	4.38	2.43	6.07	0.67	0.19	0.60	0.04	0.01
136.65	0.99	10.12	1.11	4.35	2.51	6.22	0.62	0.17	0.40	0.03	0.00
137.61	1.24	30.94	0.80	3.27	1.83	5.57	0.57	0.25	0.96	0.02	0.01
138.75	0.84	10.64	0.99	4.39	2.23	20.46	0.79	0.49	1.05	0.10	0.01
139.44	0.93	10.94	1.15	4.55	2.47	7.50	0.77	0.26	0.75	0.03	0.01
140.50	0.87	12.09	1.02	4.05	2.20	7.24	0.63	0.50	0.64	0.03	0.00
141.60	0.92	11.48	1.11	4.45	2.27	7.79	0.58	0.23	0.78	0.05	0.01
142.65	0.99	14.33	1.03	4.97	2.29	9.56	0.89	0.32	2.01	0.07	0.01
143.78	1.02	12.21	1.03	4.55	2.63	6.62	0.48	0.34	0.85	0.02	0.01
144.84	1.01	11.30	1.06	4.68	2.59	7.45	0.58	0.22	0.50	0.03	0.00
145.69	1.09	12.43	1.15	4.92	2.81	6.62	0.51	0.31	0.51	0.03	0.00
146.82	0.94	10.50	1.12	4.27	2.38	83.71	0.45	0.21	0.40	0.03	0.00
147.94	1.10	13.04	1.23	5.09	2.70	10.87	0.54	0.25	0.77	0.04	0.00
149.96	0.92	10.28	0.95	3.93	2.06	6.59	0.41	0.17	0.43	0.04	0.01
151.07	0.96	10.95	0.98	4.01	2.22	6.71	0.43	0.24	0.46	0.03	0.00
151.81	1.09	14.32	1.49	6.72	2.72	20.74	1.41	0.34	1.93	0.10	0.01
152.37	0.98	14.04	1.30	5.34	2.42	5.68	0.94	0.41	1.55	0.03	0.00
152.87	1.00	12.50	1.37	6.00	2.28	14.21	1.30	0.36	2.16	0.06	0.01
153.98	1.14	17.50	1.15	5.87	1.94	6.60	1.52	0.22	1.89	0.03	0.01
154.80	1.15	14.04	1.39	6.58	2.65	9.80	1.40	0.24	1.97	0.04	0.01
155.93	1.05	12.58	1.27	5.65	2.30	8.62	1.30	0.29	2.24	0.06	0.01
157.00	1.52	21.52	1.21	5.98	2.13	8.41	1.37	0.31	2.15	0.04	0.01
157.97	1.12	11.52	1.54	6.02	2.51	9.01	1.44	0.19	1.84	0.05	0.01
158.94	1.31	13.64	1.72	6.80	3.36	15.56	1.54	0.27	2.04	0.11	0.01
160.07	1.21	13.87	1.62	6.50	2.92	13.48	1.43	0.33	1.97	0.08	0.00
161.00	1.37	13.55	1.51	7.41	2.86	7.19	1.90	0.35	3.09	0.03	0.01
161.58	1.13	14.09	1.57	7.68	2.88	8.79	2.00	0.31	3.29	0.04	0.01
162.72	1.15	12.56	1.61	7.17	2.99	8.99	1.63	0.32	4.43	0.03	0.01
163.77	1.03	15.15	1.50	7.70	2.45	46.38	2.18	0.26	2.15	0.38	0.01
164.91	2.20	44.79	1.18	4.15	3.44	15.64	1.31	0.34	1.71	0.14	0.01
166.04	0.83	14.92	1.85	4.93	3.59	6.99	1.67	0.33	0.67	0.04	0.01
167.11	2.00	23.14	2.51	6.70	7.63	9.97	1.97	0.35	1.13	0.06	0.01

Sample	V (ppm)	Mn (ppm)	Co (ppm)	Ni (ppm)	Cu (ppm)	Zn (ppm)	As (ppm)	Se (ppm)	Mo (ppm)	Cd (ppm)	Sb (ppm)
167.89	2.14	97.85	0.44	1.21	1.46	3.52	0.23	0.09	0.53	0.04	0.01
168.99	1.40	24.87	1.83	5.74	6.99	24.31	1.37	0.64	0.94	0.26	0.01
170.08	0.86	15.75	1.43	4.70	3.54	4.76	1.30	0.19	0.45	0.03	0.00
171.21	1.05	19.93	1.71	4.76	4.01	6.40	1.40	0.16	0.70	0.03	0.00
172.31	0.98	21.22	1.42	4.54	3.16	8.45	1.02	0.27	0.52	0.05	0.00
173.20	1.46	23.69	1.85	7.04	4.56	8.10	1.60	0.35	0.67	0.04	0.00
174.23	1.08	19.56	1.16	4.13	2.57	4.78	0.56	0.33	0.32	0.03	0.00
175.26	0.99	16.78	1.06	2.84	1.71	4.66	0.89	0.17	0.43	0.00	0.01
176.24	1.28	19.59	1.41	4.34	2.61	7.90	0.79	0.26	0.43	0.02	0.01
176.71	1.34	16.22	1.25	3.14	3.03	6.62	1.09	0.21	0.22	0.02	0.01
177.77	1.92	28.30	1.28	4.10	2.84	5.91	0.85	0.30	0.18	0.03	0.00
178.77	1.49	19.78	1.26	3.40	2.32	7.02	0.59	0.29	0.17	0.03	0.00
179.79	1.72	22.86	1.43	3.59	2.95	10.59	0.73	0.43	0.24	0.03	0.00
180.91	1.54	18.39	1.74	3.61	2.33	6.96	1.17	0.33	0.26	0.03	0.01
181.79	1.54	19.71	2.14	3.97	2.96	7.56	1.41	0.19	0.23	0.03	0.00
182.88	1.58	17.62	1.72	4.34	2.64	6.66	1.47	0.11	0.25	0.03	0.00
184.01	1.61	25.80	1.62	4.35	2.76	6.05	0.79	0.22	0.22	0.04	0.00
184.91	1.20	20.95	1.33	1.95	1.08	7.16	2.24	0.12	0.33	0.01	0.01
185.75	5.81	146.8	0.69	1.73	1.82	5.95	0.96	0.59	0.16	0.03	0.00
186.83	2.22	16.66	1.68	4.81	2.37	6.91	1.04	0.08	0.20	0.02	0.00
187.88	2.01	16.05	3.65	10.77	3.09	9.24	3.02	0.09	0.46	0.04	0.01
189.07	1.94	14.24	1.65	5.51	2.20	5.65	1.49	0.06	0.36	0.01	0.01
190.01	1.85	29.57	1.23	3.81	1.74	4.68	1.00	0.17	0.36	0.01	0.01
190.15	2.17	18.81	1.35	4.54	3.62	9.91	1.07	0.25	0.24	0.02	0.00
190.91	1.63	35.09	1.02	3.73	1.72	5.35	0.81	0.15	0.27	0.02	0.01
191.94	2.78	19.20	2.23	6.13	2.60	16.40	1.86	0.14	0.57	0.05	0.01
193.07	2.35	10.68	1.68	4.65	2.32	6.66	1.67	0.09	0.40	0.03	0.01
194.02	17.88	240.4	1.95	4.66	1.26	13.95	2.63	0.32	0.23	0.03	0.01
195.18	14.16	14.61	3.06	6.84	4.13	7.21	11.64	0.09	0.69	0.03	0.01
196.27	3.12	23.27	1.63	5.39	2.29	8.22	1.40	0.26	0.32	0.03	0.01
196.40	3.19	17.66	1.26	4.19	1.91	6.96	1.19	0.22	0.19	0.02	0.00
197.46	3.52	20.08	1.93	6.43	3.70	8.42	2.39	0.36	0.30	0.04	0.01
197.97	4.08	20.28	2.33	6.49	4.20	9.77	2.27	0.39	0.29	0.03	0.01
199.11	3.60	16.86	1.71	5.34	3.19	8.49	1.81	0.27	0.33	0.03	0.01
199.96	3.30	14.43	1.65	5.25	3.31	7.42	1.91	0.17	0.21	0.03	0.00
200.39	9.88	387.1	0.27	0.58	0.18	1.70	0.50	0.11	0.25	0.02	0.00
201.09	2.58	18.50	1.80	3.94	1.91	5.82	2.03	0.11	0.31	0.02	0.00
202.07	2.53	16.22	2.16	5.99	2.26	7.69	1.62	0.09	0.68	0.03	0.01
202.65	2.50	20.10	1.36	4.23	2.51	9.05	1.50	0.11	0.29	0.02	0.01
203.70	2.24	12.80	1.39	4.24	2.52	5.43	1.27	0.12	0.35	0.02	0.01
204.66	3.16	19.94	1.66	5.25	2.81	8.05	1.44	0.22	0.25	0.04	0.01
205.48	2.65	15.32	1.69	5.20	3.07	8.47	1.51	0.12	0.46	0.02	0.01
205.65	2.53	15.05	1.48	4.81	2.97	6.50	1.20	0.14	0.25	0.03	0.00
207.57	2.45	11.52	1.47	3.94	2.18	6.44	1.39	0.12	0.58	0.02	0.01

Sample	V (ppm)	Mn (ppm)	Co (ppm)	Ni (ppm)	Cu (ppm)	Zn (ppm)	As (ppm)	Se (ppm)	Mo (ppm)	Cd (ppm)	Sb (ppm)
208.63	1.84	8.94	1.25	3.50	1.93	5.12	0.98	0.10	0.29	0.02	0.01
209.80	1.97	54.04	0.39	1.19	0.47	17.13	0.37	0.16	0.43	0.02	0.01
210.75	2.82	13.11	1.98	5.99	2.29	8.58	1.70	0.13	0.39	0.03	0.00
211.88	3.73	30.47	1.59	4.03	1.93	12.46	1.49	0.32	0.27	0.04	0.01
213.57	2.21	11.57	1.49	3.93	1.47	5.19	1.27	0.14	0.41	0.03	0.01
213.79	2.24	24.16	0.76	2.52	2.43	18.90	0.55	0.19	0.15	0.03	0.00
214.91	2.53	11.97	1.31	3.64	2.38	6.24	0.87	0.25	0.41	0.02	0.01
218.02	2.35	55.26	1.85	7.26	1.43	4.89	1.50	0.16	0.20	0.03	0.01
219.06	3.52	16.83	1.78	4.24	2.00	8.04	1.46	0.16	0.32	0.03	0.01

Sample	Hf (ppm)	Ta (ppm)	Th (ppm)	U (ppm)
126.18	0.03	0.04	0.13	0.05
127.26	0.20	0.32	0.58	0.12
128.33	0.18	0.31	0.60	0.12
129.15	0.21	0.34	0.62	0.13
130.25	0.18	0.30	0.55	0.12
131.25	0.16	0.29	0.55	0.12
132.15	0.17	0.27	0.57	0.12
133.30	0.19	0.33	0.58	0.13
133.65	0.16	0.34	0.55	0.12
134.60	0.19	0.32	0.59	0.13
135.60	0.18	0.27	0.55	0.12
136.60	0.17	0.25	0.55	0.12
136.65	0.20	0.18	0.74	0.13
137.61	0.15	0.31	0.51	0.13
138.75	0.17	0.15	0.65	0.14
138.75	0.17	0.37	0.56	0.15
139.44	0.18	0.28	0.56	0.13
140.50	0.16	0.27	0.56	0.14
141.60	0.39	0.26	0.54	0.10
142.65	0.16	0.28	0.52	0.17
143.78	0.20	0.30	0.56	0.13
144.84	0.16	0.23	0.54	0.12
145.69	0.19	0.33	0.56	0.12
146.69	0.18	0.22	0.54	0.12
146.69	0.16	0.26	0.53	0.12
146.82	0.18	0.17	0.70	0.13
146.82	0.17	0.28	0.54	0.12
147.94	0.16	0.30	0.54	0.12
148.85	0.18	0.25	0.51	0.11
151.07	0.18	0.28	0.61	0.15
151.87	0.15	0.29	0.50	0.16
152.37	0.14	0.25	0.46	0.17
152.87	0.16	0.35	0.52	0.17
153.98	0.15	0.26	0.49	0.18
155.93	0.17	0.27	0.49	0.14
156.05	0.16	0.14	0.60	0.24
157.97	0.15	0.31	0.52	0.16
158.94	0.15	0.36	0.50	0.15
160.07	0.16	0.33	0.51	0.16
161.00	0.13	0.12	0.52	0.21
161.58	0.16	0.18	0.58	0.22
162.72	0.16	0.17	0.54	0.19
163.77	0.16	0.15	0.61	0.22
164.91	0.10	0.08	0.41	0.15
166.04	0.16	0.17	0.55	0.16

Sample	Hf (ppm)	Ta (ppm)	Th (ppm)	U (ppm)
167.11	0.14	0.15	0.46	0.23
167.89	0.06	0.07	0.07	0.09
168.99	0.16	0.32	0.40	0.26
170.08	0.14	0.34	0.48	0.17
171.21	0.15	0.35	0.48	0.17
172.31	0.18	0.31	0.54	0.17
173.20	0.17	0.16	0.58	0.13
174.23	0.19	0.15	0.63	0.11
174.23	0.19	0.27	0.57	0.12
175.26	0.21	0.16	0.62	0.11
176.24	0.21	0.16	0.71	0.12
176.71	0.18	0.14	0.63	0.10
177.77	0.20	0.19	0.70	0.12
178.77	0.19	0.18	0.62	0.10
179.79	0.25	0.18	0.79	0.13
180.91	0.13	0.10	0.39	0.19
181.79	0.20	0.13	0.60	0.10
182.88	0.22	0.22	0.72	0.11
184.01	0.20	0.15	0.63	0.10
184.91	0.37	0.14	0.73	0.11
185.75	0.14	0.10	0.35	0.07
185.75	0.13	0.22	0.30	0.08
186.83	0.17	0.27	0.55	0.12
186.83	0.25	0.23	0.43	0.09
187.88	0.23	0.23	0.45	0.09
189.01	0.25	0.22	0.47	0.10
190.01	0.37	0.14	0.54	0.11
190.15	0.30	0.14	0.74	0.10
190.91	0.31	0.11	0.44	0.09
191.94	0.24	0.12	0.45	0.09
193.07	0.22	0.12	0.53	0.12
194.02	0.15	0.06	1.11	0.09
195.18	0.20	0.17	0.95	0.10
195.18	0.25	0.20	1.18	0.13
196.27	0.22	0.16	0.55	0.09
196.40	0.20	0.14	0.48	0.09
197.46	0.20	0.15	0.62	0.11
197.97	0.20	0.15	0.60	0.10
199.11	0.21	0.16	0.71	0.12
199.96	0.20	0.15	0.70	0.11
200.39	0.04	0.04	0.18	0.02
201.09	0.21	0.16	0.60	0.10
202.07	0.21	0.15	0.60	0.10
202.65	0.22	0.18	0.68	0.12
203.70	0.18	0.14	0.61	0.10

Sample	Hf (ppm)	Ta (ppm)	Th (ppm)	U (ppm)
204.66	0.20	0.15	0.60	0.11
205.48	0.19	0.14	0.62	0.10
205.65	0.19	0.15	0.62	0.10
207.57	0.21	0.14	0.60	0.11
208.63	0.21	0.14	0.63	0.11
209.86	0.39	0.12	0.46	0.08
210.75	0.25	0.16	0.68	0.13
211.88	0.26	0.12	0.46	0.09
213.07	0.27	0.12	0.48	0.09
213.79	0.25	0.09	0.30	0.05
214.91	0.25	0.12	0.45	0.08
216.02	0.24	0.16	0.59	0.11
216.96	0.27	0.09	0.41	0.08
218.02	0.17	0.10	0.30	0.05
219.06	0.31	0.14	0.52	0.11

Sample	La (ppm)	Ce (ppm)	Pr (ppm)	Nd (ppm)	Sm (ppm)	Eu (ppm)	Gd (ppm)	Tb (ppm)	Dy (ppm)	Ho (ppm)	Er (ppm)	Tm (ppm)	Yb (ppm)	Lu (ppm)
126.18	1.09	3.16	0.43	2.17	0.68	0.19	0.75	0.10	0.51	0.08	0.18	0.02	0.10	0.01
127.26	1.88	3.64	0.42	1.64	0.29	0.06	0.24	0.03	0.21	0.04	0.13	0.02	0.12	0.02
128.33	1.97	3.81	0.44	1.76	0.32	0.06	0.28	0.04	0.23	0.04	0.14	0.02	0.13	0.02
129.15	1.99	3.86	0.45	1.77	0.33	0.07	0.29	0.04	0.24	0.04	0.14	0.02	0.13	0.02
130.25	1.81	3.53	0.41	1.58	0.29	0.06	0.25	0.03	0.22	0.04	0.13	0.02	0.12	0.02
131.25	1.84	3.67	0.44	1.75	0.35	0.08	0.32	0.04	0.26	0.04	0.14	0.02	0.13	0.02
132.15	1.84	3.42	0.40	1.54	0.28	0.06	0.24	0.03	0.21	0.04	0.12	0.02	0.11	0.02
133.30	1.88	3.73	0.43	1.66	0.30	0.06	0.26	0.03	0.22	0.04	0.13	0.02	0.13	0.02
133.65	1.83	3.54	0.42	1.63	0.31	0.07	0.27	0.04	0.22	0.04	0.13	0.02	0.12	0.02
134.60	1.93	3.73	0.44	1.74	0.34	0.07	0.30	0.04	0.24	0.04	0.14	0.02	0.13	0.02
135.60	1.83	3.52	0.41	1.57	0.28	0.05	0.24	0.03	0.20	0.04	0.12	0.01	0.11	0.02
136.60	1.86	3.70	0.43	1.73	0.34	0.07	0.30	0.04	0.24	0.04	0.13	0.02	0.12	0.02
137.61	1.67	3.36	0.39	1.55	0.30	0.07	0.29	0.04	0.22	0.04	0.13	0.02	0.12	0.02
138.75	1.89	4.10	0.49	2.06	0.51	0.12	0.49	0.07	0.38	0.06	0.18	0.02	0.15	0.02
139.44	1.88	3.71	0.42	1.65	0.30	0.06	0.27	0.03	0.22	0.04	0.13	0.02	0.12	0.02
140.50	1.96	4.17	0.50	2.16	0.50	0.11	0.49	0.06	0.37	0.06	0.18	0.02	0.14	0.02
141.60	1.55	3.52	0.38	1.47	0.25	0.05	0.22	0.03	0.18	0.03	0.11	0.01	0.12	0.02
142.65	1.80	3.73	0.42	1.74	0.34	0.07	0.33	0.04	0.26	0.05	0.14	0.02	0.12	0.02
143.78	1.92	3.81	0.44	1.77	0.34	0.07	0.31	0.04	0.25	0.04	0.14	0.02	0.13	0.02
144.84	1.79	3.54	0.41	1.61	0.31	0.06	0.27	0.04	0.22	0.04	0.13	0.02	0.12	0.02
145.69	1.84	3.61	0.42	1.64	0.30	0.06	0.27	0.04	0.22	0.04	0.13	0.02	0.12	0.02
146.69	1.86	3.64	0.42	1.66	0.31	0.06	0.28	0.04	0.23	0.04	0.13	0.02	0.11	0.02
146.69	1.84	3.65	0.42	1.69	0.31	0.06	0.28	0.04	0.23	0.04	0.13	0.02	0.12	0.02
146.82	2.36	4.67	0.53	1.91	0.34	0.08	0.30	0.04	0.25	0.04	0.15	0.02	0.13	0.02
146.82	1.82	3.56	0.40	1.59	0.29	0.06	0.25	0.03	0.21	0.04	0.12	0.02	0.12	0.02
147.94	1.80	3.62	0.42	1.65	0.31	0.06	0.27	0.04	0.22	0.04	0.12	0.02	0.11	0.02

Sample	La (ppm)	Ce (ppm)	Pr (ppm)	Nd (ppm)	Sm (ppm)	Eu (ppm)	Gd (ppm)	Tb (ppm)	Dy (ppm)	Ho (ppm)	Er (ppm)	Tm (ppm)	Yb (ppm)	Lu (ppm)
148.85	1.70	3.39	0.39	1.58	0.29	0.06	0.27	0.03	0.22	0.04	0.12	0.01	0.11	0.02
151.07	2.06	4.02	0.47	1.84	0.35	0.07	0.31	0.04	0.25	0.05	0.14	0.02	0.13	0.02
151.87	1.82	3.80	0.41	1.61	0.30	0.07	0.28	0.04	0.22	0.04	0.13	0.02	0.12	0.02
152.37	1.67	3.53	0.40	1.65	0.34	0.07	0.30	0.04	0.24	0.04	0.13	0.02	0.11	0.02
152.87	1.87	3.98	0.44	1.77	0.34	0.08	0.32	0.04	0.25	0.04	0.14	0.02	0.13	0.02
153.98	1.68	3.35	0.38	1.47	0.28	0.06	0.24	0.03	0.20	0.04	0.11	0.01	0.11	0.02
155.93	1.67	3.37	0.38	1.57	0.30	0.06	0.27	0.04	0.22	0.04	0.12	0.01	0.11	0.01
157.97	1.80	3.69	0.42	1.64	0.31	0.06	0.28	0.04	0.22	0.04	0.13	0.02	0.12	0.02
158.94	1.78	3.67	0.42	1.63	0.30	0.06	0.28	0.04	0.21	0.04	0.12	0.02	0.11	0.02
160.07	1.64	3.34	0.37	1.46	0.28	0.06	0.25	0.03	0.21	0.04	0.12	0.02	0.11	0.02
167.89	0.32	0.63	0.07	0.28	0.06	0.01	0.06	0.01	0.05	0.01	0.03	0.00	0.03	0.00
168.99	1.64	3.73	0.45	1.97	0.53	0.13	0.58	0.08	0.45	0.07	0.20	0.02	0.15	0.02
170.08	1.76	3.63	0.41	1.63	0.31	0.06	0.28	0.04	0.23	0.04	0.13	0.02	0.12	0.02
171.21	1.67	3.35	0.38	1.52	0.27	0.06	0.24	0.03	0.21	0.04	0.13	0.02	0.12	0.02
172.31	1.80	3.78	0.43	1.71	0.33	0.07	0.31	0.04	0.26	0.05	0.15	0.02	0.14	0.02
174.23	1.93	4.16	0.46	1.81	0.35	0.07	0.31	0.04	0.25	0.05	0.15	0.02	0.14	0.02
185.75	1.06	2.70	0.32	1.49	0.41	0.11	0.44	0.06	0.31	0.05	0.14	0.02	0.11	0.02
186.83	1.83	3.57	0.41	1.59	0.29	0.06	0.25	0.03	0.21	0.04	0.12	0.02	0.11	0.02
186.83	1.33	2.81	0.31	1.17	0.19	0.04	0.17	0.02	0.16	0.03	0.11	0.02	0.12	0.02
187.88	1.37	2.99	0.32	1.23	0.20	0.04	0.17	0.02	0.16	0.03	0.11	0.01	0.11	0.02
189.01	1.55	3.18	0.34	1.26	0.19	0.04	0.17	0.02	0.16	0.03	0.12	0.02	0.12	0.02
136.65	2.38	4.71	0.55	1.95	0.36	0.07	0.30	0.04	0.25	0.04	0.15	0.02	0.14	0.02
138.75	2.09	4.55	0.54	2.06	0.48	0.12	0.47	0.06	0.36	0.06	0.18	0.02	0.15	0.02
156.05	2.11	4.41	0.50	1.88	0.36	0.08	0.33	0.04	0.25	0.05	0.15	0.02	0.13	0.02
161.00	1.76	3.64	0.40	1.46	0.27	0.06	0.24	0.03	0.20	0.04	0.12	0.01	0.11	0.01
161.58	1.90	3.87	0.43	1.52	0.27	0.06	0.25	0.03	0.20	0.04	0.12	0.01	0.12	0.02

Sample	La (ppm)	Ce (ppm)	Pr (ppm)	Nd (ppm)	Sm (ppm)	Eu (ppm)	Gd (ppm)	Tb (ppm)	Dy (ppm)	Ho (ppm)	Er (ppm)	Tm (ppm)	Yb (ppm)	Lu (ppm)
162.72	1.82	3.68	0.40	1.45	0.25	0.06	0.24	0.03	0.19	0.03	0.12	0.01	0.11	0.01
163.77	2.02	4.29	0.47	1.72	0.30	0.07	0.28	0.03	0.23	0.04	0.14	0.02	0.13	0.02
164.91	1.64	3.60	0.39	1.40	0.24	0.06	0.23	0.03	0.18	0.03	0.11	0.01	0.09	0.01
166.04	2.15	4.72	0.53	2.01	0.38	0.08	0.34	0.04	0.27	0.05	0.15	0.02	0.13	0.02
167.11	1.86	3.95	0.43	1.63	0.31	0.07	0.30	0.04	0.25	0.05	0.15	0.02	0.13	0.02
173.20	1.80	3.78	0.42	1.50	0.27	0.06	0.26	0.03	0.22	0.04	0.14	0.02	0.13	0.02
174.23	2.09	4.49	0.49	1.79	0.32	0.07	0.29	0.04	0.24	0.04	0.14	0.02	0.13	0.02
175.26	1.86	3.88	0.42	1.50	0.26	0.05	0.22	0.03	0.20	0.04	0.13	0.02	0.12	0.02
176.24	2.19	4.53	0.49	1.74	0.30	0.07	0.29	0.04	0.24	0.05	0.16	0.02	0.15	0.02
176.71	1.96	4.24	0.45	1.59	0.27	0.05	0.22	0.03	0.19	0.04	0.13	0.02	0.12	0.02
177.77	2.20	4.71	0.53	1.94	0.37	0.08	0.35	0.04	0.29	0.05	0.17	0.02	0.15	0.02
178.77	1.96	4.09	0.45	1.62	0.29	0.06	0.26	0.03	0.22	0.04	0.14	0.02	0.13	0.02
179.79	2.50	5.48	0.61	2.24	0.43	0.10	0.40	0.05	0.32	0.06	0.19	0.02	0.17	0.02
180.91	1.45	3.23	0.37	1.40	0.28	0.06	0.26	0.03	0.21	0.04	0.12	0.01	0.11	0.01
181.79	1.88	4.15	0.44	1.58	0.25	0.05	0.21	0.03	0.18	0.03	0.13	0.02	0.12	0.02
182.88	2.26	4.82	0.50	1.76	0.28	0.06	0.24	0.03	0.21	0.04	0.15	0.02	0.15	0.02
184.01	2.12	4.60	0.50	1.84	0.32	0.06	0.26	0.03	0.22	0.04	0.14	0.02	0.13	0.02
184.91	1.98	4.67	0.49	1.77	0.29	0.06	0.25	0.03	0.21	0.04	0.14	0.02	0.13	0.02
185.75	1.19	3.04	0.36	1.50	0.40	0.11	0.42	0.05	0.30	0.05	0.15	0.02	0.11	0.01
190.01	1.91	4.34	0.47	1.69	0.29	0.06	0.27	0.04	0.24	0.04	0.15	0.02	0.15	0.02
190.15	2.17	5.24	0.56	2.02	0.34	0.07	0.28	0.03	0.22	0.04	0.14	0.02	0.13	0.02
190.91	1.35	2.86	0.32	1.17	0.21	0.05	0.21	0.03	0.20	0.04	0.13	0.02	0.13	0.02
191.94	1.35	2.82	0.31	1.12	0.19	0.04	0.18	0.02	0.17	0.03	0.12	0.01	0.12	0.01
193.07	1.72	3.65	0.41	1.45	0.23	0.04	0.18	0.02	0.17	0.03	0.12	0.01	0.12	0.02
194.02	1.69	4.01	0.41	1.36	0.24	0.05	0.23	0.04	0.26	0.05	0.20	0.03	0.22	0.03
195.18	1.62	3.31	0.33	1.03	0.13	0.03	0.12	0.02	0.12	0.03	0.11	0.02	0.14	0.02

Sample	La (ppm)	Ce (ppm)	Pr (ppm)	Nd (ppm)	Sm (ppm)	Eu (ppm)	Gd (ppm)	Tb (ppm)	Dy (ppm)	Ho (ppm)	Er (ppm)	Tm (ppm)	Yb (ppm)	Lu (ppm)
195.18	2.02	4.11	0.41	1.26	0.16	0.03	0.14	0.02	0.16	0.03	0.14	0.02	0.18	0.02
196.27	1.75	3.65	0.39	1.42	0.24	0.05	0.23	0.03	0.19	0.04	0.13	0.02	0.13	0.02
196.40	1.53	3.20	0.36	1.29	0.22	0.05	0.20	0.03	0.18	0.03	0.12	0.01	0.12	0.02
197.46	1.98	4.17	0.46	1.69	0.31	0.07	0.30	0.04	0.25	0.05	0.16	0.02	0.15	0.02
197.97	1.83	3.95	0.44	1.61	0.31	0.07	0.30	0.04	0.25	0.05	0.16	0.02	0.15	0.02
199.11	2.19	4.81	0.52	1.92	0.34	0.07	0.30	0.04	0.26	0.05	0.17	0.02	0.16	0.02
199.96	1.95	4.33	0.48	1.70	0.27	0.05	0.22	0.03	0.20	0.04	0.14	0.02	0.14	0.02
200.39	0.30	0.85	0.10	0.39	0.09	0.02	0.09	0.01	0.09	0.01	0.05	0.01	0.05	0.01
201.09	1.71	3.85	0.40	1.37	0.21	0.04	0.17	0.02	0.17	0.03	0.12	0.01	0.12	0.02
202.07	1.76	3.60	0.38	1.31	0.19	0.04	0.17	0.02	0.16	0.03	0.12	0.01	0.12	0.02
202.65	2.00	4.17	0.45	1.57	0.24	0.05	0.21	0.03	0.19	0.04	0.14	0.02	0.14	0.02
203.70	1.70	3.52	0.38	1.33	0.21	0.04	0.17	0.02	0.16	0.03	0.12	0.02	0.12	0.02
204.66	1.89	4.02	0.44	1.61	0.29	0.06	0.26	0.03	0.23	0.04	0.15	0.02	0.14	0.02
205.48	1.77	3.67	0.40	1.38	0.22	0.04	0.18	0.02	0.18	0.03	0.13	0.02	0.13	0.02
205.65	1.75	3.52	0.37	1.29	0.20	0.04	0.19	0.02	0.18	0.04	0.13	0.02	0.13	0.02
207.57	1.91	4.04	0.44	1.57	0.25	0.05	0.21	0.03	0.19	0.04	0.13	0.02	0.13	0.02
208.63	1.97	4.15	0.45	1.57	0.24	0.05	0.19	0.02	0.17	0.03	0.12	0.02	0.13	0.02
209.86	1.20	2.88	0.32	1.24	0.24	0.05	0.22	0.03	0.20	0.04	0.12	0.01	0.11	0.01
210.75	2.18	4.57	0.50	1.75	0.28	0.05	0.23	0.03	0.21	0.04	0.15	0.02	0.14	0.02
211.88	1.65	3.52	0.39	1.42	0.26	0.05	0.24	0.03	0.20	0.04	0.12	0.01	0.11	0.01
213.07	1.46	3.16	0.35	1.33	0.25	0.06	0.24	0.03	0.20	0.04	0.13	0.02	0.12	0.02
213.79	0.70	1.46	0.17	0.63	0.13	0.03	0.14	0.02	0.14	0.03	0.09	0.01	0.08	0.01
214.91	1.29	2.90	0.33	1.29	0.27	0.06	0.26	0.03	0.23	0.04	0.13	0.02	0.12	0.02
216.02	1.83	3.97	0.44	1.59	0.29	0.06	0.25	0.03	0.22	0.04	0.14	0.02	0.13	0.02
216.96	1.20	2.63	0.30	1.14	0.21	0.04	0.19	0.02	0.16	0.03	0.10	0.01	0.09	0.01
218.02	0.89	2.05	0.23	0.90	0.18	0.04	0.18	0.02	0.16	0.03	0.10	0.01	0.08	0.01

Sample	La (ppm)	Ce (ppm)	Pr (ppm)	Nd (ppm)	Sm (ppm)	Eu (ppm)	Gd (ppm)	Tb (ppm)	Dy (ppm)	Ho (ppm)	Er (ppm)	Tm (ppm)	Yb (ppm)	Lu (ppm)
219.06	1.93	4.05	0.45	1.59	0.26	0.05	0.23	0.03	0.19	0.03	0.13	0.02	0.12	0.02